VYSOKÉ UČENÍ TECHNICKÉ V BRNĚ
BRNO UNIVERSITY OF TECHNOLOGY

FAKULTA ELEKTROTECHNIKY A KOMUNIKAČNÍCH TECHNOLOGIÍ
ÚSTAV VÝKONOVÉ ELEKTROTECHNIKY A ELEKTRONIKY

FACULTY OF ELECTRICAL ENGINEERING AND COMMUNICATION
DEPARTMENT OF POWER ELECTRICAL AND ELECTRONIC ENGINEERING

FAULT-TOLERANT CONTROL OF A FLUX-SWITCHING PERMANENT MAGNET SYNCHRONOUS MACHINE

DOKTORSKÁ PRÁCE
DOCTORAL THESIS

AUTOR PRÁCE **Ing. MUSTAFA OSMAN ELRAYAH ABOELHASSAN**
AUTHOR

BRNO 2013

VYSOKÉ UČENÍ TECHNICKÉ V BRNĚ
BRNO UNIVERSITY OF TECHNOLOGY

FAKULTA ELEKTROTECHNIKY A KOMUNIKAČNÍCH TECHNOLOGIÍ
ÚSTAV VÝKONOVÉ ELEKTROTECHNIKY A ELEKTRONIKY

FACULTY OF ELECTRICAL ENGINEERING AND COMMUNICATION
DEPARTMENT OF POWER ELECTRICAL AND ELECTRONIC ENGINEERING

FAULT-TOLERANT CONTROL OF A FLUX-SWITCHING PERMANENT MAGNET SYNCHRONOUS MACHINE

ROBUSTNÍ ŘÍZENÍ SYNCHRONNÍHO STROJE S PERMANENTNÍMI MAGNETY A SPÍNANÝM TOKEM

DOCTORAL THESIS
DOKTORSKÁ PRÁCE

AUTOR PRÁCE Ing. MUSTAFA OSMAN ELRAYAH ABOELHASSAN
AUTHOR

VEDOUCÍ PRÁCE Prof. Ing. JIŘÍ SKALICKÝ, CSc.
SUPERVISOR

BRNO 2013

This Page Intentionally Left Blank

ABSTRAKT

Je jasné, že nejúspěšnější konstrukce zahrnuje postup vícefázového řízení, ve kterém každá fáze může být považována za samostatný modul. Provoz kterékoliv z jednotek musí mít minimální vliv na ostatní, a to tak, že v případě selhání jedné jednotky ostatní mohou být v provozu neovlivněny. Modulární řešení vyžaduje minimální elektrické, magnetické a tepelné ovlivnění mezi fázemi řízení (měniče). Synchronní stroje s pulzním tokem a permanentními magnety se jeví jako atraktivní typ stroje, jejíž přednostmi jsou vysoký kroutící moment, jednoduchá a robustní konstrukce rotoru a skutečnost, že permanentní magnety i cívky jsou umístěny společně na statoru.

FS-PMSM jsou poměrně nové typy střídavého stroje stator-permanentní magnet, které představují významné přednosti na rozdíl od konvenčních rotorů - velký kroutící moment, vysoký točivý moment, v podstatě sinusové zpětné EMF křivky, zároveň kompaktní a robustní konstrukce díky umístění magnetů a vinutí kotvy na statoru. Srovnání výsledků mezi FS-PMSM a klasickými motory na povrchu upevněnými PM (SPM) se stejnými parametry ukazuje, že FS-PMSM vykazuje větší vzduchové mezery hustoty toku, vyšší točivý moment na ztráty v mědi, ale také vyšší pulzaci díky reluktančnímu momentu. Pro stroje buzené permanentními magnety se jedná o tradiční rozpor mezi požadavkem na vysoký kroutící moment pod základní rychlostí (oblast konstantního momentu) a provozem nad základní rychlostí (oblast konstantního výkonu), zejména pro aplikace v hybridních vozidlech.

Je předložena nová topologie synchronního stroje s permanentními magnety a spínaným tokem odolného proti poruchám, která je schopná provozu během vinutí naprázdno a zkratovaného vinutí i poruchách měniče. Schéma je založeno na dvojitě vinutém motoru napájeném ze dvou oddělených vektorově řízených napěťových zdrojů. Vinutí jsou uspořádána takovým způsobem, aby tvořila dvě nezávislé a oddělené sady. Simulace a experimentální výzkum zpřesní výkon během obou scénářů jak za normálního provozu, tak za poruch včetně zkratových závad a ukáží robustnost pohonu za těchto podmínek.

Tato práce byla publikována v deseti konferenčních příspěvcích, dvou časopisech a knižní kapitole, kde byly představeny jak topologie pohonu a aplikovaná řídící schémata, tak analýzy jeho schopnosti odolávat poruchám.

KLÍČOVÁ SLOVA: Letecký, Vysokorychlostní, Nadbytek, Odolné proti poruchám, Frekvenční měniče, Odolnost vůči poruchám stroje, Dvojité trojfázové stroje, Pulzní tok permanentní magnety synchronního stroje, Vícefázové motory, Vícefázové pohony, Vektorové řízení, Polem orientované vektorové řízení, Pulsní šířková modulace, Napěťový měnič, Synchronní stroj s permanentními magnety, Servomotor, Nelineární řízení, Řízení zpětnou vazbou, Polohové řízení, Řízení rychlosti, Proudová regulace, Zpětný náraz, Regulace odbuzováním, Normální provozní podmínky, Chybový provozní stav, Porucha naprázdno, Porucha zkratem, Jednofázové poruchy, Nerovnováha tří fází, Brzdný moment, Bezpečnostně kritické aplikace.

ABSTRACT

It has become clear that the most successful design approach involves a multiple phase drive in which each phase may be regarded as a single-module. The operation of any one module must have minimal impact upon the others, so that in the event of that module failing the others can continue to operate unaffected. The modular approach requires that there should be minimal electrical, magnetic and thermal interaction between phases of the drive. Flux-Switching permanent magnet synchronous machines (FS-PMSM) have recently emerged as an attractive machine type virtue of their high torque densities, simple and robust rotor structure and the fact that permanent magnets and coils are both located on the stator.

Flux-switching permanent magnet (FS-PMSM) synchronous machines are a relatively new topology of stator PM brushless machine. They exhibit attractive merits including the large torque capability and high torque (power) density, essentially sinusoidal back-EMF waveforms, as well as having a compact and robust structure due to both the location of magnets and armature windings in the stator instead of the rotor as those in the conventional rotor-PM machines. The comparative results between a FS-PMSM and a traditional surface-mounted PM (SPM) motor having the same specifications reveal that FS-PMSM exhibits larger air-gap flux density, higher torque per copper loss, but also a higher torque ripple due to cogging -torque. However, for solely permanent magnets excited machines, it is a traditional contradiction between the requests of high torque capability under the base-speed (constant torque region) and wide speed operation above the base speed (constant power region) especially for hybrid vehicle applications.

A novel fault-tolerant FS-PMSM drive topology is presented, which is able to operate during open- and short-circuit winding and converter faults. The scheme is based on a dual winding motor supplied from two separate vector-controlled voltage-sourced inverter drives. The windings are arranged in a way so as to form two independent and isolated sets. Simulation and experimental work will detail the driver's performance during both healthy- and faulty- scenarios including short-circuit faults and will show the drive robustness to operate in these conditions.

The work has been published in ten conference papers, two journal papers and a book chapter, presenting both the topology of the drive and the applied control schemes, as well as analysing the fault-tolerant capabilities of the drive.

KEYWORDS: Aerospace, High speed, Redundancy, Fault-Tolerant, AC motor drives , Fault-Tolerant machines, Dual three-phase machines, Flux-Switching permanent magnet synchronous machine (FS-PMSM), Multi-phase motors, Multi-phase drives, Vector-control, Field-oriented vector-control, Pulse-width modulation (PWM), Voltage source inverter (VSI), Permanent magnet synchronous machine (PMSM), Servomotor, Nonlinear-control, Feedback-control, Position control, Speed control, Current control, Backlash, Field-weakening control, Normal-operating condition (Healthy), Faulty-operating condition (Unhealthy), Open-circuit fault, Short-circuit fault, Single-phase fault, Balance three-phase fault, Braking torque, Safety-critical application.

BIBLIOGRAFICKÁ CITACE

ABOELHASSAN, M. O. E. **Robustní řízení synchronního stroje s permanentními magnety a spínaným tokem**. Brno: Vysoké učení technické v Brně, Fakulta elektrotechniky a komunikačních technologií, 2013. 168 s. Vedoucí dizertační práce **prof. Ing. Jiří Skalický, CSc.**

PROHLÁŠENÍ AUTORA O PŮVODNOSTI PRÁCE

Prohlašuji, že dizertační práci na téma *Fault-Tolerant Control of a Flux-Switching Permanent Magnet Synchronous Machine* jsem vypracoval samostatně pod vedením školitele a s využitím odborné literatury a dalších informačních zdrojů, které jsou všechny citovány v práci a uvedeny v seznamu literatury.

Jako autor uvedené dizertační práce dále prohlašuji, že v souvislosti s vytvořením této dizertační práce jsem neporušil autorská práva třetích osob, zejména jsem nezasáhl nedovoleným způsobem do cizích autorských práv osobnostních a jsem si plně vědom následků porušení ustanovení § 11 a následujících autorského zákona č. 121/2000 Sb., včetně možných trestněprávních důsledků vyplývajících z ustanovení § 152 trestního zákona č. 140/1961 Sb.

V Brně dne…………………………….............Podpis autora ……………………………….......

ACKNOWLEGMENT

This research project focuses on the development of fault-tolerant control strategies of novel flux-switching permanent magnet synchronous machines for aerospace applications. The research was fully funded and supported by the Ministry of Education, Youth and Sports of the Czech Republic under project *MSM0021630516* and the Nottingham, Department of Electrical and Electronic Engineering, which is gratefully acknowledged. First of all I would like to express my deepest appreciation and sincere gratitude to my supervisors prof. Ing. Jiří Skalický, CSc and Prof. Dr. Chris Gerada for their continuous support, encouragement, and valuable advice throughout the progress of this project. I would also like to take this opportunity to express heartfelt gratitude to Dr. Andrew Goodman, Dr. Lee Empringham Dr. Liliana De Lillo for their friendship in due course of development of the thesis, constant support, precious advice and technical support, encouragement, guidance and direction without which the thesis would not have taken shape.

I am very grateful to the staff and all my colleagues in the Department of Power Electrical and Electronic Engineering at Brno University of Technology. I gratefully acknowledged the staff of the Power Electronics, Machines and Control (PEMC) Research Group at the University of Nottingham for their support, valuable discussions, and providing both theoretical and practical help to carry out this research. Many thanks also go to all of the technicians. Among them I would like to give special thanks to Andy Matthews, Kevin Padgett, and Colin Astill for their steady support during the experimental stage.

Appreciation is extended to those others who have made my research more interesting and enjoyable, they are too many to mention, but particularly Dr. Sudarat Khwan-on and Dr. Abdurrahman Saeid. I would also like to thank all of my friends for their friendship and support over the last three years.

Finally, and above of all, I owe greatest debt of gratitude and thanks to Allah, my parents, my sisters and my brothers for their infinite patience, providing continuous guidance and wholehearted support, encouragement throughout the thesis. They helped me to regain enthusiasm, strength and determination during the difficult times.

Mustafa Osman Elrayah Aboelhassan

Nottingham, United Kingdom

August 2013.

LIST OF CONTENTS

LIST OF FIGURES

LIST OF TABLES

LIST OF BASIC SYMBOLS AND ACRONYMS

SYMBOL		*DEFINITION*
v_a, v_b, v_c		Phase voltages in the stator windings as, bs, and cs, respectively
v_{a1_ref}, v_{b1_ref}, v_{c1_ref}, v_{a2_ref}, v_{b2_ref}, v_{c2_ref}		Reference voltages
$v^r{}_{sd}, v^r{}_{sq}, v^r{}_{s0}$		Instantaneous values of direct-, quadrature-, and zero - axis stator voltage components respectively and expressed in the rotor reference frame
$v_{d1}, v_{q1}, v_{d2}, v_{q2},$		Controlled voltages
v_D, v_Q		Damper winding voltage
v_f		Excitation voltage applied to the rotor winding *f*
E		Back-EMF voltage
$\overline{i_s^r}$		Space phasor of the stator currents expressed in the rotor reference frame
$\left\lvert\overline{i_s^r}\right\rvert$		Rotor current modulus
$\overline{i_s'^s}$		Space phasor of the stator currents expressed in the stationary reference frame
$\left\lvert\overline{i_s'^s}\right\rvert$		Stator current modulus
i_a, i_b, i_c		Instantaneous values of the stator currents in stator phases a, b, and c Respectively
$i_{a1}, i_{b1}, i_{c1}, i_{a2}, i_{b2}, i_{c2}$		Phase currents in the stator windings
i_d, i_q		Controlled currents
$i^r{}_{sd}$		Direct axis of the stator current in rotor reference frame (Flux component)

$i^{r}{}_{sq}$		Quadrature-axis of the stator current in rotor reference frame (Torque component)
$i^{r}{}_{sd},\ i^{r}{}_{sq},\ i^{r}{}_{s0}$		Instantaneous values of direct-, quadrature-, and zero - axis stator current components respectively and expressed in the rotor reference fame
$i_{d1}, i_{d2}, i_{q1}, i_{q2}$		Controlled currents
$i_{d1}{}^{*}\quad i_{d2}{}^{*}, i_{d2}{}^{*}\quad i_{q2}{}^{*}$		Reference currents
$i_{sD},\ i_{sQ}$		Instantaneous values of direct,- and quadrature axis stator current *components respectively and expressed in stationary reference frame*
R_s, R_r		Resistances of the stator (armature-resistance) and rotor windings, respectively
$R_s,\ R_f$		Resistance of the rotor winding (field-resistance), respectively
$\psi_{as}, \psi_{bs}, \psi_{cs}$		Stator flux linkages
$\psi_{a1}, \psi_{b1}, \psi_{c1}, \psi_{a2}, \psi_{b2}, \psi_{c2}$		Stator flux linkages
$\psi^{r}{}_{sd}, \psi^{r}{}_{sq}, \psi^{r}{}_{s0}$		Instantaneous values of direct-, quadrature-, and zero-axis stator flux linkages expressed in the rotor reference frame
ψ_{f}		Rotor (Excitation) flux linkage
ψ_{PM}		Permanent magnet flux per pole
ψ_{m}		Magnitude of the flux linkages established by the permanent-magnet
L_{ss}, L_{rr}		Self-inductances of the stator and rotor windings, respectively

L_{aa}, L_{bb}, L_{cc}		Self-inductances of the stator windings
L_{ab}, L_{ac}, L_{ba}, L_{bc}, L_{ca}, L_{cb}		Mutual inductances between the stator phases.
L_d		Direct inductance
L_q		Quadurature inductance
L_{sd}, $L_{sq,}$ L_0		Stator inductance in *d*,*q*,*0* axis respectively
L_{sd}		Inductance along the magnet axis
L_{sq}		Inductance along an axis in quadrature to the magnet axis
L_{df}		Mutual inductance between the armature- and field-winding
L_m, L_{ls}		Stator magnetizing and stator leakage inductances, respectively
L_{mq}, L_{md}		Magnetizing inductances in the quadrature and direct axes
$\overline{\mathrm{L}}_{\mathrm{m}}$		The average value of the magnetizing inductance
$\mathrm{L}_{\Delta\mathrm{m}}$		Half the amplitude of the sinusoidal variation of the magnetizing inductance
L_f		Excitation winding inductance
$\Re_{mq} = \Re_{md}$		Magnetizing reluctance
ω_k		Angular velocity of the general reference frame
ω_s		Angular velocity of the synchronous reference frame
ω_m, θ_m		Mechanical angular velocity and displacement, respectively
ω_r, θ_r		Electrical angular velocity and displacement, respectively

θ_r		Instantaneous rotor angle (*angular position of the rotor*)
ϑ		Instantaneous rotor angle (electrical angular displacement)
T_e		Instantaneous value of electromagnetic torque developed by the motor
T_L		Load-torque (required torque to drive the load referred to the motor shaft) applied
P		Number of electrical poles
J		Equivalent moment of inertia of the drive system
$J_{m(\text{total})}$		Total system ineria referred to motor shaft
B_m		Viscous friction coefficient
$B_{m(\text{total})}$		Total system viscous friction referred to motor shaft
K_t		Torque constant
N_s, N_r		Number of turns of the stator and rotor windings, respectively
β_s		The angle of the stator current vector (with respect to the direct axis of the Stationary reference frame)
δ		Current load (torque) angle
$(^r)$		Superscript denotes to define variable in rotor reference frame
PM		Permanent Magnet
(*)		Superscript denotes the complex conjugate
IPM		Surface inset PM
SPM		Surface-mounted PM
DSPM		Doubly-salient permanent magnet machine
FRPM		Flux-reversal permanent magnet machine

FSPMSM		Flux switching permanent magnet synchronous machine
rpm		Revolutions per minute
sec		Second
AC		Alternation current
DC		Direct current
SC		Short-circuit
OC		Open-circuit
MTPA		Maximum torque per ampere
PWM		Pulse-Width modulation
VSI		Voltage source inverter
GTO		A gate turn-off thyristor
IGBT		Insulated gate bipolar transistor
MOSFET		Metal oxide semiconductor field effect transistor
d, q		Rotating frame d- and q- axis components
A/D		Analogue to digital converter
R/D		Resolver to digital converter
DSP		Digital Signal processor
FPGA		Field programmable gate array
HPI		Host port interface daughter card
EMIF		External memory interface
IDE		Integrated development environment
EMI		Electromagnetic interference
CCS		Code composer studio

1 INTRODUCTION

1.1 Literature Review (FS-PMSM, Fault-Tolerant)

The Performance of brushless AC machines having magnets in the rotor is compromised due to the poor cooling and high speed limitation. Whilst in the stator PM machine (*permanent magnet are located on the stator*), the temperature rise in the permanent magnet can be controlled much easier. The rotor of these machines is very simple and robust; therefore it can be operated at a very high speed. Recently, three novel topologies of stator PM machines have been proposed, doubly-salient PM (*DSPM*) machines, flux-reversal PM (*FRPM*) machines, and flux-switching PM (*FSPM*) machines [1]. The FS-PM machine is a competitive candidate for brushless **AC** drives [2], due to the higher torque density (*ratio of torque capability to volume and is expressed in unit Torque per volume*).

Flux-switching machines are gaining an increasing popularity in high performance drives due to their numerous advantages over other brushless machines [3], [4]. Their rotor structure is similar to that of a switched reluctance machine with all the associated advantages in terms of robustness and construction simplicity. They are however an AC machine having a sinusoidally varying permanent-magnet flux-linking each phase winding with rotor rotation. They can thus be sinusoidally driven and have the associated advantages of sinusoidally excited machines including a smooth output torque and constant input power in steady-state balanced operation. The output torque can be dynamically controlled using vector-control algorithms. A control scheme for a fault-tolerant flux-switching machine design will be presented. The machine itself was designed to have two-sets of three-phase windings, each supplied from a separate three-phase converter drive. The drive system behaviour in healthy-conditions and when it undergoes a variety of faults will be looked at and results from an experimental drive system will be detailed.

Fault tolerance is often adopted in safety-critical drive systems such as aerospace drives to reach the required drive system reliability levels with minimum overall weight and component count. The fundamental concept is to have redundancy in the components which are more likely to fail rather than have redundancy at the drive system level. This usually requires isolation (thermally, electrically, magnetically and physically) from each component to avoid failure propagation [5]. Electrical machines can be made to be fault tolerant in different configurations depending on the nature of faults they need to tolerate. The failures which are more likely to occur in an electrical drive system are those related to the converter drive including sensors; active and passive components; and related driving, control, and protection circuitry. Within the machine itself, the main failure modes which need accounting for are winding and bearing failures. Bearing failures are progressive and diagnostic, and prognostic techniques can be employed to cater for these. With electrical failures in the converter and machine, remedial action needs to be taken to ensure drive operation in safety-critical applications.

Different machine topologies have been proposed for such applications. PM machines have often been chosen based on their higher specific torque and power density [6]. Concentrated wound machines designed to have a high phase inductance and low phase-phase mutual inductance that are fed from separate converters were shown to fulfil these fault-tolerant requirements. The main challenge with the design of such machines is the magnet permanent field excitation which cannot be disabled in case of a fault unless some type of complex mechanical mechanism or active magnet shunts are used as reviewed in [7]. These are often not acceptable due to increased complexity and weight and due to their implication on the system reliability. The requirement for high inductance to limit the short-circuit current results in a low machine power factor, and if the machine is used in a variable speed application, the braking-torque generated when the machine is running at low speeds can be significant.

1.2 Thesis Objective

This work is based on a dual three-phase channel machine. Each machine (three-phase channel) is fed from a separate three-phase converter. In case of a phase open-circuit fault in one of the machine drive units, the post-fault control strategy is to disable the faulty unit and deliver power with the remaining healthy unit. In case of a short-circuit fault, the post-fault control strategy is to apply a balanced short-circuit through the converter and again continue operation with the healthy unit, this time having to additionally overcome the braking-torque produced by the faulty unit.

The purpose of this research is to provide a novel fault-tolerant flux-switching permanent magnet synchronous machine drive topology, which is able to operate during open- and short-circuit winding and converter faults. Simulation and experimental work will detail the driver's performance during both healthy- and faulty-scenarios including short-circuit faults and will show the drive robustness to operate in these conditions.

The control strategies have been implemented for a novel fault-tolerant FS-PMSM showing their respective implications on drive operation. This work will present the modelling and implementation of a fault-tolerant vector-control strategy for a flux-switching machine and will highlight the implications of adopting such a system.

The main objectives of the research described in this thesis are:

- The development of a fault-tolerant FS-PMSM to drive under open- and short-circuit operating conditions.
- The development of fault-tolerant control strategies of novel flux-switching synchronous machines for aerospace applications.
- Improving machine dynamic performance through applying a torque compensation scheme.
- Field-weakening control of FS-PMSM

1.3 Thesis Layout

In order to describe the output research objective above, this thesis is organized into eight chapters. The layout of the thesis is described below;

CHAPTER 1 INTRODUCTION

This chapter provides a literature review of previous research on fault tolerant drive systems which particularly focus on FS-PMSM. Permanent magnet machines are high performance devices; there are two torque components that affect their output performance. The first is called ripple torque, which is produced from the harmonic content of the current and voltage waveforms in the machine. The second, called cogging torque, occurs due to the physical structure of the machine. Cogging torque is produced by the magnetic attraction between the rotor permanent magnets with the stator slots. It is an undesired effect that contributes to the output ripple, vibration, and noise in the machine [8]. The performance of brushless **AC** machines having magnets in the rotor is compromised due to the poor cooling and high limitation. Whilst in the stator machine (permanent magnets are located on the stator), the temperature rise in the permanent magnet can be much easier controlled. The rotor of these machines is very simple and robust; therefore it can be operated at a very high speed. Recently, three novel topologies of stator permanent magnet machine have been proposed, doubly-salient permanent magnet machines (DSPM), flux-reversal permanent magnet machines (FRPM), and flux-switching permanent magnet machines (FS-PM). The Flux-switching permanent magnet machine is a competitive candidate for brushless **AC** drives, due to the higher torque density (ratio of torque capability to volume and is expressed in unit Torque per volume).

CHAPTER 2 POSITION CONTROL OF PM SYNCHRONOUS AC SERVOMOTOR BASED ON VECTOR CONTROL

This chapter reviews the mathematical model of a permanent magnet servomotor using *d-q axis*. The *d-q* model of the PM-servomotor synchronous motor can be derived from the well-known model of the synchronous machine without the equations of the damper windings on the rotor and field current dynamics removed. The *d-q* model of the PM-servomotor has been developed on a rotor reference frame; it is done by converting the three-phase voltages and currents to *d-q* variables by using Park's transformation. The mathematical model for the PM-servomotor has been verified and designed in MATLAB-SIMULINK. The complete servodrive consists of a PMSM provided with a resolver, of a voltage source converter with sinusoidal PWM and of a feedback-control structure for the current, speed and position. The vector-control of a PMSM is derived from the rotor position because the flux complies with the position of the permanent magnets on the rotor. This chapter mainly focuses on position vector-control of the PM-servomotor. The PM-servomotor needs continuous knowledge of the rotor position, i.e. of the magnetic flux position. The proposed motor supplied by a voltage source inverter (VSI-PWM) with IGBTs (*insulated gate bipolar transistors*), which is controlled by a digital circuit is based on the stator current feedback information.

CHAPTER 3 FLUX SWITCHING PERMANENT MAGNET SYNCHRONOUS MACHINED

This Chapter has discusses a dual three-phase FS-PMSM which was designed to have two sets of three-phase winding. The winding are arranged in a way so as to form two independent and isolated sets. This chapter will give a description of the concept and operation principles of FS-PMSM. A summary of the mathematical model for dual three-phase FS-PMSM (a, b, c) has been provided.

CHAPTER 4 FSPMSM DRIVE SYSTEM

This chapter presents fault tolerant drive topologies based on a voltage source inverter. In [9], voltage source inverters have evolved as the most preferred power conversion method for AC drive applications. At this point in time hard switching techniques continue to dominate the market, ranging from MOSFET semiconductor switches (application at low power range), Bipolar Darlington transistor and the IGBT (application at medium power range) up to GTO inverters (applied at megawatt power level). Drive system reliability can be typically improved by increasing the number of machine-converter units, or the number of phases, or the number of winding channels or a combination of the aforementioned in order to ensure continued operation in case of a fault occurring. In this Chapter a novel fault-tolerant flux-switching permanent magnet synchronous machine supplied from two separate vector-controlled and voltage sourced inverter drives has been shown and described. A field-weakening control has been focused on MTPA in order to make the system dynamics higher for instantaneous torque control. A field-weakening scheme to maintain the maximum torque capability over the entire high speed range is presented.

CHAPTER 5 FAULT TOLERANT FSPMSM DRIVE CONTROL

Safety critical motor drive systems are becoming more important in many areas such as aerospace, transportation, medical and military applications. In these applications, any failure of motor drives may result in catastrophic loss of property and human life. Therefore, the motor drives utilized in safety critical applications must be fault-tolerant, and they should continue to operate until the system is stopped safely [10]. The main aim of fault-tolerant drive system is to continue the operation of the drive in a satisfactory way in the presence of a fault. This means that the control and a minimum level of performance should be kept after a fault occurs. It should be noted that when operating with a fault, the system efficiency is typically reduced. Since operation with a fault represents an abnormal condition, the system efficiency is a secondary concern as long as the system is thermally able to accommodate the increased losses safely. Those additional losses during post-fault operation are typically modest and dependent on the selected topology [11]. In this Chapter a Fault-Tolerant Control strategy for an innovative Dual Flux-Switching Permanent Magnet Motor Drive in both healthy- and faulty- conditions has been described in sufficient detail.

CHAPTER 6 SIMULATION RESULTS

This chapter shows the simulation results verifying the proposed model of a flux-switching permanent magnet motor drive under healthy- and faulty-operation conditions. Short-circuit fault as well as open-circuit faults have been considered.

CHAPTER 7 EXPERIMENTAL IMPLEMENTAION AND RESULTS

A single motor fault-tolerant drive system may be sufficient in many critical applications; it does not offer any redundancy if the motor drive system with a single motor module is out of operation. In order to provide redundancy, a dual fault-tolerant motor drive system has been proposed [12]. Most applications now use a microprocessor or a microcontroller using a digital modulation technique. The objective of Pulse-width modulation is to control the inverter output voltage and harmonics reduction. Disadvantages of PWM are an increase in switching losses due to high PWM frequency, reduction of available voltage and EMI problems due to high order harmonics. The harmonics of order three and multiples of three of voltage source inverter or six step voltage source inverter (“six step” because of the presence of six “steps” in the line to neutral (phase) voltage waveform) are absent from both line to line and line to neutral voltages and are consequently absent from the currents. The output amplitude of VSI in three-phase inverter can be controlled by only DC voltage. The field-oriented scheme is implemented on a control board consisting of a Texas Instrument TI C6713 processor and Actel ProAsic3 FPGAs. The PWM switching signals are transmitted to the gate drivers using high performance fiber optic links. The motor unit is fed from separate converter units. The rotor position is obtained from a resolver transducer. The 6-stator pole, 7-rotor pole flux-switching machine was constructed from 0.35mm silicone steel laminations and samarium cobalt permanent magnets. The machine was totally enclosed and naturally ventilated. This chapter presents a steady state and transit performance of a dual-fed FS-PMSM to verify the steady state performance of the machine unit and transit behaviour of the machine during both healthy- and faulty-operating conditions. In this Chapter torque compensation scheme has been proposed to improve the machine’s dynamic performance. In this Chapter also a single-phase short-circuit has been introduced.

CHAPTER 8 CONCLUSION AND FUTURE WORK

Summarizes the conclusions of the work and recommendations for future work.

2 POSITION CONTROL OF PM SYNCHRONOUS AC SERVOMOTOR BASED ON (FOC)

2.1 Concept and Operation Principles of PMSM

Synchronous machines have a three-phase stator structure that houses the armature windings. Most synchronous machines have either electromagnetic excitations or permanent magnets (PM) on their rotors. Larger synchronous motors usually have a symmetrical damper winding in order to reduce the effects of harmonics and negative sequence current components produced by the power converter; a damper winding (short-circuited windings which represent paths for induced rotor currents) also tends to lower the transient reactance of the machine and thus facilitates commutation. AC power is fed to the stator of the synchronous motor whilst the rotor winding is fed by DC voltage from a separate source and generates the magnetic field. The rotor can be designed either cylindrically (non-salient) or as a salient pole. More information can be found in [13]. In addition, cylindrical rotor synchronous motors have a uniform air-gap and a rotor flux distributed sinusoidally in space. This combines with the three-phase stator flux, which in the air-gap produces a sinusoidal pattern of mutual flux, resulting in a sinusoidal torque pattern [14]. However, the rotor magnetic field locks onto the stator rotating magnetic field and rotates at the same speed (rotor rotates synchronously with the rotating flux of the stator). The rotor speed is a function of the supply frequency and number of magnetic poles in the stator. The three-phase stator windings of a sinusoidal permanent magnet AC machine are placed on multiple slots of laminated core and electrically spaced 120^o, in order to approximate sinusoidal distribution.

PMSM have a polyphase winding in the stator that can be concentrated or distributed. The rotor has a steel core, with permanent magnets mounted on its surface or inset. Smaller motors, such as synchronous servomotors (see *Figure 2.4*) with a permanent magnet usually do not possess damper windings but, there is a slight electrical damping effect due to the eddy currents in the magnets; of course, all the mechanical damping of the drive can now be achieved by control. More details can be found in refs. [15]. Furthermore, the permanent magnet synchronous motor (PMSM) is used for the servo application; excitation is provided by a permanent magnet instead of a field-winding.

The PM material will affect directly the performance of the motor. As magnetic materials there are three classes of PMs currently used for electric motors:

- Alnicos (*Al, Ni, Co, Fe*). The main advantage of Alnico is its high magnetic remnant flux density and low temperature coefficients.
- Ceramics (*ferrites*), e.g., barium ferrite ($BaO\times6Fe_2O_3$) and strontium ($SrO\times6Fe_2O_3$) have lower costs, however they demagnetise easily. A ferrite material has a higher coercive force than Alnico, but at the same time has a lower remnant magnetic flux density. Temperature coefficients are relatively high.
- Rare-earth materials, i.e., samarium-cobalt (*SmCo*) and neodymium iron-boron (*NdFeB*). A detailed explanation can be found in [16]. Rare-earth materials have a high energy density and can lead to compact designs. On the other hand they feature high conductivity, which can cause high eddy current losses.

Alternatively, there exists mainly four types of implementation for mounting the magnets, which can either be:

- Surface-mounted PM ((*SPM*) $L_{sd} = L_{sq}$),

There's two ways to magnetize the magnet either radically or sometimes circumferentially. An external high conductivity non-ferromagnetic cylinder is sometimes used to protect the PMs against the demagnetizing action of armature reaction and centrifugal force. Furthermore, it provides an asynchronous starting torque, and acts as a damper. If rare-earth PMs are used, the synchronous reactance in the *d* and *q axis* are practically equal (small saliency) [16].

Moreover, the machine can be considered to have smoother air-gap flux density destitution with the surface-mounted magnets. This is due to the fact that the incremental permeability (μ_r =1=*permeability of the air*) of the magnets with regards to the external field is approximately unity. This machine also has high resistivity and thus the machine can be considered to have a large effective air gap, which makes the effect of saliency negligible (*d-axis* magnetizing inductance is equal to *q-axis* magnetizing inductance, $L_{md}=L_{mq}=L_m$). In addition, the synchronous inductance $L_s = L_{sl}$ *(Leakage inductance of armature winding per phase)*+L_m *(Magnetizing inductance armature reaction*) is small because of the large air-gap, thus an armature effect is negligible.

- surface inset PM ((*IPM*) $L_{sd} < L_{sq}$),

Surface inset PM is a salient pole machine which means that ($L_{sd} \neq L_{sq}$), thus both magnet and reluctance-torque are produced. Furthermore, the magnets (subpolar) are directly inset under the rotor surface.

The magnetic circuit of the rotor can be either laminated or made of solid steel. If a magnetic circuit of the rotor is laminated, a starting cage winding or external nonferromagnetic cylinder is required. On the other hand the *q-axis* synchronous reactance is greater than that in the *d-axis*, whereas, the back-EMF (electromotive force is the potential generated by a current carrying conductor when it is exposed to magnetic field, EMF is measured in volts) induced by the PMs is lower than that in surface PM rotors.

- Interior PM ($L_{sd} < L_{sq}$)

Magnetic permeability and reluctance are not constant. Both, the magnet torque (arises from the interaction of the rotor magnet flux and *q-axis* stator current component) and reluctance torque component (due to saliency (*variation of magnetic reluctance*)) are produced with Interior PM. Interior PM can be considered to have a uniform air-gap. The interior-magnet rotor is radically magnetized and has alternately poled magnets.

Three types of PM machine with buried interior PM exist and can be placed axially, radially, or inclined into the rotor. Due to a smaller magnet pole area at interior PM than the rotor surface, the air-gap flux density on the open-circuit is less than the flux density in the magnet. The magnetic circuit of interior PM significantly changes when the steel pole piece covers each magnet. Since the *q-axis* magnetic flux can pass through the steel pole pieces with crossing the PMs, the synchronous reactance in the *d-axis* is smaller than that in the *q-axis*. The magnet Interior PM Machines are well protected against centrifugal forces thus are recommended for high speed operation. Such a configuration is shown in adjacent *Figure 2.1.*

Figure 2.1 Interior permanent Magnet

(Source: R. Dutta, M. Rahman, "Design and Control of Interior Permanent Magnet Motor Drives," Uni. of New South Wales, Sydney 2052, Australia).

- buried inside the rotor

Next is the buried-magnet rotor which has circumferentially magnetized **PMs** embedded in deep slots. The synchronous reactance in the *q-axis* is greater than that in the *d-axis*. On the other hand, a starting asynchronous torque is produced with the aid of both a cage winding incorporated in slots in the rotor pole shoes (laminated core) and solid salient pole shoes made of mild steel. In addition, the width of the iron bridge between the inner ends of the neighbouring magnets has to be carefully chosen. However, when the magnets are buried inside the rotor (each magnet is covered by a steel pole piece), thus, high permeance paths are produced for the magnetic fluxes across these poles and also in space *quadrature* to the magnetic flux. Consequently, the effects of saliency arise.

More importantly is that PMAC machines with salient rotors can offer useful performance characteristics when excited with EMF, providing more flexibility for adopting a variety of rotor geometries and a variety of IPM or buried magnets as alternatives to the SPM design.

Due to their high power density and, consequently, the smaller size, permanent magnet synchronous motors have in recent years evolved as the preferred solution for positioning drives on machine tools and robots, where the motors are to be integrated into the mechanical load. The quality of servo is given by its time response and frequency bandwidth. Recently, faster response is becoming an increasingly common industrial requirement; therefore servo drive systems are continuously improve in performance. There are three major components of the PM-servomotor drive system which are PM-servomotor, power converter, and a controller. A controller compares the system reference with the system feedback and generates an error signal that represents the difference between the desired (*reference signal*) operating point and the actual system operating value. Some of the disciplines related to these components are electric machine design, electric machine modelling, sensing and measurement techniques, signal processing, power electronic design and electric machine control.

The control objectives are to have zero steady state error and good dynamic response (*fast, small overshoot*). Feedback control makes the system insensitive to disturbances and parameters variation. A Servomechanism is a feedback system consisting of a sensing element, amplifier, and servomotor, using an automatic control of a mechanical device [17]. It is an automatic device used to correct the performance of a mechanism by means of an error sensing negative feedback. A Servomechanism can be applied only to systems in which the mechanical position or one of its derivatives (*velocity, acceleration*) can be controlled by a feedback and error correction signals. AC servo is an electrical drive with a PMSM provided with a resolver, supplied by a voltage source inverter with PWM. The control structure of the servo consists of additional feedback: of the inner current closed loop, of a speed close loop and position close loop. This Chapter mainly focuses on position vector-control of the PM-servomotor. The proposed motor supplied by a voltage source inverter (VSI-PWM) with IGBTs (insulated gate bipolar transistors), which is controlled by a digital circuit is based on the stator current feedback information. In [18], IGBT transistors have high input resistance and require small control power because they are voltage controlled devices with small ON-state voltage drop, independent of the current. The DC link of the voltage source inverter must have negligible impedance (*near to the ideal voltage source*), which ensures the large capacitance. The three-phase inverters supplying voltages and currents of adjustable frequency and magnitude to the stator are an important element of adjustable speed drive systems employing servomotors (VSI-PWM and DSP implementation will be considered in more details in *Section 4.2*. The mathematical model of the PM-servomotor in *d-q axis* is briefly described.

2.2 Mathematical Model for PM Synchronous AC Servomotor (*d, q*)

A system mathematical model is one or more equations that describe the relationship between the system variables, often its inputs and outputs. For physical systems, these equations are derived from studying the physical properties of the system such as mechanics, fluids, electrical, thermodynamics, etc. To understand system performance, a mathematical model of the plant is required, which eventually enables the design control system to achieve a particular specification. The study of the control provides us with a process for analysing and understanding the behaviour of a system. This Chapter reviews the mathematical model of a permanent magnet servomotor using the *d-q axis*. The *d-q* model of the PM servomotor synchronous motor can be derived from the well-known model of the synchronous machine without the equations of the damper windings and field current dynamics removed. The *d-q* model of the PM-servomotor has been developed on a rotor reference frame; it is done by converting the three phase voltages and currents to *d-q* variables by using the Park's transformation. The mathematical model of PM-servomotor has been verified and designed in MATLAB-SIMULINK.

2.2.1 Park's Transformation and Dynamic *d-q* Modelling

Mathematical transformations are often used to decouple variables, to facilitate the solutions of difficult equations with time varying coefficients, or to refer all variables to a common reference frame [19] Park's transformation is a phase transformation (*coordinate transformation*) between the three-physical phases in a three-phase system (*see Figure 2.3*). This transformation is also known as the *d-q* transformation or Blondel's transformation. Further information can be found in refs [20]. In addition dynamic *d-q* modelling is used to study the motor during transient and steady-state conditions.

The phase quantities in the (*a, b, and c*) phases vary periodically in steady-state. Furthermore, the self- and mutual-inductances between stator circuits and rotor circuits will vary with the rotor position *Figure 2.2* shows the self-inductances of the stator windings as well as the mutual-inductances between the stator and rotor windings which are functions of the rotor angular position. However, in the model used herein, Park's transformation is applied to the stator variables (*voltage, current, flux linkage*), which replaces the variables associated with the stator windings with variables associated with fictitious windings that rotate with the rotor.

This change of variables has the effect of eliminating the angular position dependence of the inductances.

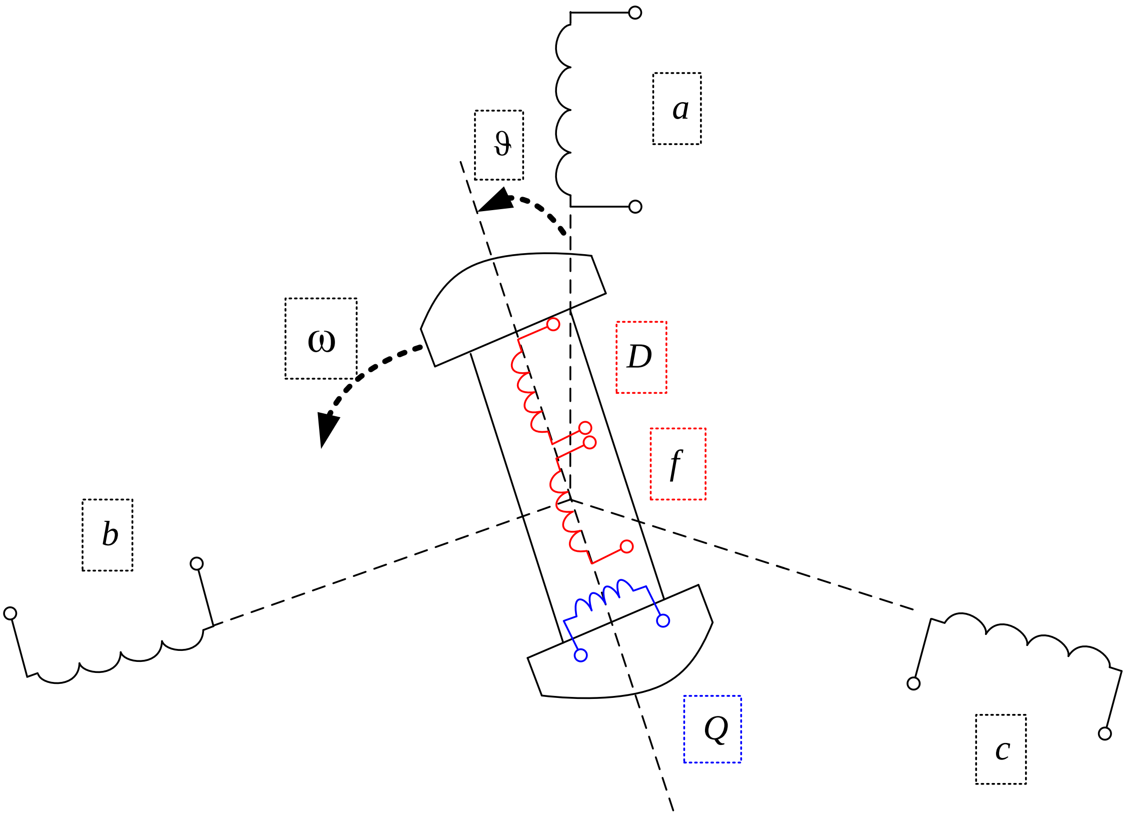

Figure 2.2 Definition of quantities in Park's transformation

According to *Figure 2.2* the salient rotor synchronous machine consist of six windings which are

- Three phase stator winding (*a*, *b*, *c*)
- Excitation winding in *d-axis* (*f*)
- Damper winding in *d-q axis* (*D*, *Q*)

Figure 2.3 shows *d-axis* space vector aligned with the direction of the rotor magnetization and the *q-axis* perpendicular to it.

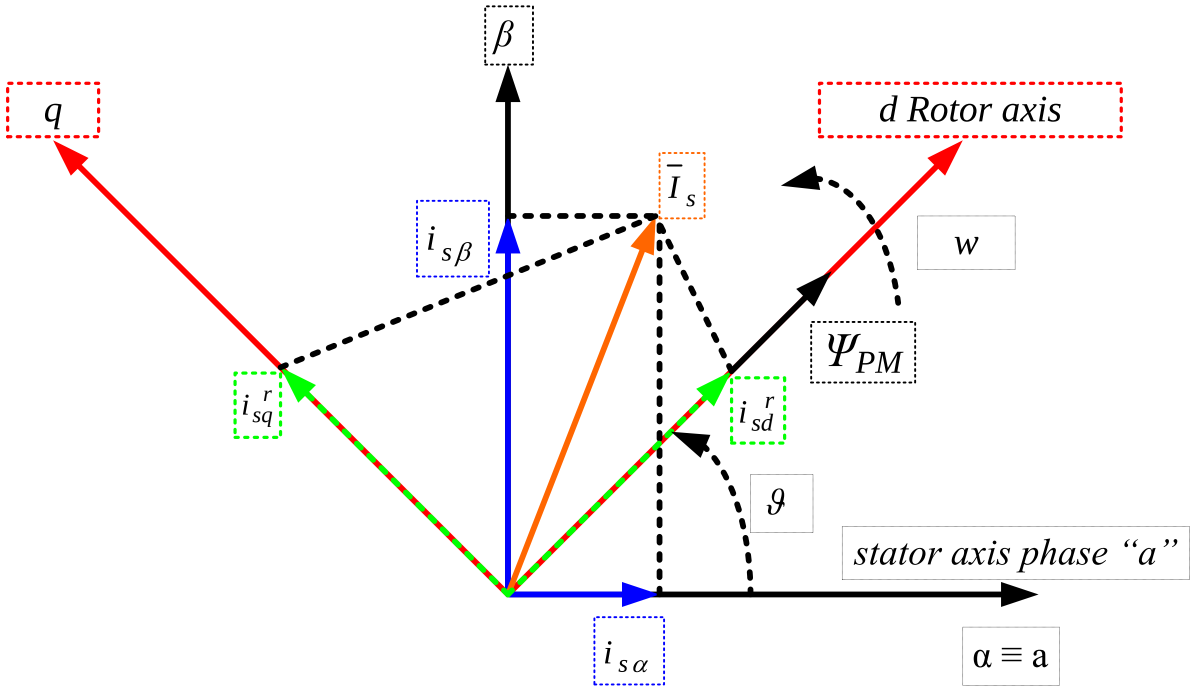

Figure 2.3 Stator current and magnet flux space vectors in the d-q rotating reference frame and its relationship with the α, β stationary reference frame

The selection of the *d-axis* leading the *q-axis* is purely arbitrary and is recommended, due to the *d-axis* current which usually causes demagnetization of the machine and should be negative in the generator reference frame. In this Park's transformation, however, assume the *d-axis* to lag the *q-axis* by (*90º*).

The transformation equation from (*a, b, c*) to (*d-q*) reference frame may be expressed as

$$\begin{bmatrix} i^r_{sd} \\ i^r_{sq} \end{bmatrix} = K \begin{bmatrix} \cos(\vartheta) & \cos\left(\vartheta - \frac{2}{3}\pi\right) & \cos\left(\vartheta + \frac{2}{3}\pi\right) \\ -\sin(\vartheta) & \cos\left(\vartheta - \frac{2}{3}\pi\right) & -\sin\left(\vartheta + \frac{2}{3}\pi\right) \end{bmatrix} \begin{bmatrix} i_a \\ i_b \\ i_c \end{bmatrix} \tag{2.1}$$

where:

$(^r)$	=	*superscript denotes to define variable in rotor reference frame.*
$\vartheta(t)$	=	*Instantaneous rotor angle [in rad]*
i^r_{sd}	=	*Direct axis of the stator current in rotor reference frame (Flux component) [in A]*

i^r_{sq}	=	*Quadrature axis of the stator current in rotor reference frame (Torque component) [in A]*
i_a i_b, i_c	=	*Instantaneous values of the stator currents in stator phases a, b, and c Respectively [in A]*
K	=	*2/3* (*transformation constant*).

The instantaneous rotor angle (ϑ *(t) electrical angular displacement*) of the rotor reference frame, between the *d-axis* of the speed of $\omega_r(t)$ (*electrical*) and *a-axis* of the stationary stator winding maybe expressed as follows:

$$\vartheta(t) = \int_0^t \omega_r\left(t\right)dt + \vartheta(0) \tag{2.2}$$

where,

$\omega_r(t)$	=	*Electrical angular velocity [in rad s^{-1}]*

The PM-servomotor requires continuous knowledge of the rotor position, i.e. of the magnetic flux position. Typical position sensors are resolvers, linear and shaft encoders (*rotary encoder*).

The inverse transformation is given by:

$$\begin{bmatrix} i_a \\ i_b \\ i_c \end{bmatrix} = \begin{bmatrix} \cos\left(\vartheta\right) & -\sin\left(\vartheta\right) \\ \cos\left(\vartheta - \frac{2}{3}\pi\right) & -\sin\left(\vartheta + \frac{2}{3}\pi\right) \\ \cos\left(\vartheta + \frac{2}{3}\pi\right) & -\sin\left(\vartheta + \frac{2}{3}\pi\right) \end{bmatrix} \begin{bmatrix} i^r_{sd} \\ i^r_{sq} \end{bmatrix} \tag{2.3}$$

By assuming a mathematical model of a PM-servomotor supplied from a symmetrical power supply consequently stator voltage and current sequence components can be omitted. Thus, the three-phase voltages and currents become

$$v_a + v_b + v_c = 0\,[V] \tag{2.4}$$

where,

v_a, v_b, v_c = *Instantaneous values of the stator voltages in phase a, b, and c Respectively [in V]*

Assume i_a, i_b, i_c are the instantaneous balanced three-phase currents:

$$i_a + i_b + i_c = 0\,[A] \tag{2.5}$$

The mathematical PM-servomotor is described by three differential equations, one for each winding. These differential equations are coupled to one another through the mutual inductance between the windings. Therefore, *d-q* can facilitate the computation of the transient solution of the servomotor model by transforming the differential equations with time varying inductances (*the equations depends on rotor position*) to differential equations with constant inductances (*inductance no longer depend on rotor position*).

2.2.2 Mathematical Model of PM Synchronous AC Servomotor

The *d-q* mathematical model of a synchronous servomotor with field and without damper windings in the rotor reference frame ($\omega_k = \omega_r = \omega_s$) can be derived in the same way as that of the permanent magnet synchronous motor and can be characterised by referring to *Equations (2.6) and (2.7)*

where

ω_k = *Angular velocity of the general reference frame [in rad s^{-1}]*

ω_s = *Angular velocity of the synchronous reference frame[rad s^{-1}]*

In [21], the proposed machine is of salient rotor design of synchronous machine. The damper winding voltage (u_D, u_Q) is equal to zero, because damper winding are short-circuited. Thus, $v_D = v_Q = 0$. The well-known voltage equations (*Electrical system equations*) of the machine for the three-phase stator winding in the rotor reference frame are as follows:

$$
\begin{aligned}
v_{sd}^{r} &= R_s i_{sd}^{r} + \frac{d\psi_{sd}^{r}}{dt} - \omega_r \psi_{sq}^{r} = R_s i_{sd}^{r} + L_d \frac{di_{sd}^{r}}{dt} - \omega_r \psi_{sq}^{r} = R_s i_{sd}^{r} + L_d \frac{di_{sd}^{r}}{dt} - \omega_r (L_q i_{sq}^{r}) \\
v_{sq}^{r} &= R_s i_{sq}^{r} + \frac{d\psi_{sq}^{r}}{dt} + \omega_r \psi_{sd}^{r} = R_s i_{sq}^{r} + L_q \frac{di_{sq}^{r}}{dt} + \omega_r \psi_{sd}^{r} = R_s i_{sq}^{r} + L_q \frac{di_{sq}^{r}}{dt} - \omega_r (L_d i_{sd}^{r} + \psi_f) \\
v_{s0}^{r} &= R_s i_{s0}^{r} + \frac{d\psi_{s0}^{r}}{dt} \\
v_f &= R_f i_f + \frac{d\psi_f}{dt}
\end{aligned}
\tag{2.6}
$$

where,

$v^r_{sd}, v^r_{sq}, v^r_{s0}$	=	*Instantaneous values of direct-, quadrature-, and zero - axis stator voltage Components respectively and expressed in the rotor reference frame [in V]*
v_f	=	*Excitation voltage applied to the rotor winding **f** [in V].*
$i^r_{sd}, i^r_{sq}, i^r_{s0}$	=	*Instantaneous values of direct-, quadrature-, and zero - axis stator current components respectively and expressed in the rotor reference fame [in A]*
i_f	=	*Excitation current in the rotor winding (Field-current)[in A]*
R_s, R_f	=	*Resistance of the stator (armature-resistance) and rotor winding (field-resistance), respectively [in Ω]*
$P=d/dt$	=	*deferential operator.*

The stator and rotor flux-linkages in *(2.6)* are related to the currents (*flux linkage current relations*) in the different windings with reference to the *d-q axis* and can be described as

$$
\begin{aligned}
\psi_{sd}^{r} &= L_d i_{sd}^{r} + L_{df} i_f = L_d i_{sd}^{r} + \psi_f \\
\psi_{sq}^{r} &= L_q i_{sq}^{r} \\
\psi_{s0}^{r} &= L_0 i_{s0}^{r} \\
\psi_f &= L_f i_f + L_{fd} i_{sd}^{r}
\end{aligned}
\tag{2.7}
$$

where,

$\Psi^r_{sd}, \Psi^r_{sq}, \Psi^r_{s0}$ = *Instantaneous values of direct-, quadrature-, and zero-axis stator flux linkages expressed in the rotor reference frame[in Wb]*

Ψ_f = *Rotor (Excitation) flux linkage [in Wb]*

L_{sd}, L_{sq}, L_0 = *Stator inductance in d,q,0 axis respectively [in H]*

L_f = *Excitation winding inductance [in H]*

L_{df} = *Mutual inductance between the armature- and field-winding [in H].*

According to the expression *(2.6) and (2.7)*, the mathematical model for a servomotor with constant PM flux linkage (Ψ_{PM}=const.) can be deduced and characterized as shown in *equations. (2.8) to (2.11).*

$$\frac{di^r_{sd}}{dt} = \frac{1}{L_d}\left[u^r_{sd} - R_s i^r_{sd} + \omega_r L_q i^r_{sq}\right] \tag{2.8}$$

where:

L_{sd} = *Inductance along the magnet axis [in H].*

$$\frac{di^r_{sq}}{dt} = \frac{1}{L_q}\left[u^r_{sq} - R_s i^r_{sq} - \omega_r (L_d i^r_{sd} + \psi_{PM})\right] \tag{2.9}$$

where:

L_{sq} = *Inductance along an axis in quadrature to the magnet axis [in H].*

The mechanical system equation (*motion equation*) represents the relationship between the differential equation of the electrical angular velocity and the torsional mechanical system this can be expressed as *(2.10).*

$$\frac{d\omega_r}{dt} = \frac{P}{J}\left[T_e - T_L\right] = \frac{1}{J}\left[\frac{3}{2}P\left(\psi_{PM} i^r_{sq}\right) - T_L\right] \tag{2.10}$$

where:

T_L	=	*load torque (required torque to drive the load referred to the motor shaft) applied [in Nm]*
J	=	*Total equivalent moment of inertia of the motor's rotor (in Kg m^2).*

It can be seen from *Equations (2.8) and (2.9)* that, the *d-q axis* voltage equations are coupled by the term $-\omega_r (L_{sq}\, i^r_{sq})$ and $\omega_r (L_{sd}\, i^r_{sd}+\Psi_f)$. These terms can be eliminated by the use of a decoupling circuit in the controller that utilizes nonlinear feedback of the coupling voltage. It requires accurate knowledge of inductances in the *d-q axis* ($L_{md} = L_{mq} = L_m$ (surface-mounted PM-servomotor)). Thus, the dynamics of the *d-q axis* currents can be represented by simple linear first order differential equations. Therefore it is possible to effectively control the current with a PI - controller. More details can be found in refs [22]. The expression for the generated electromagnetic (*driving*) torque by a servomotor can be written

$$
\begin{aligned}
T_e &= \frac{3}{2}P\left[\mathrm{Im}\left\{\overline{\psi}^*_s\, \overline{i}_s\right\}\right]=\frac{3}{2}P\left[\mathrm{Im}\left\{\left(\psi^r_{sd}-j\psi^r_{sq}\right)\left(i^r_{sd}+ji^r_{sq}\right)\right\}\right]=\frac{3}{2}P\left\{\psi^r_{sd}\, i^r_{sq}-\psi^r_{sq}\, i^r_{sd}\right\}\\
\overline{\psi}^*_s &= \left(\psi^r_{sd}-j\psi^r_{sq}\right)\\
\overline{i}_s &= \left(i_{sd}+ji_{sq}\right)
\end{aligned}
\tag{2.11}
$$

where

T_e	=	*Instantaneous value of Electromagnetic Torque developed by the motor [in Nm]*
P	=	*Number of poles*
(*)	=	*Superscript denotes the complex conjugate*
$\overline{i^r_s}$	=	*Space phasor of the stator currents expressed in the rotor reference frame [in A]*
ψ_s	=	*Stator flux linkage [in Wb]*

Substituting *Equations (2.7) into Equation (2.11)* yields the equation of developed Electromagnetic torque which can be rearranged to the form:

$$T_e = \frac{3}{2}P\Big[\Big(L_d\, i^r_{sd}\, i^r_{sq} + \psi_{PM}\, i^r_{sq} - L_q\, i^r_{sq}\, i^r_{sd}\Big)\Big] = \frac{3}{2}P\left[\underbrace{\Big(\psi_{PM}\, i^r_{sq}\Big)}_{\text{Magnetic torque}} + \underbrace{\Big(\big(L_d - L_q\big) i^r_{sd} i^r_{sq}\Big)}_{\text{Reluctance torque}}\right] \tag{2.12}$$

The first term of equation *(2.12)* is the mutual- reaction torque occurring between i^r_{sq} and the permanent magnet flux, and the second term corresponds to reluctance-torque due to reluctance variations (*difference in d and q reluctance or inductance*). The motor used in this thesis is a servomotor which means that $L_{sd}=L_{sq}=L_s$, due to the same reluctance paths in the rotor *d* and *q axis*, thus the reluctance-torque is equal to zero.

The mathematical model is quite significant for synthesizing the concept of field-oriented control. Vector control strategy uses the space vector model of the PM-servomotor to accurately control the speed and the torque in both steady state- and transient-operation. However, the *field-oriented control* method is one of the classes of vector-control strategies. Field-oriented control (*FOC*) has become widely used as a method of enabling the permanent magnet synchronous machine to realize a dynamic performance equal or superior to that of the DC machine. The concept of field-oriented control is to accomplish a decoupled control of torque and flux linkage magnitude. A detailed description about FOC will be given in *Section 4.3*. The *q-axis* stator current (*in the rotor reference frame*) can be obtained by considering the following transformation (*form of the stator current vector expressed in rotor reference frame*),

$$\overline{i^r_s} = i^r_{sd} + j i^r_{sq} \tag{2.13}$$

Likewise, the stator current vector expressed in the stator (*stationary*) reference fame is

$$\overline{i'^s_s} = i^s_{sD} + j i^s_{sQ} = \left|\overline{i'^s_s}\right| e^{j\beta_s} \tag{2.14}$$

where,

$\overline{i'^s_s}$ = *Space phasor of the stator currents expressed in the stationary reference frame [in A]*

i_{sD}, i_{sQ} = *instantaneous values of direct,- and quadrature axis stator current components respectively and expressed in stationary reference frame [in A]*

$\left|\overline{i'^{s}_{s}}\right|$ = *Stator current modulus [in A].*

β_s = *The angle of the stator current vector (with respect to the direct axis of the Stationary reference frame)[in rad].*

Space phasor of the stator $\overline{i^r_s}$ can be defined as

$$\overline{i^r_s} = i^r_{sd} + ji^r_{sq} = \left|\overline{i^r_s}\right| e^{i(\beta_s - \vartheta)} \tag{2.15}$$

Where,

$\left|\overline{i^r_s}\right|$ = *rotor current modulus [in A].*

The stator current vector $\overline{i^r_s}$ can be resolved into two components along the *d-q axis*.

$$\begin{bmatrix} i^r_{sd} \\ i^r_{sq} \end{bmatrix} = \left|\overline{i^r_s}\right| \begin{bmatrix} \cos(\beta_s - \vartheta) \\ \sin(\beta_s - \vartheta) \end{bmatrix} = \left|\overline{i^r_s}\right| \begin{bmatrix} \cos(\delta) \\ \sin(\delta) \end{bmatrix} \tag{2.16}$$

It should be noted that the *d-axis* current i^r_{sd} is referred to as flux producing current whilst the *q-axis* current i^r_{sq} which is perpendicular to i^r_{sd}, is the torque-producing current. However, FOC keeps the *direct* current at its rated value whilst controlling the *quadrature* current independently. Thus, a high performance drive can be realized with decoupled control of *direct* and *quadrature* currents.

A vector control AC servo below the rated speed is determined by the condition $i^r_{sd} = 0$ (assume no field-weakening range where the inverter voltage limit is reached, then $i^r_{sd} \neq 0$ (*negative*) and the torque angle $\delta > 90^o$). Then the *PM Synchronous AC Servomotor* stator vector is perpendicular to the rotor magnetization vector (*Motor currents are applied to the stator winding producing a stator vector, perpendicular to the rotor flux*). Hence, the *q-axis* stator current in the rotor reference frame is given as follows

$$i_{sq} = \left|\overline{i_s^r}\right| \sin\left(\beta_s - \vartheta\right) = \left|\overline{i_s^r}\right| \sin\left(\delta\right) \tag{2.17}$$

It can be noted from *(2.17)* that, for a fixed value of the current load (*torque*) angle *δ [in rad]*, the behaviour of the system is very similar to a DC machine and its steady state torque control principles are possible.

$$T_e = \frac{3}{2}\frac{P}{2}\left\{ \psi_{PM} \underbrace{\left|i_s^r\right| \sin\left(\delta\right)}_{i_{sq}^r} \right\} \tag{2.18}$$

Ψ_{PM}	=	*rms value of the magnitude of the field flux linkage of the permanent magnet in the air gap established by the permanent magnet [in Wb].*

The electromagnetic torque developed by the servomotor is proportional to i^r_{sq} (*assume no field-weakening*) *and* is usually expressed as a function of the angle *δ*. The maximum torque/ampere (*maximum torque per stator current*) is obtained when $\delta = 90^o$ (*the vector of the flux is perpendicular to the vector of the current*). The principle of the vector-control is that the stator current has to be driven so, that at every position of the rotor (position of the magnetic flux) is applied $\delta = 90^o$. Consequently, the Electromagnetic torque expression for *PM Synchronous AC Servomotor* can be simplified to (2.19)

$$T_e = \frac{3}{2}\frac{P}{2}\left\{ \psi_{PM} i_{sq}^r \right\} = K_t i_{sq}^r \tag{2.19}$$

where T_e is the electromagnetic torque of the motor, *P* is the number of poles of the motor and K_t is the torque constant of the PMSM

Equation (2.19) forms the basis of rotor oriented vector-control schemes, which use a position sensor. However due to rotor speed, ω_r, a voltage *E* (*back EMF*), is induced to the stator windings and can be determined as

$$E = j\omega_r \psi_{PM} \tag{2.20}$$

On the other hand, the parameter values of the *PM Synchronous AC Servomotor* used in Simulation is listed in

Table 2. 1

Parameters	Values
Continuous stall torque [in *Nm*]	7.5
Peak torque selection max [in *Nm*]	22.5
High inertia [in $kgcm^2$]	6.7
Standard inertia [in $kgcm^2$]	4.7
Standard motor weight [in *kg*]	8.3
Winding thermal time constant [in *s*]	22.1
Maximum torque pulsation [in *Nm*]	0.1
Parameters	**Values**
Rated speed [in *rpm*]	3000
Rated torque [in *Nm*]	6.8
Rated current [in *A*]	4.7
Rated power [in *kW*]	2.14
Number of pole-pairs [-]	3
R (ph-ph) [in Ω]	2.50
L (ph-ph) [in *mH*]	10.9
Ψ_{PM} [in Wb]	0.26

Table 2. 1 PM Synchronous AC Servomotor-UNIMOTOR UM-95UMD300CACAA

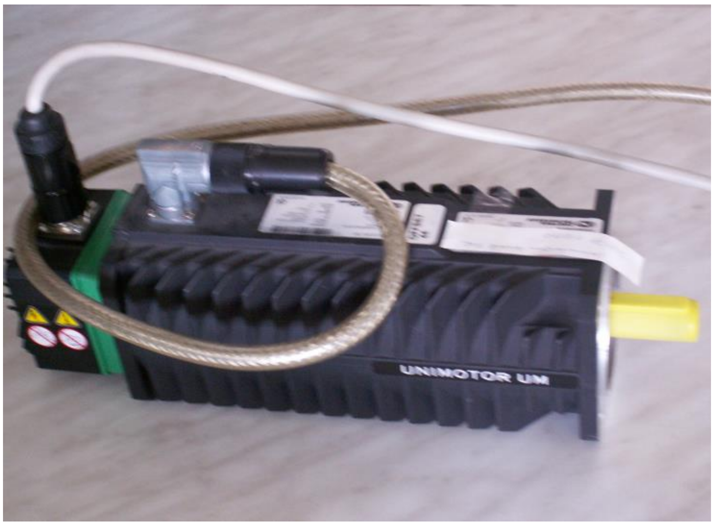

Figure 2.4 PM Synchronous AC Servomotor-UNIMOTOR UM-95UMD300CACAA

2.3 Controller Design

Feedback is both a mechanical, process and a signal mediated response that is looped back to control the system within itself. This loop is called the feedback loop. A control system usually has input and output to the system, when the output of the system is fed back into the system as part of its input, it is called the "feedback". Cascade control is used to enable a process having multiple lags to be controlled with the fastest possible response to process disturbances including set point changes. Cascade control is widely used within industrial processes. Conventional cascade schemes have two distinct features with two nested feedback control loops, there is a secondary control loop located inside a primary control loop. The primary loop controller is used to calculate the set-point for the inner (secondary) control loop. The inner loop (secondary, slave loop) in a cascade control strategy should be tuned before the outer look (primary, master loop). After the inner loop is tuned and closed, the outer loop should be tuned using knowledge of the dynamics of the inner loop. The most common use of cascaded control structure is: Inner current closed loop followed by the speed loop and the outermost position loop superimposed on the speed loop. Many systems require nested control loops to control several variables. The most used methods for controller design are (*OM-Optimal magnitude design method*), and (*SO-Symmetrical optimum method*). When designing the control parameters, it is necessary to proceed from the inmost loop (*current or torque*) through the nested loop (*speed control*) to the outer loop (*position*). A detailed description of controller design is found in refs [23].

2.3.1 Closed Loop Current-Control

Closed loop current control gives the permanent magnet servo drive the ability to change the current and torque produced by the motor very rapidly. The current-controllers are inner closed loops for the speed-controller. The current-control loop was designed according to the optimal magnitude (*OM*) criterion. Hence maximal overshoot of the current is 4.3%. The transfer function for the controller designed by the optimal magnitude method is:

$$F_{Ri}(p) = \frac{\left(1+\tau_i p\right)}{\tau_0} = \frac{\left(1+0.00436p\right)}{0.048p} \tag{2.21}$$

Transfer function of designed controller is usually the PI type.

2.3.2 Closed Loop Speed-Control

The outer speed control loop was designed according to the symmetrical optimum (SO) criterion. Hence rise time is equal to $0.75\tau_1$. Transfer function for the controller designed by the symmetrical optimum method is:

$$F_{R\omega} = \frac{\left(1+\tau_1 p\right)}{\tau_0} = \frac{\left(1+0.0056p\right)}{0.039409p} \tag{2.22}$$

The transfer function of the designed controller is the PI type. In current (torque) and speed loops, proportional control without integral control input leads to steady-state error. The actual value of the speed-feedback can be obtained as a time derivation of the position. On the other hand, the difference between the actual and set speed is known as the speed error. The task of the speed-controller is to keep the speed error as small as possible, preferably equal to zero.

2.3.3 Closed Loop Position-Control

Industrial motion-control systems utilise the electromagnetic torque or force generated by servomotors in order to effectuate controlled motion of work pieced, tools, or machine parts [24]. The relationship between the mechanical aspects of the complete system and the motor drive needs to be fully understood. Even with the best control system and algorithms available, it will not perform to the specification if the load cannot be accelerated or decelerated to the correct speed within the required time and if that speed cannot be held to the required accuracy (follow the required motion within the allowable error). More details can be found in refs [19].

According to the position sensor location, the position measuring principles can be grouped into indirect (see *Figure 2.5*) and direct position measuring (see *Figure 2.6*). Indirect measuring has the rotary position sensor in the motor shaft. The advantage of indirect measuring is that the non-linearity of the mechanical gears is outside the closed loop position, which has a positive impact on its quality and it makes it easier to set up. The position sensor of direct measuring can be either linear (*when resulting motion is linear*) or rotary (*when resulting motion is rotational*) position sensors. Non-linearity of the mechanical transmission in this case is inside the closed loop position (*remotely mounted on the load itself*), therefore, precision position control is comparing to indirect measuring. However difficulties arise when setting up dynamics.

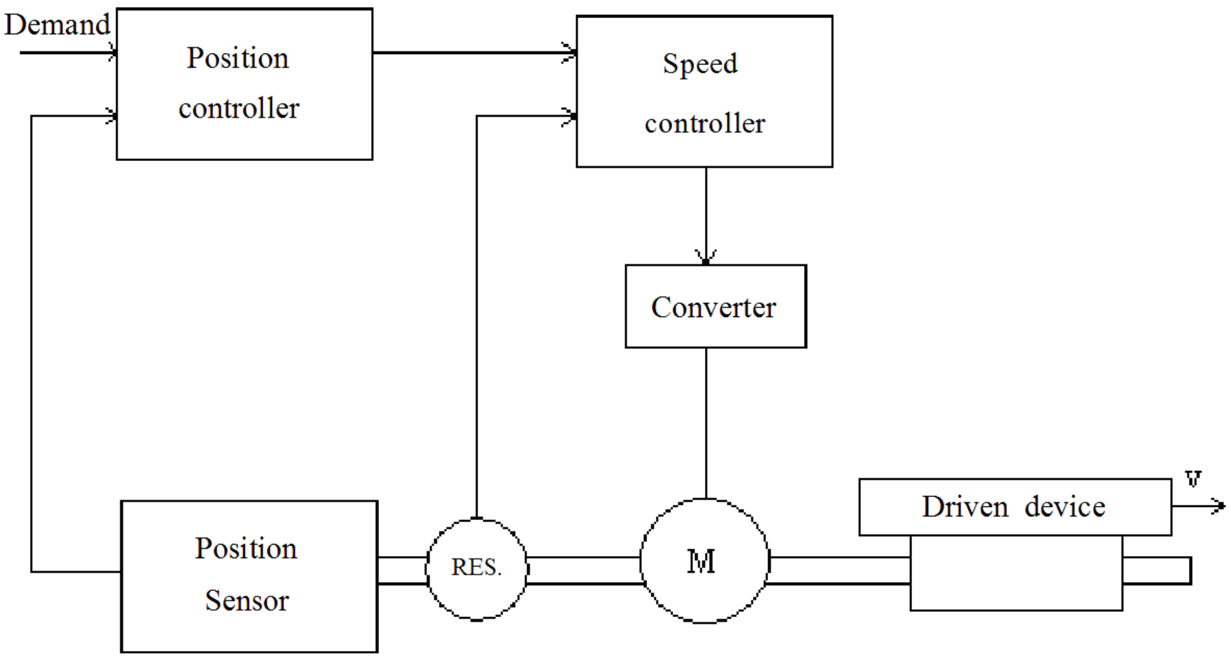

Figure 2.5 Block diagram of indirect position measuring

Figure 2.5 presents the block diagram of the Electric Motion Control of a PM-servomotor which consists of a number of elements. The main purpose is to minimize the error between the actual speed, position and their demand. On this basis, an outer servo loop maintains the demanded position with a displacement measuring sensor, whilst the inner speed loop with a motor mounted encoder (*or other speed sensing device*) precisely controls the motor speeds. Moreover an inner current loop can precisely control the motor currents (*both field and torque producing*)

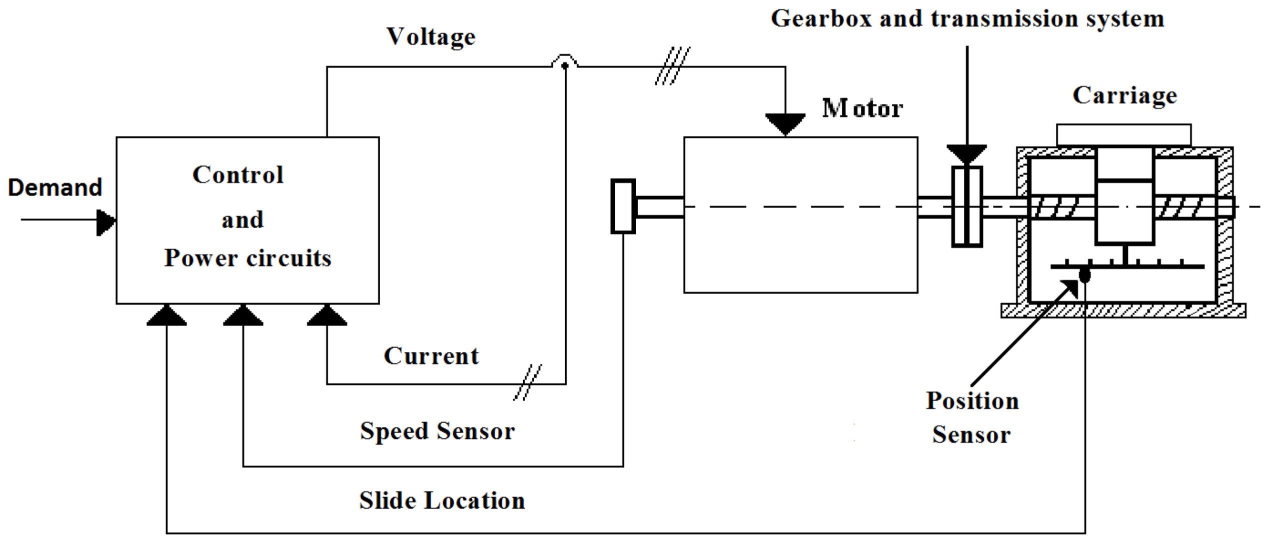

Figure 2.6 Block diagram of an advanced electric motion control system

(The output carriage is connected to the ball screws nut)

The servomotor drives the ball screw directly, whilst the ball nut (*see Figure 2.6 and Figure 2.7*) Controls the direction of motion depending on the direction of motor rotation. Moreover the rotary motion of the motor is converted to linear motion of a ball nut which pushes on the compression springs that transfer forces to the load. In addition, the calculation of the force on the load can be done by measuring the compression of the spring which can be provided by position transducers.

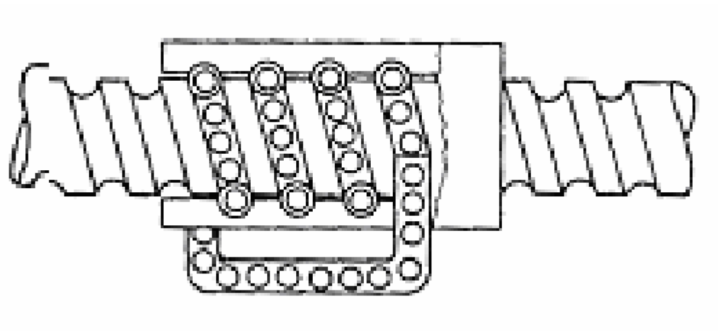

Figure 2.7 The cross section of ball screws, the circling balls are clearly visible

In order to optimize the performance of the complete system, the characteristics of these elements must be carefully determined. On the other hand a motion control system consists of five elements:

- The current controller, and motor
- Position or Speed controller (*control speed and position of one or a number of axes, either individually or when undertaking a coordinating move*). Motion controllers are able to implement the main control algorithms and provide the interface between the motion control system, the main control system, and/or the user.
- In order to provide feedback of the load's position and speed to the controller, the encoders and transducers are required
- The task of the transmission system is to take the motor output, undertake the required speed changes, and, if required, enable a rotary to linear translation
- Due to the load **(***Driven elements greatly influences the operation of the complete system*), a number of parameters including moment of inertia, external loads and friction can vary as a function of time, therefore it should be fully determined at the start of the design process. More details can be found in refs [25]

For Successful implementation of a motor drive system, some requirements need to be considered:

I. System Integration (*cooling, compatibility with existing system, bearing and couplings, mechanical fittings*)

II. Load (*motion profile, dynamic response, external forces, acceleration and deceleration, maximum speed*)

III. Environmental factors (*climatic and humidity ranges, electromagnetic compatibility (EMC), electrical supply specifications and compatibility, safety and risk*)

IV. Life Cycle Costs (*initial, operational, maintenance, and disposal costs*)

The position controller is derived from the transfer function of a closed speed loop. Proportional gain is given as a proportion of angular speed ω_r and angular position difference between desired (ϑ^*) and actual (ϑ) value of angular position.

$$k_v = \frac{\omega_r{}^*}{\underbrace{\vartheta^* - \vartheta}_{Rotary\,motion}} = \frac{v^*}{\underbrace{x^* - x}_{Linear\,motion}} = \frac{\omega_r}{\Delta\vartheta} = \frac{v}{\Delta x} \tag{2.23}$$

Where:

k_v	=	*Gain of the position controller*
ω_r*	=	*Reference value of electrical angular velocity [rad/s]*
ϑ*	=	*Reference value of electrical angular displacement (rotor angle)[rad]*
ϑ	=	*Actual value of electrical angular displacement (rotor angle)[rad]*
v*	=	*Reference value of linear velocity (shows how fast an object is moving in a straight line in particular direction)[km/hr or m/s or mph (miles per hour)]*
x*	=	*Reference value of position [km or m or miles]*
x	=	*Actual value of position [km or m or miles]*

For Position-controller design, the position gain is chosen to have a periodic step response to reach the reference in the shortest possible time without any overshoot (*Critically damped (ζ= 1)*)

2.3.4 Backlash with Direct/Indirect Position Control

The use of gears in power transmission, instrumentation, and as an integral part of position devices has become almost ubiquitous. Consequently, any faults in gear transmission severely affect the performance of such systems. These faults can be diverse and, depending on the situation, can affect the performance of the system considerably. Common examples of such faults are broken gear teeth, backlash between the teeth, interference between the teeth, and eccentric mounting of mating gears. Almost all gear transmissions require some clearance, called backlash to accommodate thermal expansion and avoid permanent friction on both the leading and trailing flanks of the teeth. Backlash may tend to zero in the case of a gear pump, for example, or may be extremely high in the case of heavy load transmissions subject to shocks and vibration. So, the amount of backlash as such is no criterion for gear quality. In marine transmissions, a certain amount of backlash is required to ensure trouble free operation of the transmission, though it should be kept small enough to reduce noise. A detailed explanation of direct/indirect position-control is found in refs [26]. A block diagram description of backlash is shown in *Figure 2.8.*

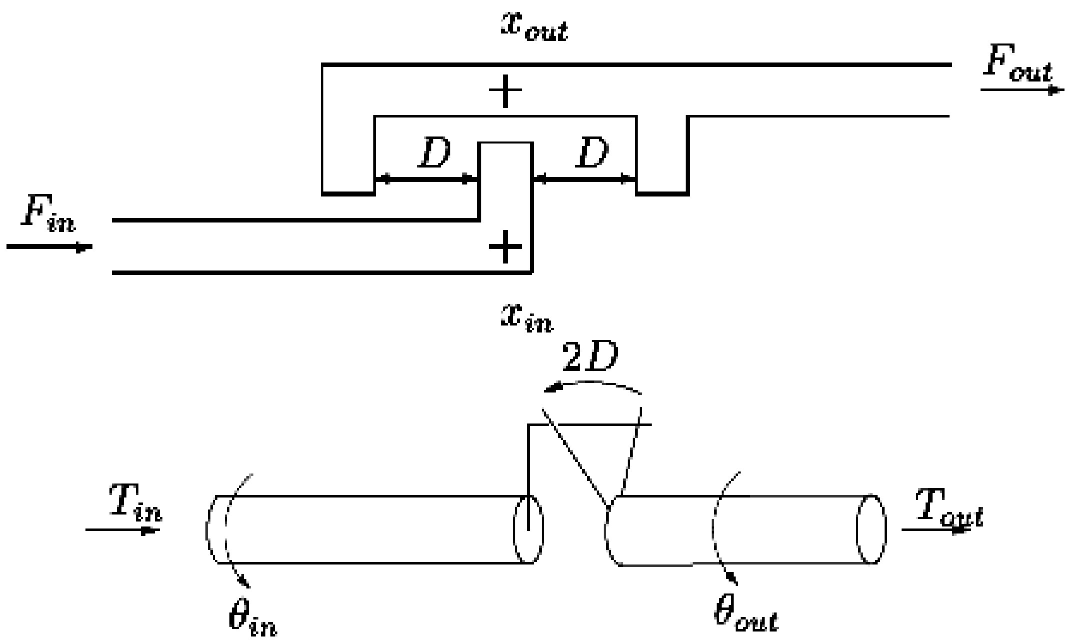

Figure 2.8 Linear and angular backlash

2.4 Simulation Results

The servomotor drives with a close-loop current giving the drive the ability to change the current (torque). *Figure 2.9* shows that the control loop of each motor is designed by two PI (PI-controller is provided for each *axis* of the reference frame) control technique. These reference currents (i^{r*}_{sd} , i^{r*}_{sq}) are compared to the actual transformed currents (i^{r}_{sd} , i^{r}_{sq}) to generate the output controlled voltages. (v^{r}_{sd} , v^{r}_{sq}) for the pulse wide modulation (PWM). Thus, the servomotor can be driven by the output voltages of the VSI. Since the flux is provided by the magnets on the rotor, the reference for the *d-axis* (flux producing current) is zero ($i^{r*}_{sd}=0$), because the flux is provided by the flux on the rotor. The reference in *q-axis* is defined as the torque-producing current (*torque produced by the motor*). In conclusion, the component of stator reference currents $i^{r*}_{sd} =0$ are constant whilst the components i^{r*}_{sq} are obtained from the speed controller. In addition the currents and voltages are D.C quantities in the-steady state, high dynamic performance is still required so that the phase delay of the current controllers is as small as possible and the effect on the outer speed controller is minimised.

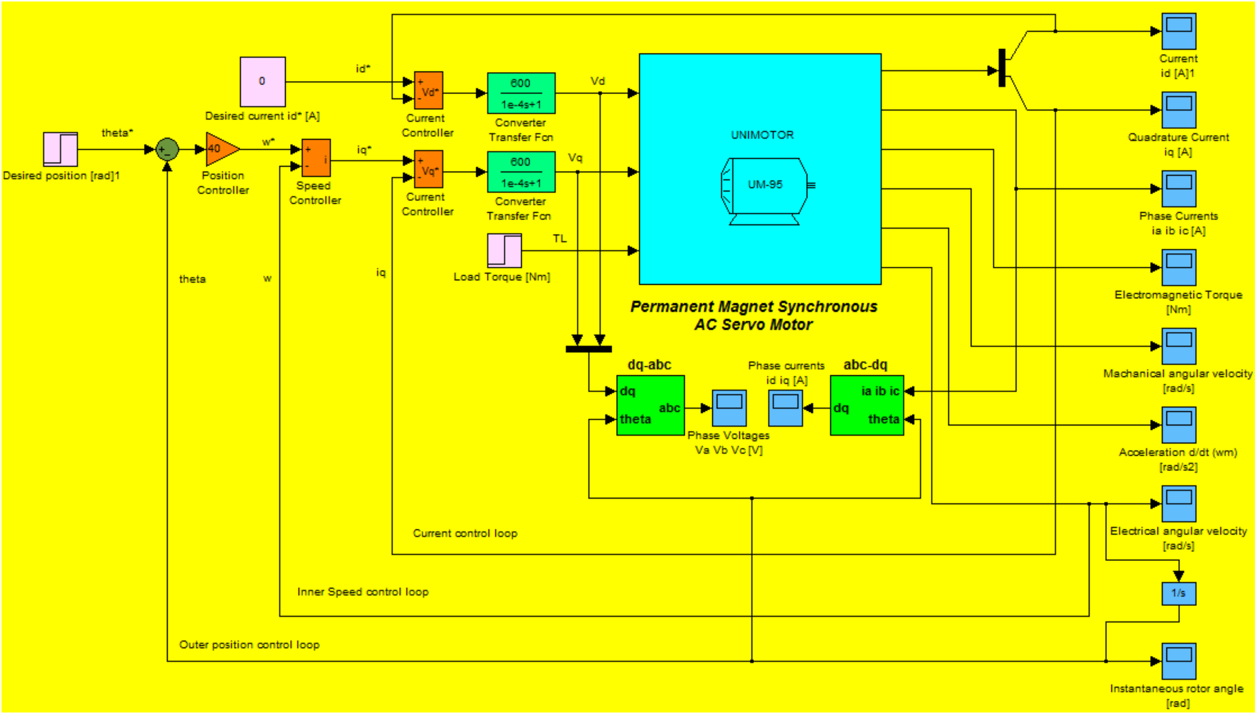

Figure 2.9 Block diagram of the position-controlled PM AC Servomotor

It can be noted that the speed of the servomotor shaft is measured and compared with a speed reference (from a sensor which is set in the motor rotation *axis*) to give speed error. Thus, the error will be modified by the speed controller (*PI*) to give a current reference i_q^* (i^{r*}_{sq}) Subsequently, it can be assumed that the motor current can be controlled to give a torque, which is proportional to the current reference. If any torque is required to hold the motor speed, the speed error must have a zero value (*non-static error at steady state*)**.** The *PI* controller has no speed error at steady-state even when torque is required to drive the load at the reference speed. When the motor speed varies from the reference level, a speed reference error is produced and hence the torque applied to the load is modified to bring the speed back to the reference level. *PI*-controller accumulates any speed error over time and builds up a current reference (*torque reference*) to provide the necessary torque for the motor system drive.

The position controller has been designed and chosen to have a periodic step response. The input reference for the controller is the imposed rotor position ($\vartheta*$), and the output is the reference value of electrical angular velocity. Furthermore, depending on the application and performance desired by the motor a position sensor with the required accuracy can be selected.

The proposed position control is tested on a *2.4kW PM Synchronous AC Servomotor in*

Table 2. 1 using ***MATLAB-SIMULINK***.

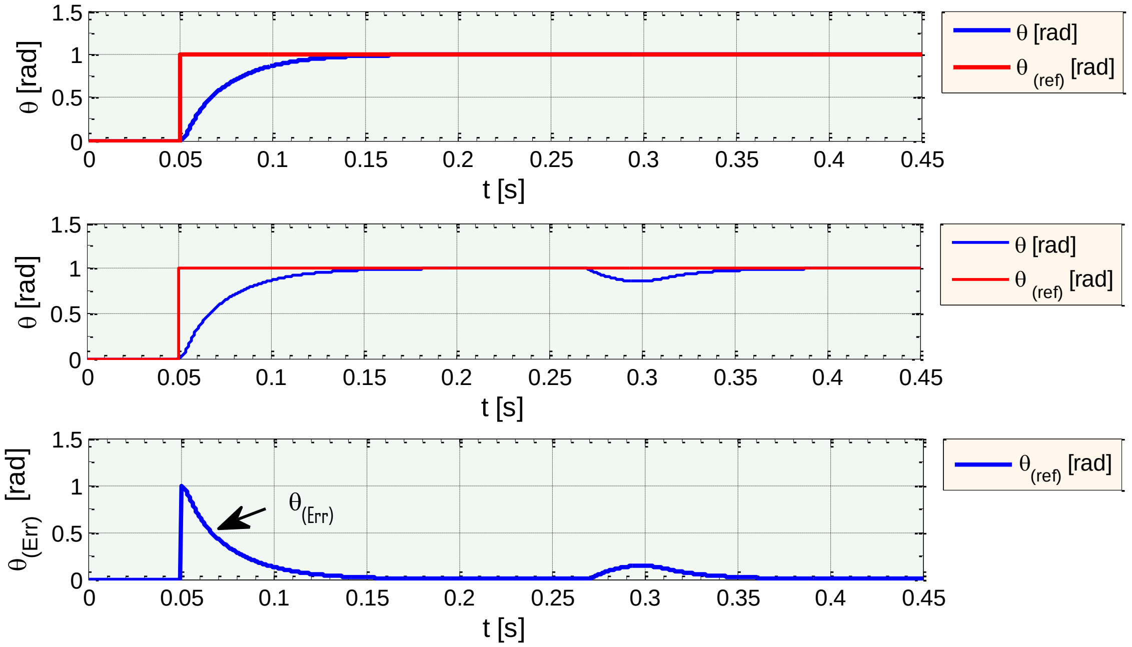

Figure 2.10 Actual and its reference rotor angular displacement ($\theta = \vartheta$) under load/no-load and the error between them

Figure 2.10 above, shows the actual (*blue line*) and the reference (*red line*) angular displacement at *load/no-load* step response and the error between them. Simulation results under load conditions considered to be of more practical interest are presented here. A load torque of T_L*=2.3Nm* is applied at *0.27s*, the compensation of it is clearly evident from the angular displacement between the actual and reference rotor angular displacement after this load torque is applied. It can be seen that the controller can effectively recover position back to the reference level at steady state. Additionally, the error between the actual and reference value under load conditions can be seen. This clearly shows that the actual value follows the reference value fairly closely.

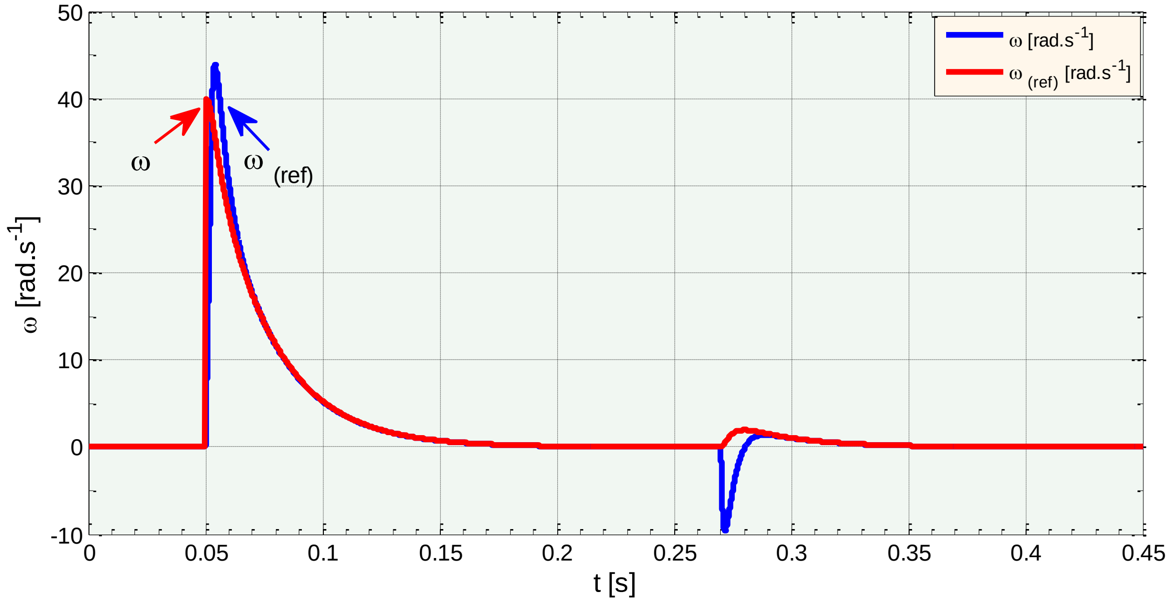

Figure 2.11 Actual and reference rotor angular velocity ($\omega = \omega_r$) step response

Figure 2.11 shows the actual and reference angular velocity response of the proposed control scheme under load conditions. At *0.05s*, when the rotor position is required to be controlled at *1 [rad]*, the motor speed increases from standstill to approximately *44 [rads^{-1}]*. After that the speed decreases slowly to maintain the actual position at the same level as the reference position.

At *t=0.27s* the load-torque is applied to the system, the motor speed drops from the reference value and then recover back to the reference value at steady-state.

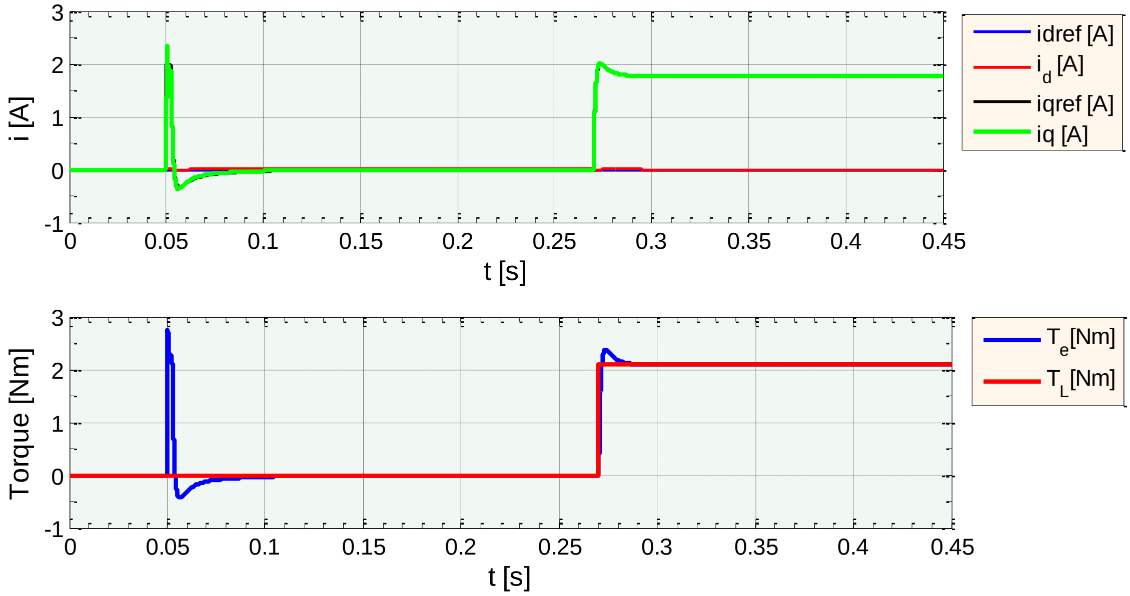

Figure 2.12 Load and electromagnetic torque and stator current components

As can be seen from *Figure 2.12* the current component $i^r_{sd}(t)$ is kept to zero in the steady-state and in the transient-state of operation this is also the case for any load condition, as required for the vector-control of *PM Synchronous AC Servomotor* up to nominal speed. The variation of $i^r_{sq}(t)$ is proportional to the variation in instantaneous load-torque. This ensures the fast dynamics response of the motor to the change in load. The initial positive and negative $i^r_{sq}(t)$ current component producing acceleration and deceleration torque $T_{el}(t)$, which counteracts the load-torque T_L. Electromagnetic torque changes at *0.27s* in response to the variation in the load-torque. The increase of $i^r_{sq}(t)$at $t=0.27s$ is required to counteract the applied load-torque.

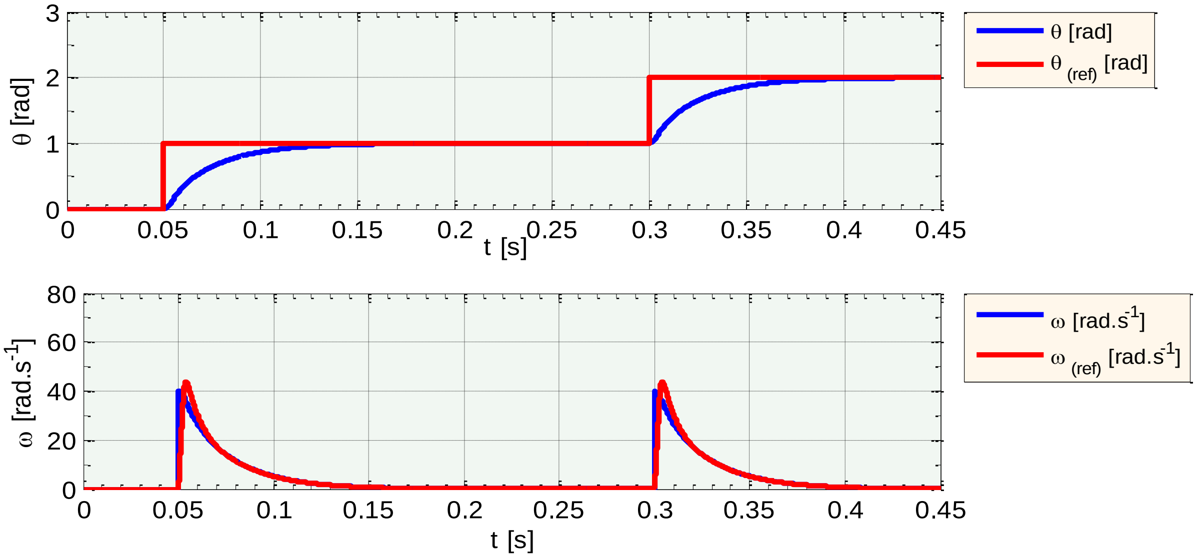

Figure 2.13 Position ($\theta = \vartheta$) and electrical angular velocity ($\omega = \omega_r$) step response with varying position reference

Figure 2.13 shows the reference and actual position and angular velocity with varying position reference at 0.3s from *1 to 2 rads*$^{-1}$. The actual position properly follows the reference position.

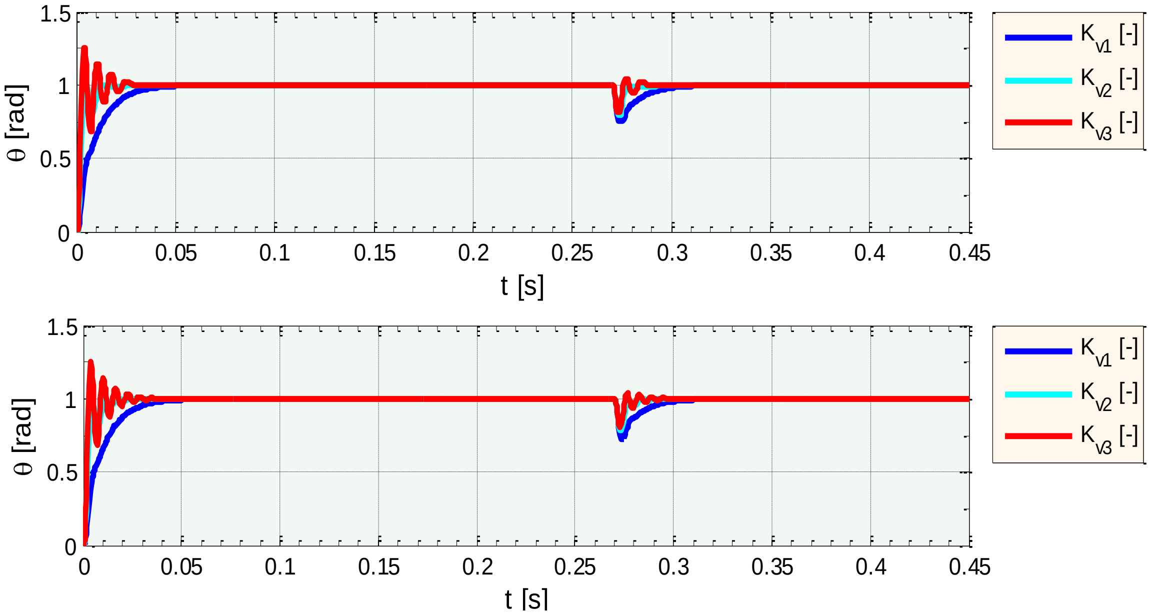

Figure 2.14 Actual rotor angular displacement under load/no-load, with/without backlash and with different proportional gain values (K_v)

Figure 2.14 shows the actual angular displacement step response with/without backlash using different proportional controller gain values. This was accomplished by varying the proportional gain (K_{v1} =20, K_{v2} = 60, k_{v3} = 90). It is apparent that as the proportional gain value is increased the system fluctuates more when reaching steady-state. Also the amplitude of these fluctuations is higher with increasing gain values, and the system reaches steady-state more slowly. However, when compared to a simple proportional control with gain value K_v = 20, the-steady state is more stable. Load-torque is applied at *0.27*s. It can be clearly seen that the controller can recover the position back to the reference level at steady-state.

2.5 Summary

Permanent Magnet-servomotor drives are widely used in Machine-tool, robotic, and other high performance applications due to their broad range of characteristics such as high speed-to-torque ratio, high system reliability, high power-to-weight ratio, four quadrant capability and an ability to produce torque at standstill. This chapter has briefly reviewed the current (fastest), speed (slower), and position (slowest) control loop of the PM-servomotor with high performance using the indirect rotor-oriented vector-control scheme. Position tracking precision, accuracy and rapidity are the standards to measure the performance of the servos system. The vector-control of the AC servo PMSM is derived from the rotor position because the flux complies with the position of the permanent magnet on the rotor. The indirect vector control requires a position sensor on the motor-shaft, which may be applied for a position feedback control. It has clearly emphasized that the satisfactory system performance depends on all the components and its associated controllers in the motor drive system, particularly, depends on its ability to provide the required speed and torque performance. Detailed MATLAB simulations results prove that the drive system operates without significant speed oscillations and with good dynamic performance and high positioning precision of the motor. This work also concentrates on the detection of backlash between mating gear teeth, for two reasons. First, it is the most common fault found in any geared systems; although some backlash is essential for any gear transmission, less than the appropriate amount results in interference between the teeth whereas excess backlash introduces looseness into the system. In either case, the result is poor performance and possible damage to the system. Second, the effect of backlash is most conspicuous when the system is subjected to non-continuous motion with frequent reversal of the direction of rotation. Mechanisms that fall into this category include robotic manipulators which have become an integral part of manufacturing automation. As the use of robotic manipulators increases, the detection of faults which can severely reduce their performance becomes increasingly important.

3 FLUX-SWITCHING PERMANENT MAGNET SYNCHRONOUS MACHINE

3.1 Introduction

Flux-switching machines can be seen as very similar, in terms of machine terminal behaviour, to PM machines as described in *section 2.1* . Having their magnets embedded in the stator will reduce the copper area available for the winding; however, as the magnets are in a flux-focusing arrangement, a relatively good torque density can be achieved. Fault-tolerant PM machines are also often limited by the maximum magnet temperature limit. This is presented in refs. [7]. Concentrated fractional pitch machines display a harmonic rich armature field which can induce substantial losses in the magnets themselves and any other rotor conducting components, particularly retaining cans. Although rotor losses are typically much lower than the stator losses, their thermal path has a much higher thermal resistance to the cooling surface, thus limiting the maximum torque achieved. This problem is generally exacerbated when a fault occurs and a fault-tolerant control is applied [27]. Although the fundamental synchronous rotating armature field is generally restored when a fault-tolerant control strategy is applied, the harmonic content of the armature field, particularly the triplen harmonics, increases the rotor losses significantly. These losses can quickly translate in high magnet temperature due to the high thermal resistance air-gap. This limits the allowed armature reaction field and consequently the torque. Flux-switching machines have an important advantage in such situations in that the magnets have a much improved thermal path to the machine housing, and rotor magnet retention is of course not needed, thus significantly reducing the overall losses and this constraint.

3.2 Concept and operation principles of FS-PMSM

Flux-switching machines have numerous inherent advantages for achieving high power density as discussed in the introductory section; however, in their basic form, they are not tolerant to short-circuit winding failures. In [28] and [29], a new design concept was introduced, which is able to make the machine fulfil the fault-tolerant requirements. In [30] and [31], a similar concept is adopted for a 12-slot-14-pole machine. Depending on the stator slot-rotor pole combination, flux-switching machines offer various possibilities to achieve a dual three-phase channel winding

[32]. For the flux-switching machine under consideration, a channel split described in *Figure 3.1* is considered [29]. The most popular slot-pole combination are 12slots-10 poles and 12slots-14poles derived from the “minimal” combination of six slots-five poles and six slots-seven poles, respectively [33]. In [34], it has been shown that the six-slot-seven-pole-based combination has a higher torque density than the more popular six-slot-five-pole configuration. Due to this and to use a reasonable electrical frequency at the relatively high speed of 7600 r/min, the chosen machine has seven rotor poles. This is equivalent to seven pole pairs for PM synchronous machines. In [35] and [36]. The control of a 12slot-10-pole flux-switching machine is considered. The control adopted is based on hysteresis current controllers, and the authors have investigated the operation of the machine from a dual three-phase converter unit under open-circuit faults. The work done in this thesis will mainly look at a machine operation with short-circuit faults which is fed by an SV-PWM control.

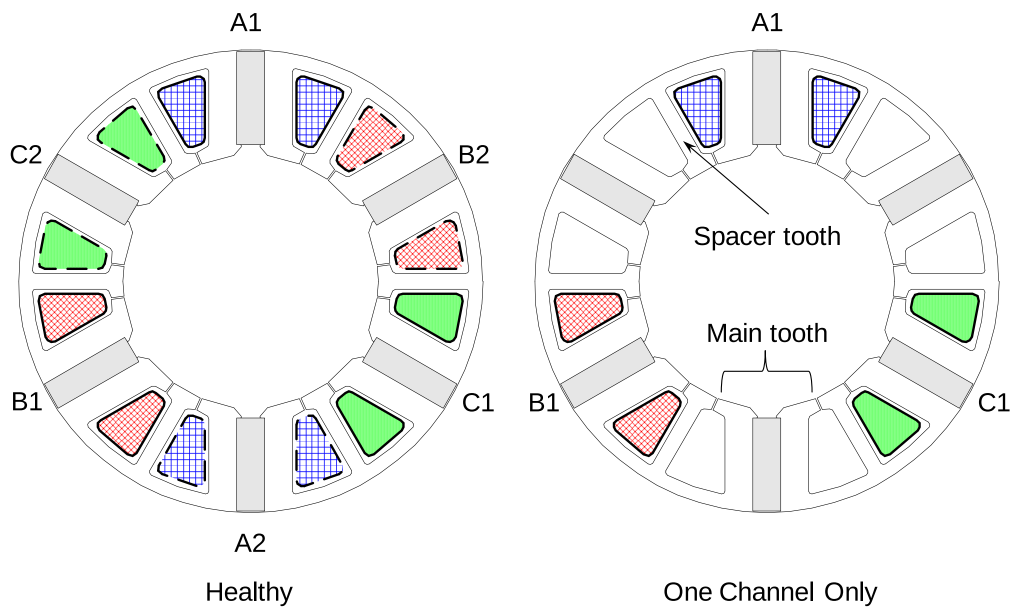

Figure 3.1 Channel split configuration of the dual channel FS-PMSM

In the event of a winding short-circuit fault due to device or winding failure, the fault current should be limited to a safe level to preserve the machine integrity. One per unit (p.u.) phase self-inductance is commonly adopted in order to limit the short-circuit current to the rated value [37], [38]. This is based on the nominal voltage, rated power, and nominal operating frequency. As discussed, another requirement is that any faulty part of the machine does not significantly influence the remaining healthy part. Winding layouts such as single-layer technologies can be used to meet these requirements [29]. In this thesis, the machine adopted uses a semi-closed slot configuration with spacer teeth to achieve 1-p.u. self-inductance as well as excellent magnetic and physical decoupling between any two coils as shown in *Figure 3.1*. The main aims of the spacer tooth, as it is in alternate concentrated-wound PM machines, are thus to minimize mutual inductance and to rule out the possibility of phase-phase faults within the machine as well as to limit failure propagation through thermal means.

The spacer-teeth thickness and the slot opening geometry are sized to meet the fault-tolerant requirements of minimal mutual-phase coupling and unity p.u. self-inductance as described in [29].

When compared to a machine of the same size but not designed to be fault-tolerant, the machine earlier produces a lower torque and has a lower factor due to the higher leaking paths. This is the same as for PM synchronous machines.

3.3 Mathematical Model for FS-PMSM (a, b, c)

The mathematical model of a dual three-phase flux-switching permanent magnet motor can be derived in the same way as that of a permanent magnet synchronous machine. A model of the machine was adopted to enable drive simulation in both healthy- and faulty- conditions. Mathematical model (a_1, b_1, c_1) and (a_2, b_2, c_2) of the dual three-phase flux-switching PM synchronous machine (FS-PMSM) will be briefly described in this section.

The phase voltages supplied to the stator windings (a_1, b_1, c_1) of the first three-phase star-connected winding set can be expressed in (3.1) to (3.3).

$$v_{a1} = r_s i_{a1} + \frac{d\psi_{a1}}{dt} \tag{3.1}$$

$$v_{b1} = r_s i_{b1} + \frac{d\psi_{b1}}{dt} \tag{3.2}$$

$$v_{c1} = r_s i_{c1} + \frac{d\psi_{c1}}{dt} \tag{3.3}$$

where i_{a1}, i_{b1}, and i_{c1} are the phase currents in the stator windings *[in A]*; is the phase resistance r_s *[in Ω]*; while ψ_{a1}, ψ_{b1}, and ψ_{c1} are the stator flux linkages of the first machine unit *[in Wb]*. Similarly, for the second winding set (a_2, b_2, c_2), the equations earlier can be rewritten with a subscript of two instead of one and can be expressed as shown in (3.4) to (3.6)

$$v_{a2} = r_s i_{a2} + \frac{d\psi_{a2}}{dt} \tag{3.4}$$

$$v_{b2} = r_s i_{b2} + \frac{d\psi_{b2}}{dt} \tag{3.5}$$

$$v_{c2} = r_s i_{c2} + \frac{d\psi_{c2}}{dt} \tag{3.6}$$

The stator flux linkages of the first and the second machine can be given using equations (3.7)-(3.9) and (3.10)-(3.12) respectively,

$$\psi_{a1} = \left(L_{ls} + \overline{L}_m\right) i_{a1} - \frac{1}{2}\overline{L}_m i_{b1} - \frac{1}{2}\overline{L}_m i_{c1} + \psi_m \sin\theta_r \tag{3.7}$$

$$\psi_{b1} = -\frac{1}{2}\overline{L}_m i_{a1} + \left(L_{ls} + \overline{L}_m\right) i_{b1} - \frac{1}{2}\overline{L}_m i_{c1} + \psi_m \sin\left(\theta_r - \frac{2}{3}\pi\right) \tag{3.8}$$

$$\psi_{c1} = -\frac{1}{2}\overline{L}_m i_{a1} - \frac{1}{2}\overline{L}_m i_{b1} + \left(L_{ls} + \overline{L}_m\right) i_{c1} + \psi_m \sin\left(\theta_r + \frac{2}{3}\pi\right) \tag{3.9}$$

$$\psi_{a2} = \left(L_{ls} + \overline{L}_m\right) i_{a2} - \frac{1}{2}\overline{L}_m i_{b2} - \frac{1}{2}\overline{L}_m i_{c2} + \psi_m \sin\theta_r \tag{3.10}$$

$$\psi_{b2} = -\frac{1}{2}\overline{L}_m i_{a2} + \left(L_{ls} + \overline{L}_m\right) i_{b2} - \frac{1}{2}\overline{L}_m i_{c2} + \psi_m \sin\left(\theta_r - \frac{2}{3}\pi\right) \tag{3.11}$$

$$\psi_{c2} = -\frac{1}{2}\overline{L}_m i_{a2} - \frac{1}{2}\overline{L}_m i_{b2} + \left(L_{ls} + \overline{L}_m\right) i_{c2} + \psi_m \sin\left(\theta_r + \frac{2}{3}\pi\right) \tag{3.12}$$

Where L_{ls} and L_m are the stator magnetizing and leakage inductances *[in H]*, respectively, while ψ_m is the magnitude of the flux linkages established by the PM *[in Wb]*. These assume that there is no coupling between the two-machine units. Although there is some mutual coupling between the two machines as shown in

Figure 3.2, this has been ignored as its mean value is relatively small compared to the coil self-inductance. The coupling reduces further as the machine is loaded.

A *d*-*q* representation of the machine can be adopted due to the sinusoidal nature of the phase flux-linkage variation with rotor position. As in conventional PM machines, the *d-axis* is taken to be aligned with the magnet flux linkage. Correspondingly, the induced Back-EMF is aligned to the quadrature axis. The electromagnetic torque is composed of two parts. The first part is the PM-torque which arises from the interaction of the magnet flux and *q-axis* stator current component. The second part is the reluctance-torque component caused by the inductance variation as a function of the rotor position. *Figure 3.3* shows the *d* and *q* inductances as a function of position. The saliency is minimal and goes virtually to zero with load. Therefore, the reluctance-torque is negligible, and the control strategy adopted is similar to that of a non-salient PM synchronous machine [39].

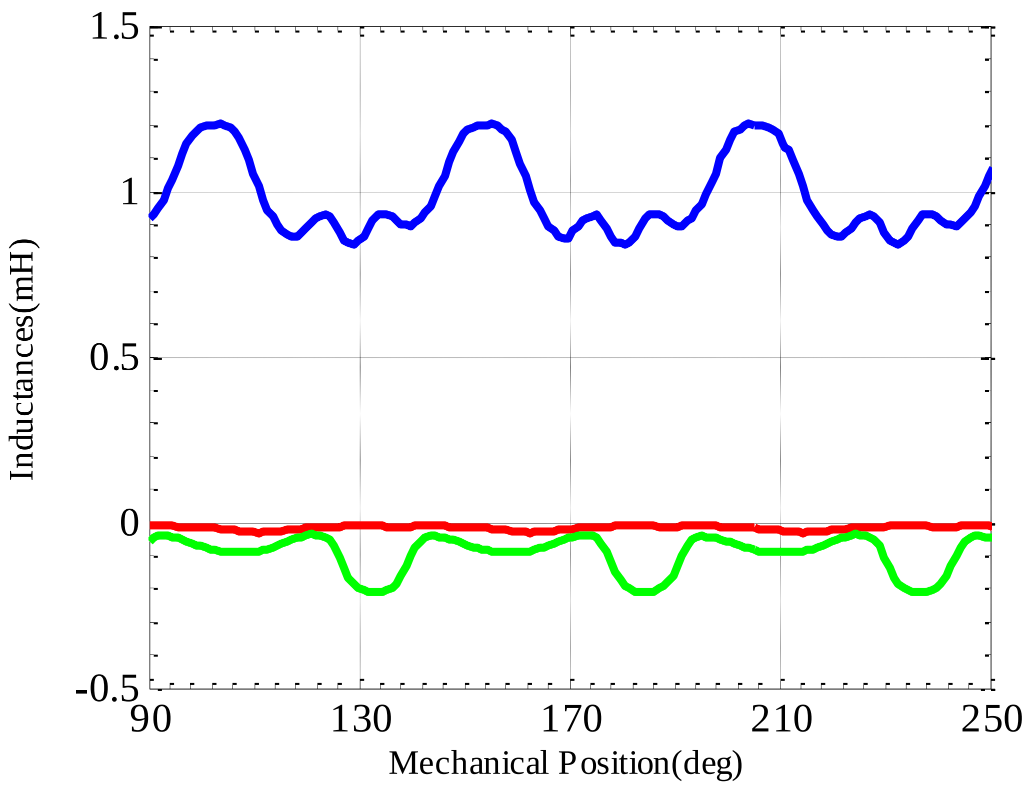

Figure 3.2 Self and mutual inductances – fault-tolerant design

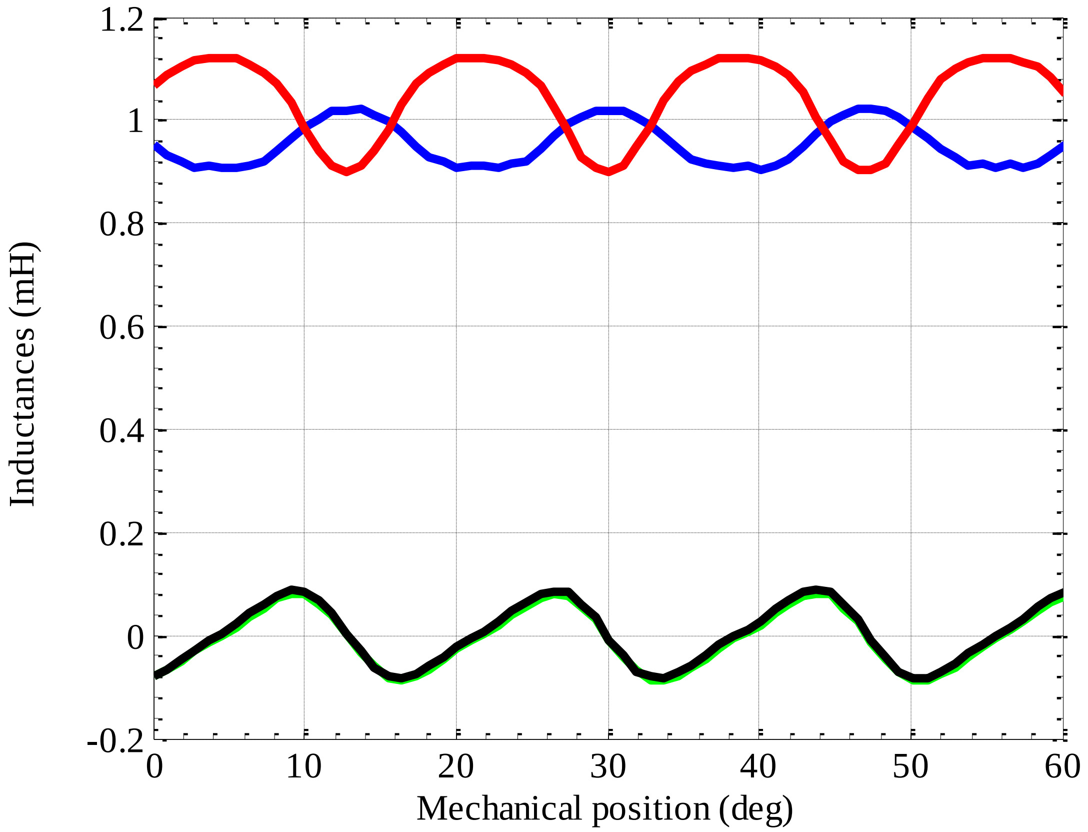

Figure 3.3 Direct and quadrature inductances – fault-tolerant design

Due to the nature of the machine, the machine parameters vary significantly with load and position. In order to have a realistic representation of the machine, finite element analysis was used to determine the PM flux linkage as a function of position and load as well as self-inductances and mutual inductances as a function of position and load.

These were integrated within the model using lookup tables.

Figure 3.2. shows the machine inductance as a function of position at no load.

The electromagnetic torque of the first machine can be calculated as (3.13) while that of the second machine can be then evaluated as in (3.14)

$$T_{e1} = \frac{P\psi_m}{2}\left(i_{a1}\cos\theta_r + i_{b1}\cos\left(\theta_r - \frac{2}{3}\pi\right) + i_{c1}\cos\left(\theta_r + \frac{2}{3}\pi\right)\right) \tag{3.13}$$

$$T_{e2} = \frac{P\psi_m}{2}\left(i_{a2}\cos\theta_r + i_{b2}\cos\left(\theta_r - \frac{2}{3}\pi\right) + i_{c2}\cos\left(\theta_r + \frac{2}{3}\pi\right)\right) \tag{3.14}$$

Therefore, the total electromagnetic torque of the dual three-phase flux-switching permanent magnet machine *[in Nm]* can be obtained from the torque of both machines, as shown in the following equation (3.15)

$$T_{e-total} = (T_{e1} + T_{e2}) \tag{3.15}$$

The realashionship between the differential equation of the electrical angular velocity and the torsional-mechanical (The drive's mechanical charakteristics) system can be expressed as in (3.16).

$$\frac{d\omega_r}{dt} = \left[\frac{P}{2J}(T_{e-total})\right] - \frac{B_m}{J}\omega_r - \frac{P}{2J}T_L \tag{3.16}$$

Where P is the number of electrical poles (i.e., twice the number of rotor poles), T_L is the load-torque applied *[in Nm]*, B_m is the viscous friction coefficient *[in N.m.s]*, and J is the equivalent moment of inertia of the drive system *[in kgcm^2]*.

It can be noted that the electrical angular velocity is the derivation of the displacement electrical angle and can be described by

$$\frac{d\theta_r}{dt} = \omega_r \tag{3.17}$$

where, ω_r and θ_r are the electrical angular velocity *[in rad.s^{-1}]* and displacement *[in rad]* of the adopted reference frame, respectively.

The parameters of prototype FS-PMSM drive are shown in

Table 3. 1

Parameters	**Values**
Total system inertia referred to motor shaft $J_{m\ (total)}$ [in $kgcm^2$]	0.0047
Total system viscous friction referred to motor shaft $B_{m\ (totat)}$ [in *N.m.s*]	0.00195
Parameters	**Values**
Rated speed [in *rpm*]	7600
Rated load torque [in *Nm*]	1.88
Nominal current $_{(rms\text{-}phase)}$ [in *A*]	7.92
Peak Current $_{(pk\text{-}phase)}$ (Phase) [in *A*]	11.2
Number of pole-pairs [-]	7
stator resistance per phase R (ph-ph) [in Ω]	0.135744
stator inductance per phase L_s (ph-ph) [in *mH*]	0.323
Direct inductance L_d (ph-ph) [in *mH*]	2.8076
Quadurature inductance L_q (ph-ph) [in *mH*]	2.8076
Permanent magnet flux per pole Ψ_{PM} [in Wb]	0.009333

Table 3. 1 The parameters of prototype FS-PMSM drive

3.4 Summary

Flux-Switching permanent-magnet (FSPM) machines have attracted considerable interest for high performance drive applications due to their high torque and power densities [40]. The configuration of the conventional brushless machine having magnets in the rotor compromised the performance due to the poor cooling and high speed limitation [41]. In stator-PM machines, the permanent magnets are located on the stator, which makes the temperature rise in the permanent magnets much easier to be controlled. The rotor is very simple and robust, so that it can be operated at a very high speed [1]. The three-phase mathematical model of permanent magnet synchronous machine is primarily studied to create the dual three-phase FS-PMSM model.

4 FS-PMSM DRIVE SYSTEM

4.1 Introduction

Drive-system reliability can be typically improved by either increasing the number of machine-converter units, the number of phases, or the number of winding channels or a combination of the aforementioned in order to ensure continued operation in case of a fault occurring.

Figure 4.1 and *Figure 4.2* show common ways how this modularity can be achieved. Increasing the number of machine units as shown in

Figure 4.1 will lead to a relatively conventional motor design but with large phase inductance. Each machine-drive unit has to deliver the required torque for the application at hand plus any additional braking-torque as a result of a faulty unit [42]. If separate-phase current control is adopted, *Figure 4.2(a)*, a specific fault-tolerant control strategy to deal with open-circuit and short-circuit faults needs to be implemented. This usually relies on a fault-detection and location algorithm to reconfigure the control accordingly. In addition, this configuration suffers from additional torque and input current ripple [43]. The work in this thesis is based on a dual three-phase channel machine similar to that in *Figure 4.2(b)*. Each machine (three-phase channel) is fed from a separate three-phase converter. In case of a phase open-circuit fault in one of the machine-drive units, the post-fault control strategy is to disable the faulty unit and deliver power with the remaining healthy unit. In case of a short-circuit fault, the post-fault strategy is to apply a balanced short circuit through the converter and again continue operation with the healthy unit, this time having to additionally overcome the braking-torque produced by the faulty unit. These types of control strategies have been implemented for both concentrated wound PM machines [44] and induction machines [37] showing their respective implications on drive operations. The work of this thesis will also present the modelling and implementation of fault-tolerant vector-control strategy for flux-switching machines and will highlight the implications of adopting such a system.

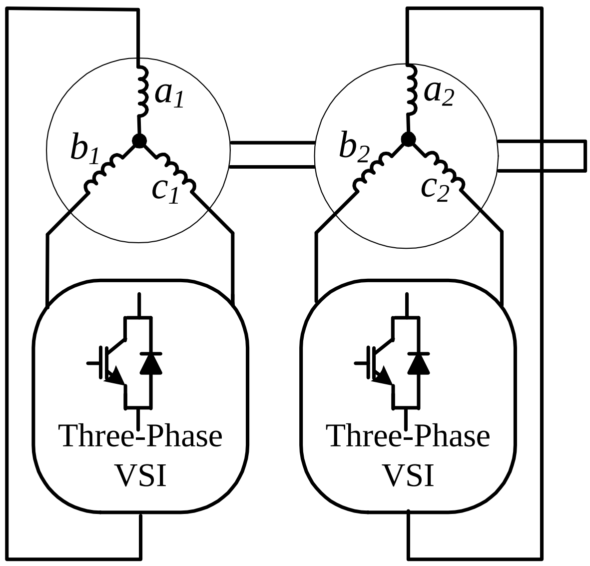

Figure 4.1 Standard two-machine setup with machines in torque-summing configuration

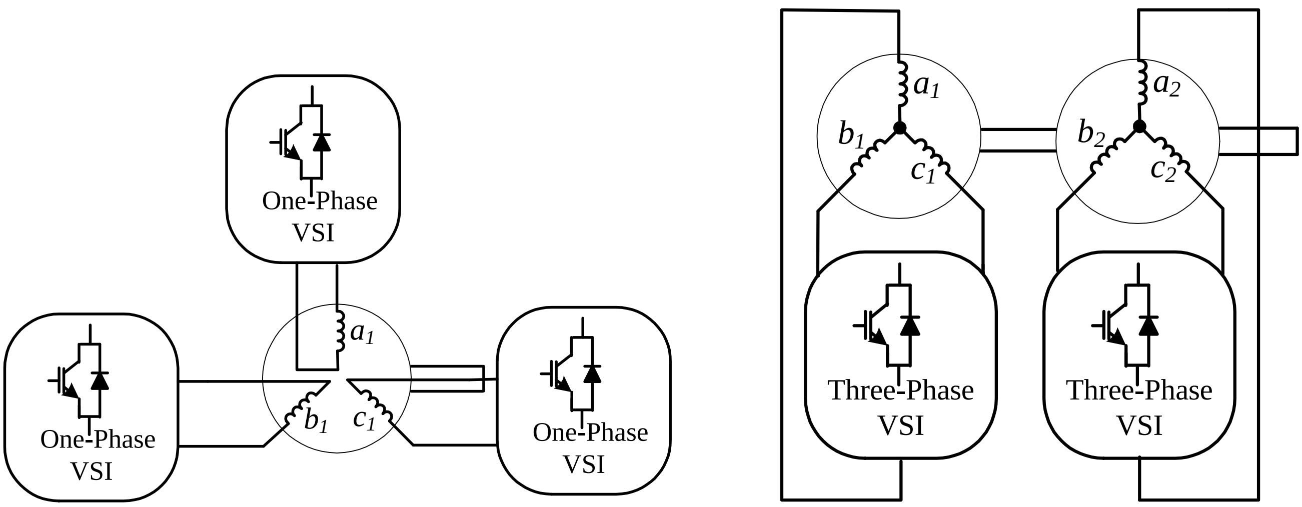

(a) (b)

Figure 4.2 Electrical redundancy (power supply and converters) can be achieved either through (a) separate phase current control or through (b) dual three-phase channel machine

4.2 Voltage Source Inverter FS-PMSM Drive

The PWM converter should meet some general conditions such as a wide range of linear operation and minimal number of switching to maintain low switching losses in power components, in addition to a minimal content of low-frequency harmonics in voltage and current, because they produce additional losses and noise in load, and also elimination of low-frequency harmonics (in the case of motors it generates a torque pulsation) and operation in the over-modulation region including square wave. The voltage source inverter flux-switching permanent magnet drive has received a considerable amount of attention in the literature [45].

A back-to-back voltage source converter consisting of an active PWM rectifier and a conventional PWM voltage source inverter is shown in *Figure 4.3*. The structure of the back-to-back converter is similar to the two-level voltage source inverter. The diode rectifier is replaced by the active PWM rectifier resulting in the ability to provide regenerative operation. The line-side PWM rectifier is controlled to regulate the dc-link voltage. Four-quadrant ac motor control can therefore be achieved.

The advantages of the back-to-back voltage source converter are sinusoidal input currents and control of the input displacement factor [46]. Compared to the two-level voltage source inverter with a diode rectifier, the control of the back-to-back voltage source converter is more complicated. Two additional controllers, a line current controller and a dc-link voltage controller, are required to obtain good performance of the drive system. Another drawback of this converter is the large dc-link capacitor, which is the bulkiest part of the converter. In order to limit the input current ripple the back-to-back converter also requires large input inductors, which increases the weight and volume of the drive [47].

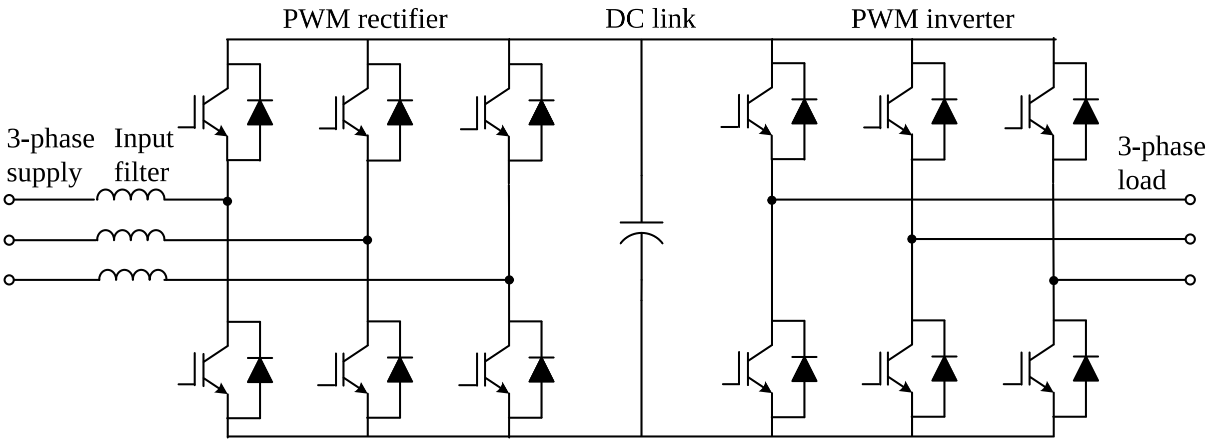

Figure 4.3 Back-to-back voltage source converter

The proposed fault tolerant flux-switching permanent magnet motor is driven by a six-phase inverter source inverter, as shown in *Figure 4.4*. Due to the fact that the considered fault-tolerant flux-switching permanent magnet motor consists of two three-phase windings connected together in one motor, this dual three-phase flux switching motor needs to be supplied by a six-phase PWM voltage source inverter with variable voltage and adjustable frequency. Consequently, this motor can effectively operate in a wide range of operating conditions. This six-phase PWM voltage source inverter is connected to a three-phase diode bridge rectifier through the dc-link capacitor.

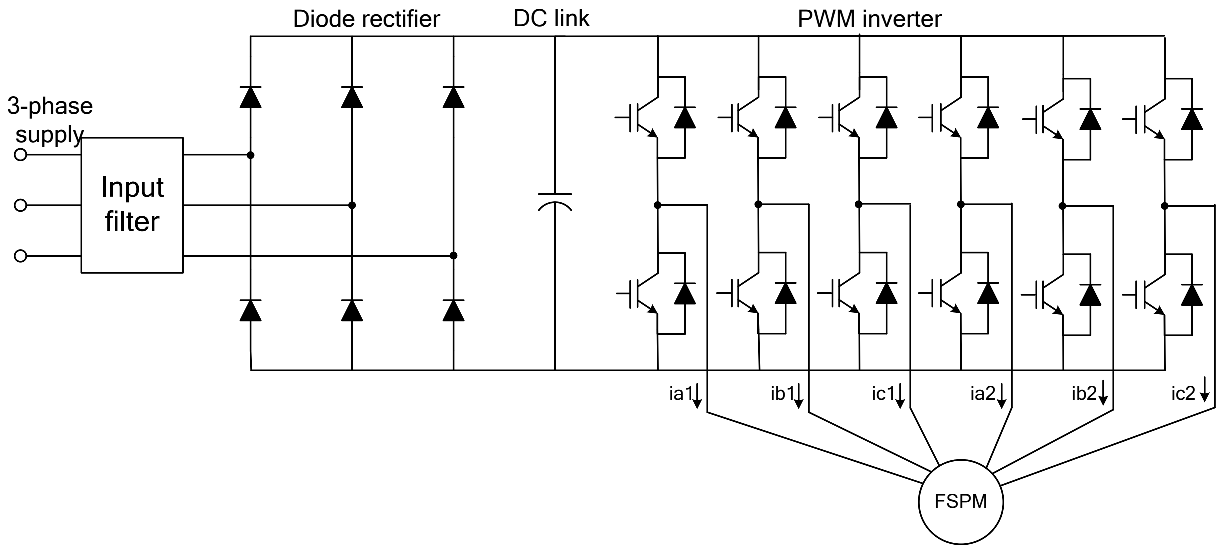

Figure 4.4 Flux-switching permanent magnet motor drive configuration

4.3 Field-Oriented Vector-Control

In order to obtain a high performance motor drive, an indirect field-oriented vector control technique is employed, this is based on decomposition of the instantaneous stator current into two components: flux current and torque-producing current.

Flux-oriented control can be classified into two parts rotor-flux oriented control or stator flux oriented control. In rotor flux-oriented control (direct-Blaschke or Indirect-Hasse) the decomposition guarantees correct current orientation in respect to rotor-flux whilst in stator-flux oriented control the decomposition guarantees correct current orientation in respect to stator-flux. More details can be found in [45]. The rotor-flux orientation is extensively used in AC drives.

The goal of the Field Oriented Control (see

Figure *4.5*) is to perform real-time control of torque variations demand, to control the rotor mechanical speed and to regulate phase currents (allows separate closed loop control of both the flux and torque, hence, achieving a similar control to that of a separately excited DC machine) in order to avoid current spikes during transient phases. To perform these controls, the electrical equations are projected from a three-phase non-rotating frame into a two co-ordinate rotating frame. This mathematical projection (Clarke & Park) greatly simplifies the expression of the electrical equations and removes their time and position dependencies. A block diagram of the indirect filed-orientated vector-control scheme is shown in

Figure 4.6, consisting of an outer speed-loop PI controller and two inner current-loop PI controllers. The measurements of the stator currents and rotor position are needed for the control scheme.

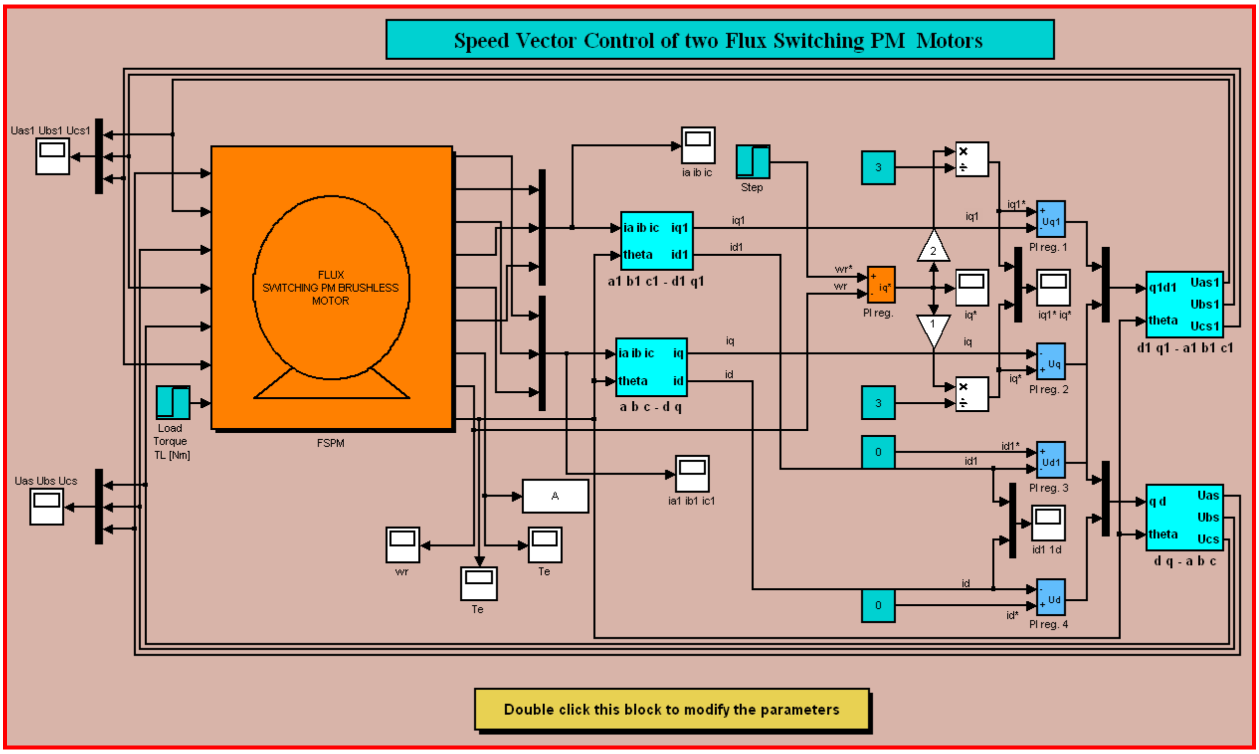

Figure 4.5 Indirect vector-control of a dual three-phase flux-switching permanent magnet motor

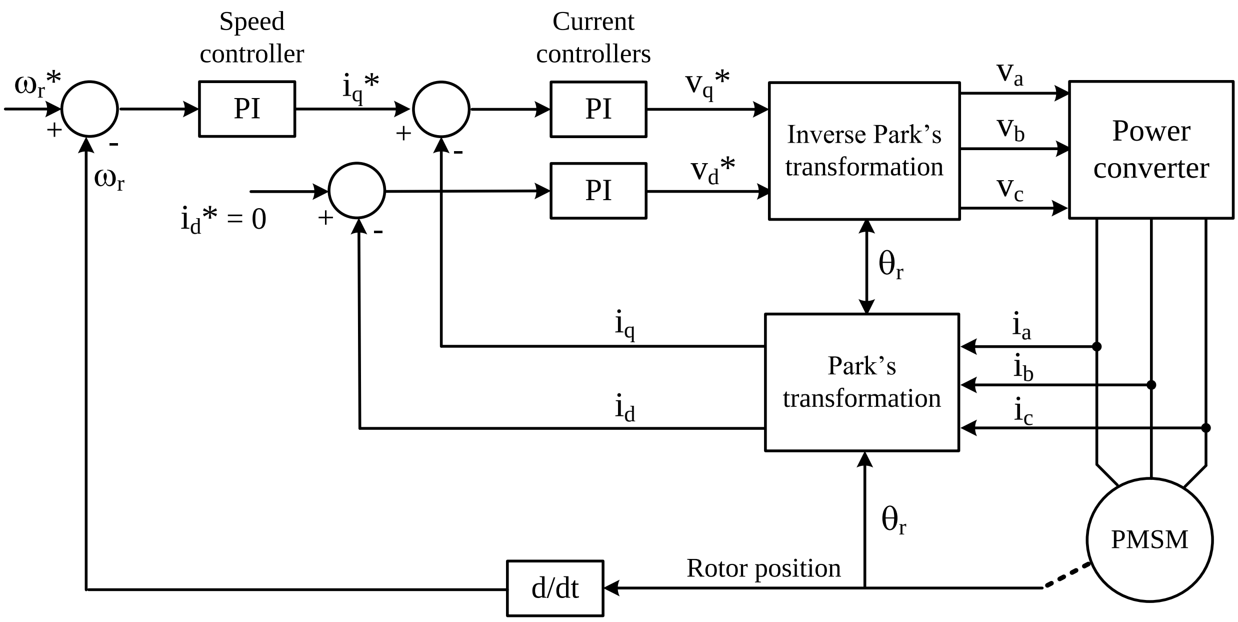

Figure 4.6 Block diagram of an indirect FOC for the PMSM drive

As can be seen in

Figure 4.6, the speed reference signal, ω_r*[in rad.s^{-1}]*, is compared to the actual speed of the motor, ω_r *[in rad.s^{-1}]*, which is obtained from the rotor position. A resolver or an encoder is mechanically mounted on the motor shaft to measure the position of the rotor. The speed of the motor is controlled by a proportional-integral (PI) controller generating a reference q-axis current signal, i_q**[in A]*. The reference d-axis and q-axis currents are then compared with the transformed currents, i_d **[in A]* and i_q *. The differences between the current references and the actual current components are processed by the current controllers, where the PI control algorithms are used.

The output of the current controllers are the reference d-axis and q-axis components, v_d* and v_q**[in V]*, of the stator voltages. These resulting voltage reference signals are converted to the three-phase voltages using the inverse Park's transformation, as expressed by

$$\begin{bmatrix} v_a \\ v_b \\ v_c \end{bmatrix} = \begin{bmatrix} \cos(\theta_r) & -\sin(\theta_r) \\ \cos(\theta_r - \frac{2\pi}{3}) & -\sin(\theta_r - \frac{2\pi}{3}) \\ \cos(\theta_r + \frac{2\pi}{3}) & -\sin(\theta_r + \frac{2\pi}{3}) \end{bmatrix} \begin{bmatrix} v_d \\ v_q \end{bmatrix} \tag{4.1}$$

The three-phase voltages, v_a, v_b and v_c, are considered as the reference voltages *[in V]* used in the modulation scheme of the power converter in order to generate the proper voltages for the motor stator windings

4.3.1 Design of the Speed-Controller

A block diagram of the speed controller for the PMSM is shown in *Figure 4.7*. The speed loop control structure consists of a PI controller, torque constant (K_t) and the s-domain PMSM model. A load torque, T_L *[in Nm]*, is considered as a disturbance.

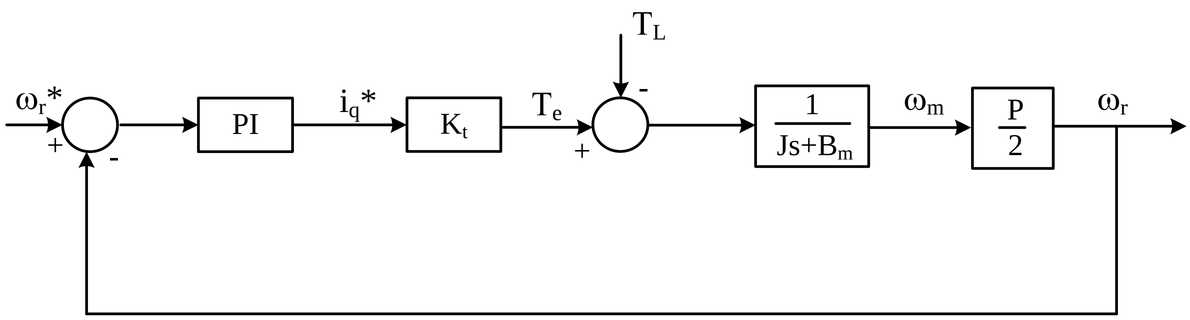

Figure 4.7 Block diagram of the PI speed controller for the PMSM

The transfer function for the PI controller can be written as:

$$\mathrm{PI(s)} = \mathrm{K_p} + \frac{\mathrm{K_i}}{\mathrm{s}} \tag{4.2}$$

where s is the Laplace operator, K_p and K_i are the proportional and integration gains of the speed PI controller.

For the design of the speed controller, the electrical speed of the motor is considered as a commanded speed. Therefore, the characteristic equation (1+G(s)H(s) = 0) for the speed control loop can be expressed as:

$$\mathrm{s}^2 + \left(\frac{\mathrm{B_m}}{\mathrm{J}} + \frac{\mathrm{K_p K_t}}{\mathrm{J}}\frac{P}{2}\right)\mathrm{s} + \frac{\mathrm{K_i K_t}}{\mathrm{J}}\frac{P}{2} = 0 \tag{4.3}$$

The characteristic equation of the second-order system can be performed by (4.4):

$$\mathrm{s}^2 + 2\xi\omega_n s + \omega_n^2 = 0 \tag{4.4}$$

where ω_n is the natural frequency *[in rad.s^{-1}]* and ξ is the damping factor.

Considering the relationship between (4.3) and (4.4) the parameter gains, K_p and K_i, for the speed controller can be obtained by (4.5) and (4.6), respectively.

$$\mathrm{K_p} = \left(2\xi\omega_n - \frac{\mathrm{B_m}}{\mathrm{J}} \right) \frac{\mathrm{J}}{\mathrm{K_t}(\mathrm{P}/2)} \tag{4.5}$$

$$\mathrm{K_i} = \omega_n^2 \frac{\mathrm{J}}{\mathrm{K_t}(\mathrm{P}/2)} \tag{4.6}$$

where the torque constant is $\mathrm{K_t} = \frac{3}{2}\frac{P}{2}\psi_{PM}$

To design the speed controller, the damping factor ξ = 0.8 is chosen and the bandwidth of the speed controller is determined at 10Hz. By using the parameters of the FS-PMSM shown in

Table 3. 1 the values of K_p and K_i are obtained as 0.0844 and 0.084285, respectively.

4.3.2 Design of the Current-Controller

The inner current controllers are designed to ensure that the measured currents are accurately regulated at the reference values with a fast dynamic response. This requires the bandwidth of the current control loop to be at least ten times faster than the speed control loop. A block diagram of the current-controllers for both the d-axis and q-axis components of the stator currents is shown in

Figure 4.8

Similarly to the speed loop control design, the characteristic equation (1+G(s)H(s) = 0) of the current controllers is considered as shown in (4.7):

$$\mathrm{s}^2 + \left(\frac{\mathrm{K_p} + r_s}{\mathrm{L_s}} \right)\mathrm{s} + \frac{\mathrm{K_i}}{\mathrm{L_s}} = 0 \tag{4.7}$$

By comparing (4.7) with the characteristic equation of the second-order system given by (4.4), the parameter gains, K_p and K_i, for the current-controllers can be obtained as:

$$\mathrm{K_p} = 2\xi\omega_{\mathrm{n}} L_s - r_s \tag{4.8}$$

$$\mathrm{K_i} = \omega_n^2 L_s \tag{4.9}$$

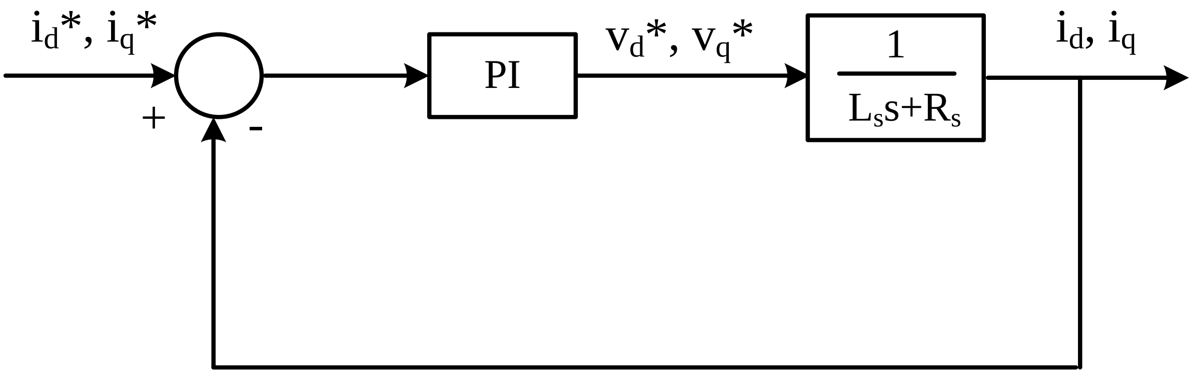

Figure 4.8 Block diagram of the PI current controllers for the PMSM

To design the current controllers, it is assumed that the current dynamics are much faster than the mechanical dynamics. In this application the bandwidth of 200Hz and the damping factor of 0.8 are designed for the current control loops, i_d and i_q, of the FS-PMSM. Considering the motor parameters listed in

Table 3. 1, the proportional and integration gains, K_p and K_i, of the current controllers are 1.25 and 1.15 respectively.

4.3.3 Vector-Control Transformation

The operating principle of a field-orientated vector-control method is based on using the coordinate transformation of the motor equations in a reference frame which rotates in synchronism with the permanent magnet flux. This control method allows decoupled control of flux and torque producing components of stator currents. Using d-axis and q-axis current controllers, independently control of motor flux and torque can be achieved. The PMSM can be controlled as a separately excited dc motor using the field-oriented vector-control method, where the torque and flux of the motor are decoupled. Thus, high performance motor drives operating in a wide range of speeds can be obtained.

The idea of the Clarke transformation is shown in *Figure 4.9.* The rotating stator current vector that is the sum of the three-phase currents can also be generated by *a- bi*-phased system placed on the fixed axis α and β. In this new frame, the expression of the torque is still dependent on the position of the rotor flux, preventing any easy solution of the electrical differential equation.

To remove this dependency, the electrical equations are projected in a two-phase ***(d,q)*** system that rotates at the speed of the electrical speed of the rotor and where the *d* axis is aligned with the electrical position of the rotor flux. In this frame, the electrical expression of the torque becomes independent from θ_r.

For transformation of any stator quantity (voltage, current, flux linkage, etc.) the transformation matrix is established [48].

The PMSM is controlled in a synchronous rotating dq reference frame with the d-axis oriented along the rotor flux vector of the motor. The three-phase stator currents are transformed into a two-phase time invariant system using Park's transformation as shown in (4.10)

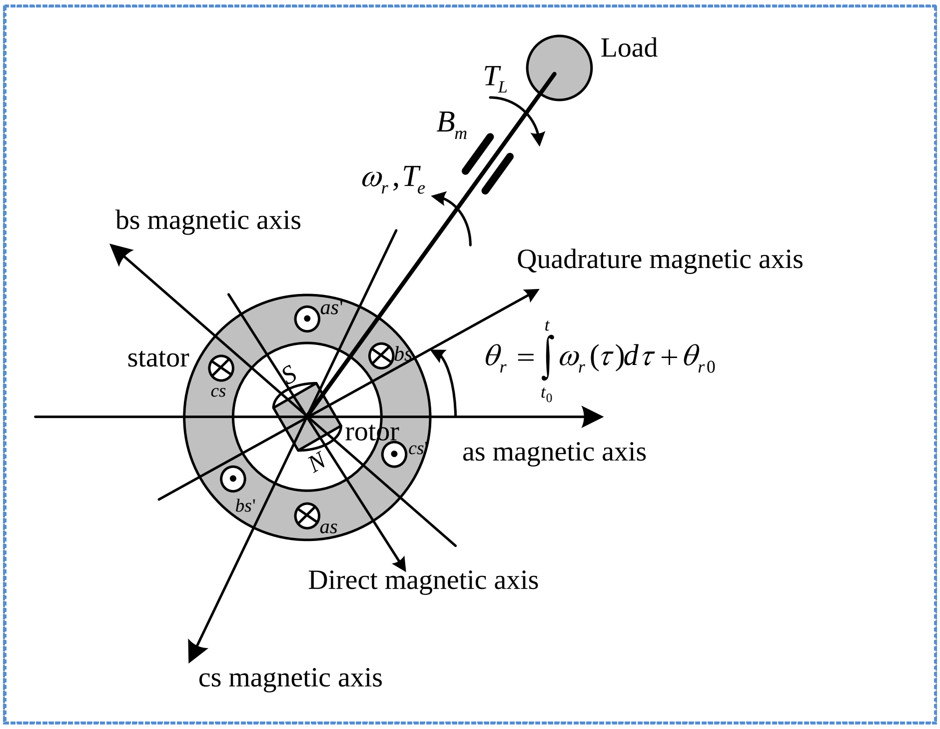

Figure 4.9 Three-phase permanent magnet synchronous motor

$$\begin{bmatrix} i_d \\ i_q \end{bmatrix} = \frac{2}{3}\begin{bmatrix} \cos(\theta_r) & \cos(\theta_r - \frac{2\pi}{3}) & \cos(\theta_r + \frac{2\pi}{3}) \\ \sin(\theta_r) & \sin(\theta_r - \frac{2\pi}{3}) & \sin(\theta_r + \frac{2\pi}{3}) \end{bmatrix} \begin{bmatrix} i_a \\ i_b \\ i_c \end{bmatrix} \tag{4.10}$$

and the inverse transformation as

$$\begin{bmatrix} i_a \\ i_b \\ i_c \end{bmatrix} = \begin{bmatrix} \cos(\theta_r) & \sin(\theta_r) \\ \cos(\theta_r - \frac{2\pi}{3}) & \sin(\theta_r - \frac{2\pi}{3}) \\ \cos(\theta_r + \frac{2\pi}{3}) & \sin(\theta_r + \frac{2\pi}{3}) \end{bmatrix} \begin{bmatrix} i_q \\ i_d \end{bmatrix} \tag{4.11}$$

The motor flux is equivalent to the d-axis current component, i_d, and an electromagnetic toque of the motor is proportional to the q-axis component, i_q, of the stator currents. Thus, i_d is called the flux producing component of the stator currents *[in A]* and i_q is called the torque generating components of the stator currents *[in A]*.

As can be seen in

Figure 4.6, the speed reference signal, ω_r* *[in rads^{-1}]*, is compared to the actual speed of the motor, ω_r *[in rads^{-1}]*, which is obtained from the rotor position. A resolver or an encoder is mechanically mounted on the motor shaft to measure the position of the rotor. The speed of the motor is controlled by a proportional-integral (PI) controller generating a reference q-axis current signal, i_q**[in A]*.

Dynamics of permanent-magnet synchronous machines in the machine variables

- Studies nonlinear analysis of permanent-magnet synchronous machines and develops nonlinear models
- Using kirchhoff's second law, one obtains three differential equations. In particular, for the as, bs, and cs stator windings, we have

$$v_a = r_s i_a + \frac{d\psi_a}{dt} \tag{4.12}$$

$$v_b = r_s i_b + \frac{d\psi_b}{dt} \tag{4.13}$$

$$v_c = r_s i_c + \frac{d\psi_c}{dt} \tag{4.14}$$

Where the flux linkages ψ_a, ψ_b, and ψ_c *[in Wb]* are given as

$$\psi_a = L_{aa} i_a + L_{ab} i_b + L_{ac} i_c + \psi_m \sin(\theta_r) \tag{4.15}$$

$$\psi_b = L_{ba} i_a + L_{bb} i_b + L_{bc} i_c + \psi_m \sin(\theta_r - \frac{2\pi}{3}) \tag{4.16}$$

$$\psi_c = L_{ca} i_a + L_{cb} i_b + L_{cc} i_c + \psi_m \sin(\theta_r + \frac{2\pi}{3}) \tag{4.17}$$

where L_{aa}, L_{bb} and L_{cc} *[in H]* are self-inductances of the stator windings. L_{ab}, L_{ac}, L_{ba}, L_{bc}, L_{ca} and L_{cb} *[in H]* are the mutual inductances between the stator phases. ψ_m is the magnitude of the flux linkage *[in Wb]*.

In matrix form, one has

$$v_{abc} = \mathbf{r}_s \mathbf{i}_{abc} + \frac{d\boldsymbol{\psi}_{abc}}{dt}, \begin{bmatrix} v_a \\ v_b \\ v_c \end{bmatrix} = \begin{bmatrix} r_s & 0 & 0 \\ 0 & r_s & 0 \\ 0 & 0 & r_s \end{bmatrix} \begin{bmatrix} i_a \\ i_b \\ i_c \end{bmatrix} + \begin{bmatrix} \frac{d\psi_a}{dt} \\ \frac{d\psi_b}{dt} \\ \frac{d\psi_c}{dt} \end{bmatrix} \tag{4.18}$$

The stator windings are displayed by 120 degree, and the flux linkages ψ_{am}, ψ_{bm}, and ψ_{cm} *[in Wb]* established by the permanent magnet, which are periodic functions of θ_r *[in rad]*, are assumed to obey the sine law. Using the magnitude of the flux linkages ψ_m *[in Wb]* established by the permanent magnet, we have $\psi_{am} = \psi_m \sin\theta_r$ (4.19)

$$\psi_{bm} = \psi_m \sin\left(\theta_r - \frac{2}{3}\pi\right) \tag{4.20}$$

$$\psi_{cm} = \psi_m \sin\left(\theta_r + \frac{2}{3}\pi\right) \tag{4.21}$$

The self and mutual inductances of the PMSM are functions of the electrical angular rotor position θ_r. Self-and mutual inductance for three-phase permanent-magnet synchronous machines can be derived using the results given for three-phase synchronous reluctance motors and can be written as follows:

$$\mathrm{L_{ac}} = \mathrm{L_{ca}} = -\frac{1}{2}\bar{\mathrm{L}}_\mathrm{m} \text{-} \mathrm{L_{\Delta m}} \cos(2\theta_\mathrm{r} + \frac{2\pi}{3}) \tag{4.22}$$

$$\mathrm{L_{bc}} = \mathrm{L_{cb}} = -\frac{1}{2}\bar{\mathrm{L}}_\mathrm{m} \text{-} \mathrm{L_{\Delta m}} \cos(2\theta_\mathrm{r}) \tag{4.23}$$

where L_{ls} is the stator leakage inductance *[in H]*, $\bar{L}_m$ is the average value of the magnetizing inductance *[in H]* and $L_{\Delta m}$ is half the amplitude of the sinusoidal variation of the magnetizing inductance *[in H]*.

Applying the expressions for inductances and driving them, we have the following equations for ψ_a, ψ_b, and ψ_c

$$\begin{aligned}\psi_a = &\left(L_{ls} + \bar{L}_m - L_{\Delta m}\cos 2\theta_r\right) i_a + \left(-\frac{1}{2}\bar{L}_m - L_{\Delta m}\cos 2\left(\theta_r - \frac{1}{3}\pi\right)\right) i_b + \\ &\left(-\frac{1}{2}\bar{L}_m - L_{\Delta m}\cos 2\left(\theta_r + \frac{1}{3}\pi\right)\right) i_c + \psi_m \sin\theta_r\end{aligned} \tag{4.24}$$

$$\psi_b = \left(-\frac{1}{2}\overline{L}_m - L_{\Delta m}\cos 2\left(\theta_r - \frac{1}{3}\pi\right)\right)i_a + \left(L_{ls} + \overline{L}_m - L_{\Delta m}\cos 2\left(\theta_r - \frac{2}{3}\pi\right)\right)i_b + \left(-\frac{1}{2}\overline{L}_m - L_{\Delta m}\cos 2\theta_r\right)i_c + \psi_m \sin\left(\theta_r - \frac{2}{3}\pi\right) \tag{4.25}$$

$$\psi_c = \left(-\frac{1}{2}\overline{L}_m - L_{\Delta m}\cos 2\left(\theta_r + \frac{1}{3}\pi\right)\right)i_a + \left(-\frac{1}{2}\overline{L}_m - L_{\Delta m}\cos 2\theta_r\right)i_b + \left(L_{ls} + \overline{L}_m - L_{\Delta m}\cos 2\left(\theta_r + \frac{2}{3}\pi\right)\right)i_b + \psi_m \sin\left(\theta_r + \frac{2}{3}\pi\right) \tag{4.26}$$

One has the following expression in matrix form for the vector of flux linkages

$$\boldsymbol{\psi}_{abc} = \mathbf{L}_s \mathbf{i}_{abc} + \boldsymbol{\psi}_m \tag{4.27}$$

$$= \begin{bmatrix} \left(L_{ls} + \overline{L}_m - L_{\Delta m}\cos 2\theta_r\right) & \left(-\frac{1}{2}\overline{L}_m - L_{\Delta m}\cos 2\left(\theta_r - \frac{1}{3}\pi\right)\right) & \left(-\frac{1}{2}\overline{L}_m - L_{\Delta m}\cos 2\left(\theta_r + \frac{1}{3}\pi\right)\right) \\ \left(-\frac{1}{2}\overline{L}_m - L_{\Delta m}\cos 2\left(\theta_r - \frac{1}{3}\pi\right)\right) & \left(L_{ls} + \overline{L}_m - L_{\Delta m}\cos 2\left(\theta_r - \frac{2}{3}\pi\right)\right) & \left(-\frac{1}{2}\overline{L}_m - L_{\Delta m}\cos 2\theta_r\right) \\ \left(-\frac{1}{2}\overline{L}_m - L_{\Delta m}\cos 2\left(\theta_r + \frac{1}{3}\pi\right)\right) & \left(-\frac{1}{2}\overline{L}_m - L_{\Delta m}\cos 2\theta_r\right) & \left(L_{ls} + \overline{L}_m - L_{\Delta m}\cos 2\left(\theta_r + \frac{2}{3}\pi\right)\right) \end{bmatrix}$$

$$* \begin{bmatrix} i_a \\ i_b \\ i_c \end{bmatrix} + \psi_m \begin{bmatrix} \sin\theta_r \\ \sin\left(\theta_r - \frac{2}{3}\pi\right) \\ \sin\left(\theta_r + \frac{2}{3}\pi\right) \end{bmatrix} \tag{4.28}$$

The matrix of inductances $\mathbf{L}_s$ is

$$\mathbf{L}_s = \begin{bmatrix} \left(L_{ls} + \overline{L}_m - L_{\Delta m}\cos 2\theta_r\right) & \left(-\frac{1}{2}\overline{L}_m - L_{\Delta m}\cos 2\left(\theta_r - \frac{1}{3}\pi\right)\right) & \left(-\frac{1}{2}\overline{L}_m - L_{\Delta m}\cos 2\left(\theta_r + \frac{1}{3}\pi\right)\right) \\ \left(-\frac{1}{2}\overline{L}_m - L_{\Delta m}\cos 2\left(\theta_r - \frac{1}{3}\pi\right)\right) & \left(L_{ls} + \overline{L}_m - L_{\Delta m}\cos 2\left(\theta_r - \frac{2}{3}\pi\right)\right) & \left(-\frac{1}{2}\overline{L}_m - L_{\Delta m}\cos 2\theta_r\right) \\ \left(-\frac{1}{2}\overline{L}_m - L_{\Delta m}\cos 2\left(\theta_r + \frac{1}{3}\pi\right)\right) & \left(-\frac{1}{2}\overline{L}_m - L_{\Delta m}\cos 2\theta_r\right) & \left(L_{ls} + \overline{L}_m - L_{\Delta m}\cos 2\left(\theta_r + \frac{2}{3}\pi\right)\right) \end{bmatrix}$$

(4.29)

It was shown that $\overline{L}_m$ and $L_{\Delta m}$ are found as

$$\overline{L}_m = \frac{1}{3}\left(\frac{N_s^2}{\Re_{mq}} + \frac{N_s^2}{\Re_{md}}\right) \text{ and } L_{\Delta m} = \frac{1}{3}\left(\frac{N_s^2}{\Re_{md}} - \frac{N_s^2}{\Re_{mq}}\right) \tag{4.30}$$

Permanent-magnet synchronous machines are round-rotor electrical machines. For round-rotor synchronous machines, the magnetic paths in the quadrature and direct magnetic axes are identical, and hence magnetizing reluctance $\Re_{mq} = \Re_{md}$ *[in H^{-1}]*. Thus,

$$\overline{L}_m = \frac{2N_s^2}{3\Re_{mq}} = \frac{2N_s^2}{3\Re_{md}} \text{ and } \qquad L_{\Delta m} = 0 \tag{4.31}$$

Hence, matrix $\mathbf{L}_s$ becomes

$$\mathbf{L}_s = \begin{bmatrix} L_{ls} + \overline{L}_m & -\frac{1}{2}\overline{L}_m & -\frac{1}{2}\overline{L}_m \\ -\frac{1}{2}\overline{L}_m & L_{ls} + \overline{L}_m & -\frac{1}{2}\overline{L}_m \\ -\frac{1}{2}\overline{L}_m & -\frac{1}{2}\overline{L}_m & L_{ls} + \overline{L}_m \end{bmatrix} \tag{4.32}$$

And the expression for the flux linkages can be simplified to

$$\psi_a = \left(L_{ls} + \overline{L}_m\right) i_a - \frac{1}{2}\overline{L}_m i_b - \frac{1}{2}\overline{L}_m i_c + \psi_m \sin\theta_r \tag{4.33}$$

$$\psi_b = -\frac{1}{2}\overline{L}_m i_a + \left(L_{ls} + \overline{L}_m\right) i_b - \frac{1}{2}\overline{L}_m i_c + \psi_m \sin\left(\theta_r - \frac{2}{3}\pi\right) \tag{4.34}$$

$$\psi_c = -\frac{1}{2}\overline{L}_m i_a - \frac{1}{2}\overline{L}_m i_b + \left(L_{ls} + \overline{L}_m\right) i_c + \psi_m \sin\left(\theta_r + \frac{2}{3}\pi\right) \tag{4.35}$$

Hence,

$$\mathbf{u}_{abc} = \mathbf{r}_s \mathbf{i}_{abc} + \frac{d\boldsymbol{\psi}_{abc}}{dt} = \mathbf{r}_s \mathbf{i}_{abc} + \mathbf{L}_s \frac{d\mathbf{i}_{ab}}{dt}\frac{d\boldsymbol{\psi}_m}{dt} \tag{4.36}$$

Where,

$$\frac{d\boldsymbol{\psi}_m}{dt} = \psi_m \begin{bmatrix} \omega_r \cos\theta_r \\ \omega_r \cos\left(\theta_r - \frac{2}{3}\pi\right) \\ \omega_r \cos\left(\theta_r + \frac{2}{3}\pi\right) \end{bmatrix} \tag{4.37}$$

Denoting

$$L_{ss} = L_{ls} + \overline{L}_m \tag{4.38}$$

Using Newton's second law the mechanical equation of the motor can be derived as

$$J\frac{d^2\theta_m}{dt^2} = T_e - B_m\omega_m - T_L \tag{4.39}$$

$$\frac{d\omega_m}{dt} = \frac{1}{J}\left(T_e - B_m\omega_m - T_L\right) \tag{4.40}$$

$$\frac{d\theta_m}{dt} = \omega_m \tag{4.41}$$

where ω_m is the mechanical angular velocity of the rotor *[rad.s^{-1}]*, θ_m is the mechanical angular position of the rotor *[rad]*, J is the moment of inertia, B_m *[N.m.s]* is the viscous coefficient, T_e is the electromagnetic torque produced by the motor *[Nm]* and T_L is the external load torque *[Nm]*.

The relationship between the mechanical and the electrical rotor speed can be considered in terms of the number of poles, P, as shown in(4.42):

$$\omega_{\mathrm{m}} = \frac{P}{2}\omega_{\mathrm{m}} \tag{4.42}$$

The electrical angular position of the rotor can be obtained by:

$$\theta_{\mathrm{m}} = \frac{P}{2}\theta_{\mathrm{m}} \tag{4.43}$$

Therefore, one obtains the following formula to calculate the electromagnetic torque for three-phase P-pole permanent-magnet synchronous motors

$$T_e = \frac{P\psi_m}{2}\left(i_a\cos\theta_r + i_b\cos\left(\theta_r - \frac{2}{3}\pi\right) + i_c\cos\left(\theta_r + \frac{2}{3}\pi\right)\right) \tag{4.44}$$

Hence, $$\frac{d\omega_m}{dt} = \frac{P\psi_m}{2}\left(i_a\cos\theta_r + i_b\cos\left(\theta_r - \frac{2}{3}\pi\right) + i_c\cos\left(\theta_r + \frac{2}{3}\pi\right)\right) - \frac{B_m}{J}\omega_m - \frac{1}{J}T_L \tag{4.45}$$

Using the electrical angular velocity ω_r and displacement θ_r, related to the mechanical angular velocity *[rad.s^{-1}]* and displacement *[rad]* as $\omega_m = \frac{2}{P}\omega_r$ and $\theta_m = \frac{2}{P}\theta_r$, the following differential equations can be used to map the torsional-mechanical transient dynamics result;

$$\frac{d\omega_r}{dt} = \frac{P^2\psi_m}{4J}\left(i_a\cos\theta_r + i_b\cos\left(\theta_r - \frac{2}{3}\pi\right) + i_c\cos\left(\theta_r + \frac{2}{3}\pi\right)\right) - \frac{B_m}{J}\omega_r - \frac{P}{2J}T_L \tag{4.46}$$

$$\frac{d\theta_r}{dt} = \omega_r \tag{4.47}$$

To control the angular velocity, one regulates the currents fed or voltages applied to the stator windings. Neglecting the viscous friction coefficient, the analysis of Newton's second law

$$T_e - T_L = J\,\frac{d\omega_m}{dt} \tag{4.48}$$

Indicates that the angular velocity increases if $T_e > T_L$, and ω_m decreases if $T_e < T_L$. Furthermore, ω_m = const if $T_e = T_L$. That is, to regulate the angular velocity, one changes the electromagnetic torque developed. The equation for the electromagnetic torque for the three-phase P-pole permanent magnet synchronous motor can be expressed as (4.49):

$$T_e = \frac{P\psi_m}{2}\left(i_a\cos\theta_r + i_b\cos\left(\theta_r - \frac{2}{3}\pi\right) + i_c\cos\left(\theta_r + \frac{2}{3}\pi\right)\right) \tag{4.49}$$

If the motor is fed by a balanced three-phase current set

$$i_a(t) = \sqrt{2}i_M\cos(\omega_r t) = \sqrt{2}i_M\cos(\omega_e t) = \sqrt{2}i_M\cos\theta_r \tag{4.50}$$

$$i_b(t) = \sqrt{2}i_M\cos\left(\omega_r t - \frac{2}{3}\pi\right) = \sqrt{2}i_M\cos\left(\omega_e t - \frac{2}{3}\pi\right) = \sqrt{2}i_M\cos\left(\theta_r - \frac{2}{3}\pi\right) \tag{4.51}$$

$$i_c(t) = \sqrt{2}i_M\cos\left(\omega_r t + \frac{2}{3}\pi\right) = \sqrt{2}i_M\cos\left(\omega_e t + \frac{2}{3}\pi\right) = \sqrt{2}i_M\cos\left(\theta_r + \frac{2}{3}\pi\right) \tag{4.52}$$

One obtains

$$T_e = \frac{P\psi_m}{2}\sqrt{2}i_M\left(\cos^2\theta_r + \cos^2\left(\theta_r - \frac{2}{3}\pi\right) + \cos^2\left(\theta_r + \frac{2}{3}\pi\right)\right) \tag{4.53}$$

Taking note that $\cos^2\theta_r + \cos^2\left(\theta_r - \frac{2}{3}\pi\right) + \cos^2\left(\theta_r + \frac{2}{3}\pi\right) = \frac{3}{2}$, We have

$$T_e = \frac{3P\psi_m}{2\sqrt{2}}i_M \tag{4.54}$$

4.4 Field-Weakening Control

The control strategy closes the design loop, the first step involves electromagnetic design, followed by thermal calculations and enclosed by selection of power electronics devices taking into account the DC bus voltage, maximum current and required switching frequency.

There are many control strategies associated with the synchronous PM machine. However the most common strategies are I_d = 0, Maximum Torque-per-Ampere (MTPA), Maximum Efficiency and Forced output power for field-weakening operation [49]. I_d = 0 control strategy takes into account magnet torque only (first term of Equation (4.55)) but does not maximize neither torque production, nor efficiency. Nevertheless, a control strategy incorporating I_d = 0 seems to beneficial for initial estimation of torque production during the design of a PM machine.

$$T_e = \frac{3}{2}P\left[\left(L_d\, i_{sd}^r\, i_{sq}^r + \psi_{PM}\, i_{sq}^r - L_q\, i_{sq}^r\, i_{sd}^r\right)\right] = \frac{3}{2}P\left[\underbrace{\left(\psi_{PM}\, i_{sq}^r\right)}_{\text{Magnetic torque}} + \underbrace{\left(\left(L_d - L_q\right) i_{sd}^r\, i_{sq}^r\right)}_{\text{Reluctance torque}}\right] \tag{4.55}$$

The MTPA (Maximum Torque Per Ampere) control strategy aims to find an optimal combination of *d*– and *q* axis currents according to Equation (4.57) such that overall torque production for a given current locus is maximized and as a result the copper losses are minimized.

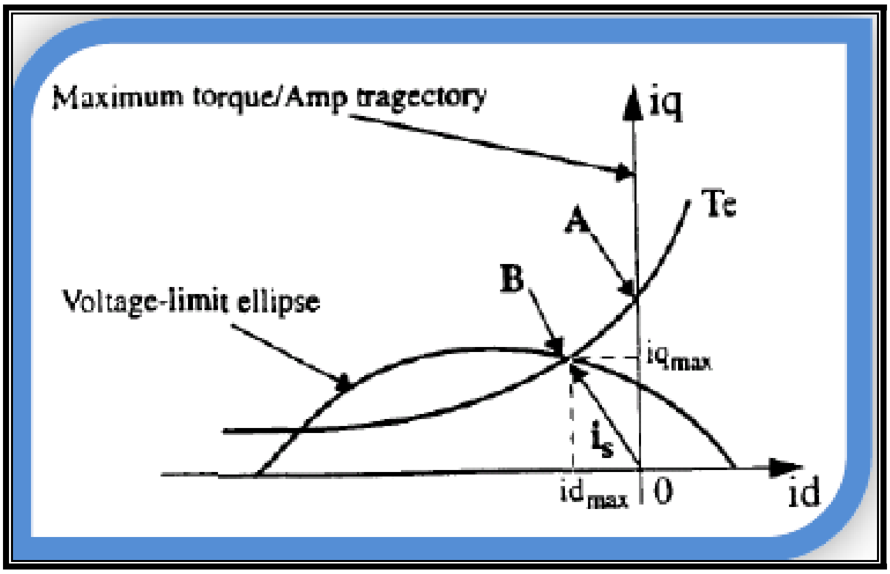

Figure 4.10 Voltgae limit in the d-q plane

The MTPA (Maximum Torque Per Ampere) control strategy is limited by the maximum available voltage. As the machine speed increases above the base speed, the availability of MTPA is limited by the voltage locus ellipses depicted in

Figure 4.10. The controller must switch, in this case, into field-weakening mode so that the negative *d*-axis current opposes back-EMF and the requested voltage does not exceed maximum supply voltage [50].

Field-weakening refers to the ability to push the machine to speeds higher than the break frequency by weakening the flux in the machine. This process allows the machine to produce torque higher than that obtainable if the flux is not weakened [49].

Under nominal load the mechanical power increases as a linear function of speed, up to the nominal power (reached when speed is equal to its nominal value). Knowing that mechanical power is proportional to the torque (T) and speed (ω) and that its nominal value has been reached when speed is equal to 7600rpm (nominal value), the torque production must be reduced if the desired speed is to be greater than 7600rpm. This is shown in *Figure 4.11*.

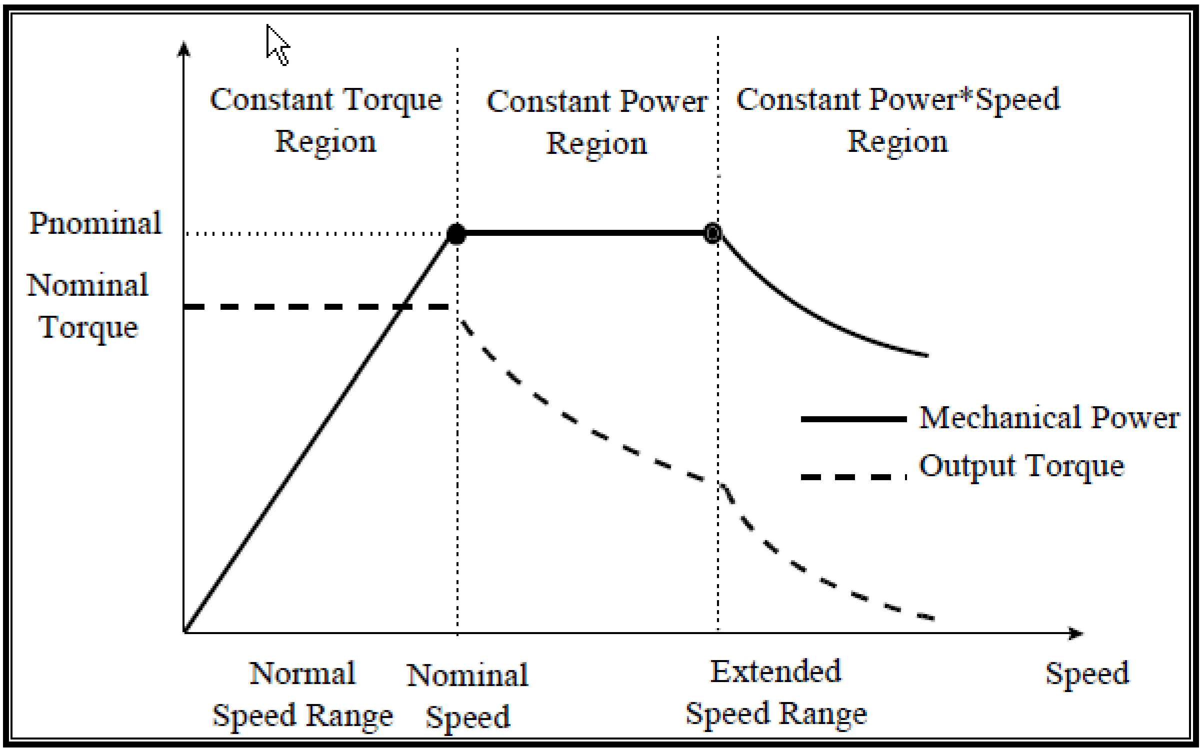

Figure 4.11 Real operation of field-weakening

In the constant power region the nominal torque production behaves like the inverse function of speed, thus allowing constant power production (P=$T\omega$).

In the constant Power*Speed region the nominal torque production behaves as the inverse function of the speed squared

The maximum torque function is equal to a constant in the first region as V (the phase voltage) increases linearly with speed. Above the nominal speed the phase voltage is maintained constant and equal to its nominal value, thus making the maximum torque an inverse function of the speed squared. This results in the curve shown in *Figure 4.12*.

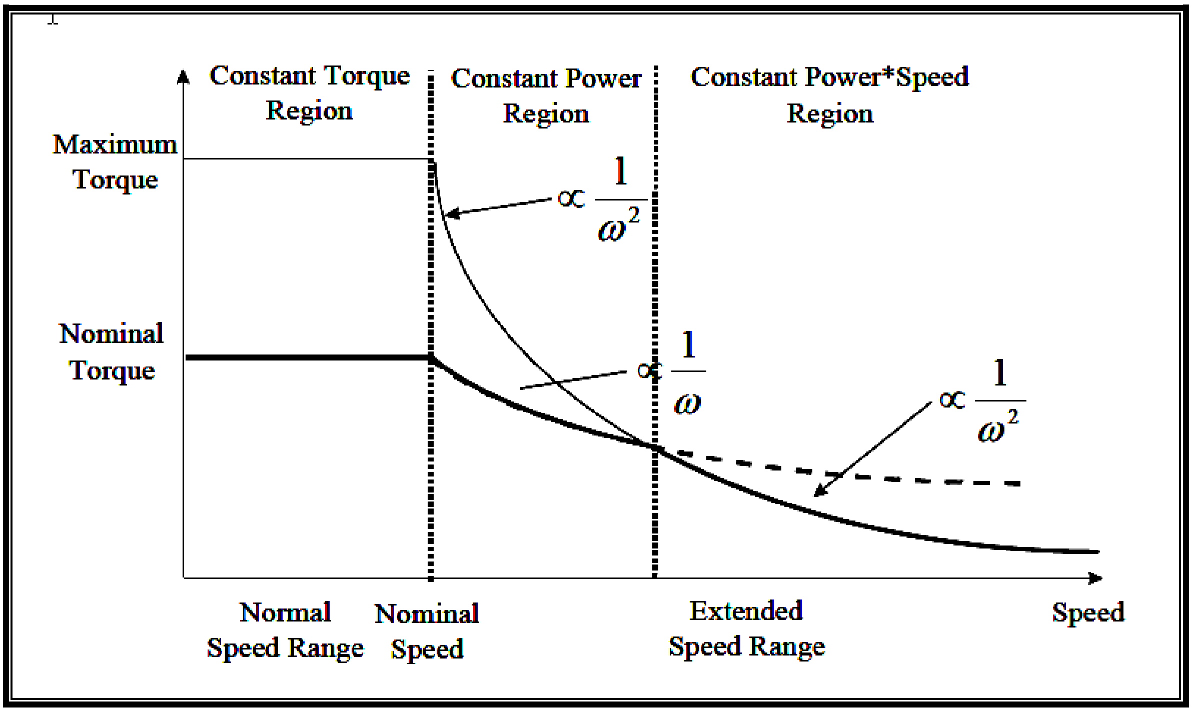

Figure 4.12 Maximum and nominal torque vs speed

In order to achieve high speeds, the stator current frequency is increased. The back-EMF ***E*** is directly proportional to the permanent magnet flux ψ_{PM} and the electrical angular velocity ω_r. In normal condition the permanent magnet flux is kept constant.

$$E = j\omega_r \psi_{PM} \tag{4.56}$$

Then a maximum stator speed is attained when *E* (back-EMF) reaches the limit output voltage of the power converter as shown in *Figure 4.13*. To reach a higher speed, the flux is reduced as an invert of the angular speed in order to keep the back-EMF constant and equal to its maximum.

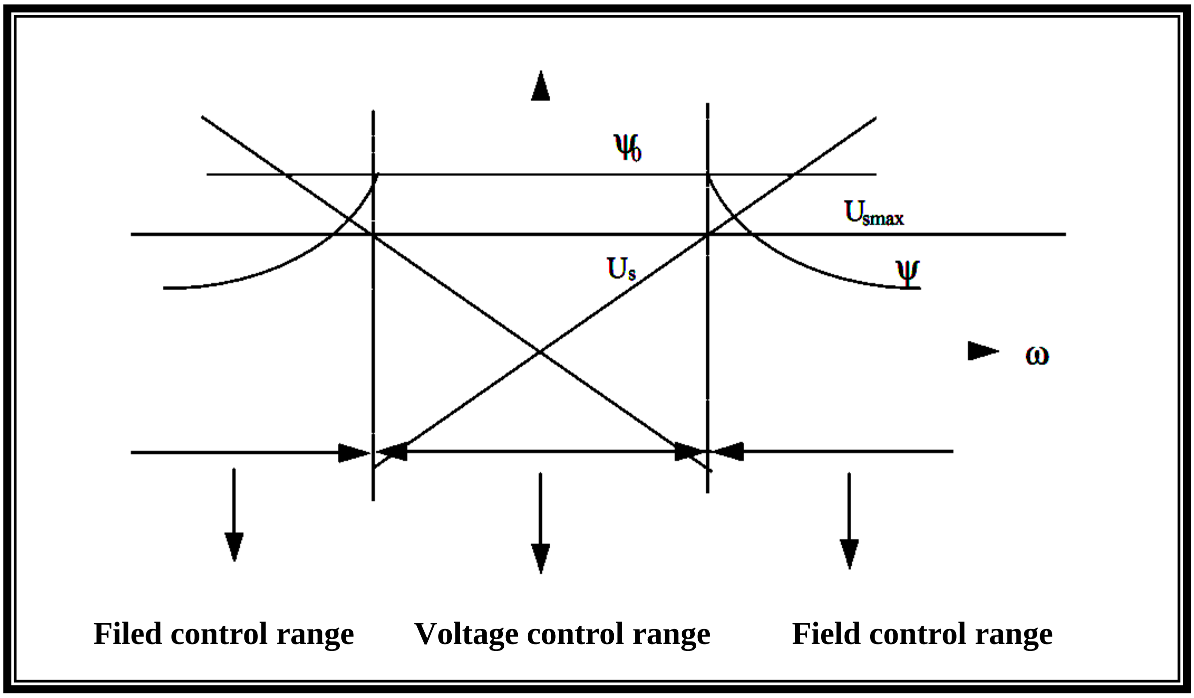

Figure 4.13 Field and voltage characteristics for high-speed control

Practically if we consider the stator current in the *d,q* rotating reference frame and its relationship with the *α,β* stationary reference frame, below the speed where the maximum output voltage is reached, the best choice is δ=±π/2 and i^r_{sd} =0. The effect of the field-weakening can be achieved by advancing the current vector beyond δ=π/2 i.e. introducing a current component in the negative d-axis. As a consequence i^r_{sq} and then the torque are reduced in order not to exceed the maximum output current i_{s_max}:

$$i_s^r = \sqrt{{i_{sd}^r}^2 + {i_{sq}^r}^2} \leq i_{s\_\max} \tag{4.57}$$

A closed loop control with field-weakening consists of feeding back a proportional integral (PI) regulator with the motor *d* and *q* axis voltages applied to the motor and calculating a new reference for the d-current component. This diagram allows us to exploit the full voltage capability of the inverter independently of the line voltage and the motor characteristics. i^r_{sd} being determined, the new i^r_{sq} limitation range set by [i^r_{sqmin} , i^r_{qmax}] is then calculated to not exceed $\mathrm{i}_{\mathrm{s\_max}}$,

4.5 Summary

The field-oriented control (FOC) or vector-control has been used to control FS-PMSM in adjustable speed drive applications. Vector-control effectively "transforms" the AC machine into a "DC machine equivalent" in which a torque producing i^r_{sd} , i^r_{sq} and field producing current may be defined. Torque and flux can thus be independently controlled as in a DC machine. In order to transform the machine into the "DC machine equivalent", the rotor flux angle (depending on the position of the rotor flux vector in space) must be known at all times. This angle defines also the position of a rotating d-q axis frame. When the d-axis of the frame is aligned with the rotor flux, the system is said to be Field-oriented. In this Chapter a field-weakening control has been described.

5 FAULT-TOLERANT FS-PMSM DRIVE CONTROL

5.1 Introduction

The concept of a fault tolerant drive is that it will continue to operate in a satisfactory manner after sustaining a fault. The term “satisfactory” implies a minimum level of performance after the fault, and will therefore be heavily influenced by system requirements.

It has been established [51] that the natural reliability of a drive system is around 1 failure in 10^5– 10^6 hrs. This is not sufficient to meet the safety critical requirement of 1 failure in 10^9 hours. The concept is that if all failures can be detected and the drive reconfigured, so that it can continue to operate with this single point failure, that the required reliability can be reached. With an elegant design combination of electric machine, power electronics and control electronics, a fault tolerant electric drive system can be made to operate fully with a range of electrical and mechanical faults.

To achieve this goal all faults must be detected with adequate speed so that the drive system can be reconfigured before the initial fault causes collateral damage and hence results in secondary faults. The fault tolerant electric drive system is then able to operate with a reduced performance but still enough to enable its critical functions to be carried out untill service can be provided [52].

A safety critical, aero-engine fuel control system must be able to demonstrate that it is extremely unlikely to cause an in-flight shut down or a loss of thrust control. Specific requirements for achieving this include [53]:

- No signal faults which cause hazardous failure
- Any fault which will cause or contribute to an in-flight shut down must have a failure rate of less than 10^{-7} failures per hour.
- Undetectable single faults which could in combination with a subsequent fault cause an in-flight shut down must have a failure rate of less than 10^{-8} failures per hour. These requirements guide the electric fuel pump drive architecture.

To guarantee fault tolerance in the whole electric drive system, the **following requirements will be necessary**:

1. Partitioning into units with redundancy
2. Isolation between units
3. Swift fault detection, identification and reporting
4. Post-fault action, i.e. fault accommodation
5. Continuing operation until repair

The types of electrical faults which can occur in a drive system:

i. Within the electrical machine

- Winding open-circuit fault
- Winding internal short-circuit
- Winding phase-ground or phase-phase s/c
- Winding short-circuit at the terminals

ii. Within the power converter

- Power device (IGBT-*Module* SKM 100GB *123 D* and diode) open-circuit faults
- IGBT and diode short-circuit faults
- IGBT gate drive failure
- DC link capacitor failure

iii. Within the control electronics

- A/D converter hardware failure
- DSP microcontroller hardware faults
- C code program operating faults (software)
- Data bus faults

iv. Within the sensor subsystem

- Current sensor faults
- DC link voltage sensor faults
- Vce-sat ON state voltage sensor faults
- Position angle sensor, i.e. resolver failure

5.2 Fault-Tolerant Control Strategy

In order to keep the motor operating at the desired speeds under both healthy and unhealthy operating condition, the field-oriented indirect vector-control technique is employed. Each machine (three-phase channel) of a dual three-phase channel flux-switching permanent magnet synchronous machine is fed from a separate three-phase converter. Naturally, degradation of motor performance occurs during faulted operation because the two remaining, unbalanced output currents result in torque pulsation in the motor. This situation leads to an increase in power losses. The pulsating-torque can also cause mechanical resonance problems. Therefore, the two healthy phase currents must be controlled to produce the same flux and torque as before the fault occurs. In this section the control strategies to maintain satisfactory performance of faults for voltage source inverter motor drives is presented. When a drive is operating in a fault-mode condition, the control algorithms need to be modified in order to insure the continuous operation of the drive with the minimum of performance degradation. In case of a phase open-circuit fault in one of the machine-drive units, the post-fault control strategy is to disable the faulty-unit and deliver power with the remaining healthy-unit. In case of a short-circuit fault, the post-fault control strategy is to apply a balanced short-circuit through the converter and again continue operation with the healthy unit, this time having to additionally overcome the braking-torque produced by the faulty-unit. A torque compensation technique has been added to improve the machine’s dynamic performance.

5.2.1 Healthy-Operation Condition

The control structure diagram of fault tolerant dual three-phase FS-PMSM operating under normal conditions is shown in *Figure 5.1.* The field-orientated indirect vector-control is employed to keep the motor running at the desired speed. The motor terminals are connected to the six-phase voltage source inverter which is modulated by the pulse width modulation (PWM) technique. The first three-phase flux-switching motor is driven by the first three legs of the voltage source inverter and the second three-phase motor is fed by the last three legs of the converter. As a result, the currents (i_{a1}, i_{b1}, i_{c1}, i_{a2}, i_{b2}, and i_{c2}) can circulate from each inverter leg to the motor stator winding constructed in the flux-switching permanent magnet motor. The first motor currents are transformed to the i_{q1} and i_{d1} by using Park's transformation as shown in (5.1), where $\theta=\theta_r$ is the electrical rotor position. In the same way for the second motor the currents i_{a2}, i_{b2}, and i_{c2} are transformed to i_{q2} and i_{d2} as written in (5.2).

$$\begin{bmatrix} i_{q1} \\ i_{d1} \end{bmatrix} = \frac{2}{3} \begin{bmatrix} \cos(\theta) & \cos(\theta - \frac{2\pi}{3}) & \cos(\theta + \frac{2\pi}{3}) \\ -\sin(\theta) & -\sin(\theta - \frac{2\pi}{3}) & -\sin(\theta + \frac{2\pi}{3}) \end{bmatrix} \begin{bmatrix} i_{a1} \\ i_{b1} \\ i_{c1} \end{bmatrix} \tag{5.1}$$

$$\begin{bmatrix} i_{q2} \\ i_{d2} \end{bmatrix} = \frac{2}{3} \begin{bmatrix} \cos(\theta) & \cos(\theta - \frac{2\pi}{3}) & \cos(\theta + \frac{2\pi}{3}) \\ -\sin(\theta) & -\sin(\theta - \frac{2\pi}{3}) & -\sin(\theta + \frac{2\pi}{3}) \end{bmatrix} \begin{bmatrix} i_{a2} \\ i_{b2} \\ i_{c2} \end{bmatrix} \tag{5.2}$$

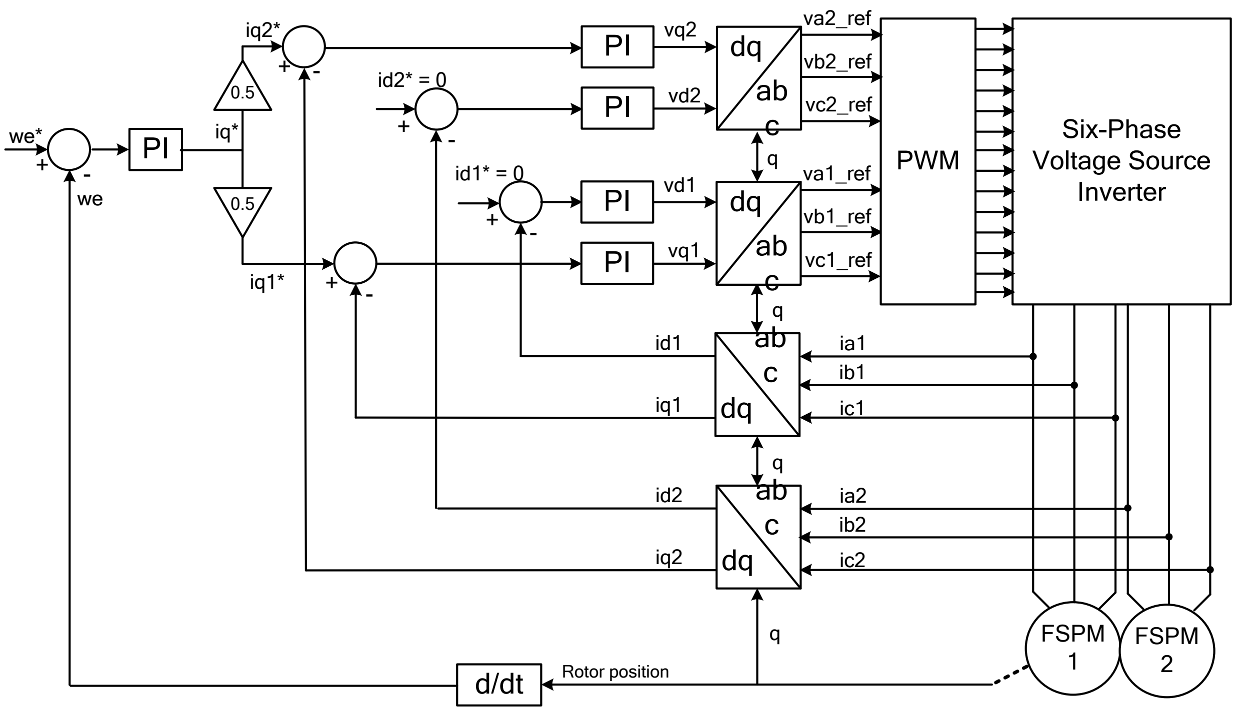

Figure 5.1 Vector-control structure of dual-three-phase flux switching permanent magnet motor under normal-operating conditions

The mechanical rotor position is obtained by using the resolver or the encoder mounted on the shaft of the motor. Then the motor electrical angular velocity calculated from the rotor position is compared to desired speed. The speed controller is designed using PI control technique to generate the q-axis reference current (i_q*) for the motor system drive. For the current controller to generate the output reference voltages for pulse-with modulator it comprises of two sets of current control loop which is designed by the PI control technique. It can be seen from *Figure 5.1* that stator currents for each motor are controlled separately. The d-axis reference currents (i_{d1}* and i_{d2}*) for each motor are set to zero, which is the same as the standard permanent magnet synchronous motor. Additionally, the q-axis reference currents (i_{q1}* and i_{q2}*) for both motors are dedicated from system reference current (i_q*) by dividing by two due to the fact that there are two motors working together under normal-operating conditions. Thus, each motor takes the same actions for the motor drive system operation. These reference transformed currents (i_{q1}*, i_{d1}* and i_{q2}*, i_{d2}*) are compared to the actual transformed currents (i_{q1}, i_{d1} and i_{q2}, i_{d2}). As a consequence, the controlled voltages (v_{q1}, v_{d1} and v_{q2}, v_{d2}) for each motor can be obtained from the PI current controller. Finally, the reference output voltages (v_{a1_ref}, v_{b1_ref}, v_{c1_ref} and v_{a2_ref}, v_{b2_ref}, v_{c2_ref}) needed for the pulse-with modulation for the first motor and the second motor can be provided by using the inverse Park's transformation as show in (5.3) and (5.4), respectively.

$$\begin{bmatrix} v_{a1\_ref} \\ v_{b1\_ref} \\ v_{c1\_ref} \end{bmatrix} = \begin{bmatrix} \cos(\theta) & -\sin(\theta) \\ \cos(\theta - \frac{2\pi}{3}) & -\sin(\theta - \frac{2\pi}{3}) \\ \cos(\theta + \frac{2\pi}{3}) & -\sin(\theta + \frac{2\pi}{3}) \end{bmatrix} \begin{bmatrix} v_{q1} \\ v_{d1} \end{bmatrix} \tag{5.3}$$

$$\begin{bmatrix} v_{a2\_ref} \\ v_{b2\_ref} \\ v_{c2\_ref} \end{bmatrix} = \begin{bmatrix} \cos(\theta) & -\sin(\theta) \\ \cos(\theta - \frac{2\pi}{3}) & -\sin(\theta - \frac{2\pi}{3}) \\ \cos(\theta + \frac{2\pi}{3}) & -\sin(\theta + \frac{2\pi}{3}) \end{bmatrix} \begin{bmatrix} v_{q2} \\ v_{d2} \end{bmatrix} \tag{5.4}$$

5.2.2 Faulty-Operation Condition

Under faulty operating conditions, the motor currents are no longer balanced sinusoidal waveforms resulting in pulsating motor torque and unsmooth motor speed. To maintain satisfactory system performance, the appropriate control strategy needs to be taken into account.

Figure 5.2 and *Figure 5.3* show the modified control structure diagram for the fault-tolerant dual three-phase flux-switching permanent magnet motor under faulty-operating conditions. The field-orientated indirect vector control is still employed to keep the motor operating uninterrupted with the satisfactory system performance compared with that under normal operating condition. In *Figure 5.2* the motor drive control structure modification is presented against a fault due to the loss of the first motor operation. Such a fault would be caused by the loss of the connection between the motor terminals and the PWM voltage source inverter legs. In the case that the first motor stops working it cannot take action for a longer period to control the motor drive system. Its three stator currents suddenly drop to zero leading to the loss of control from the first motor. By losing one motor operation the speed of the motor decreases considerably. In order to recover motor speed back to the desired level and to maintain the system performance the remaining motor needs to take more responsibility. It can be seen from *Figure 5.2.* that it is essential to set the i_{q2}* to be the same as i_q*. By following this solution the speed of the motor can return to the command speed. In addition, the system drive can continue to operate the same as during normal-operating condition. However, the remaining motor needs to have the capability of having a higher current rating. *Figure 5.3* presents the vector-control structure of the dual three-phase flux-switching permanent magnet motor when the second motor is disabled.

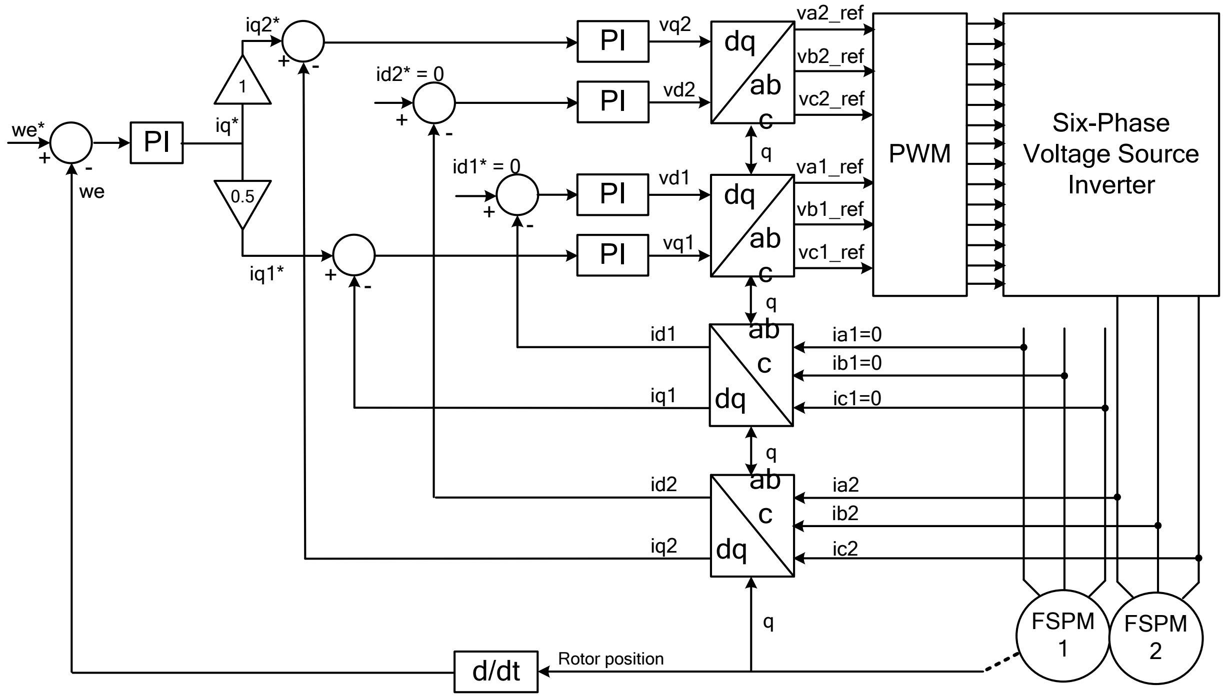

Figure 5.2 Vector-control structure of dual-three-phase flux-switching permanent magnet motor under fault-operating condition (the first motor is disabled).

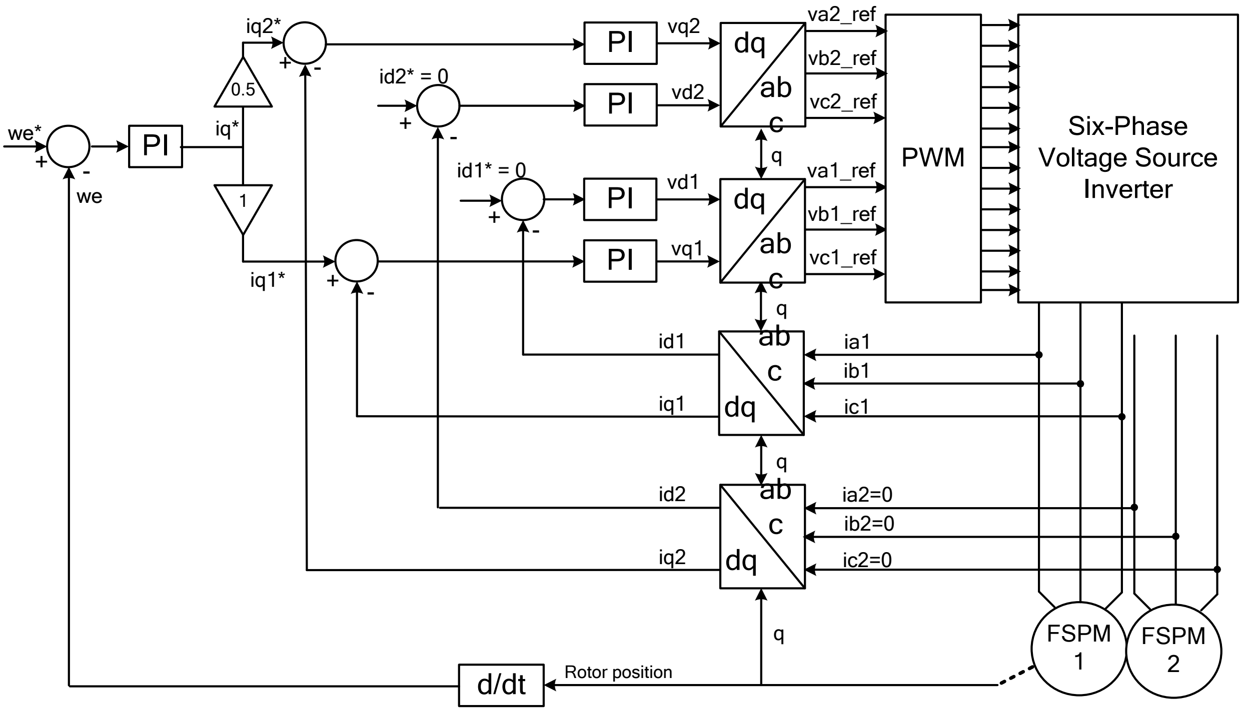

Figure 5.3 Vector-control structure of dual-three-phase flux-switching permanent magnet motor under fault-operating condition (the second motor is disabled).

5.3 Summary

The aim of this chapter is to describe the implementation of a fault tolerant vector-control scheme applied to a dual-fed Flux-Switching Permanent Magnet Synchronous Machine (FS-PMSM). Drive control is maintained during both open-circuit and fault-circuit faults by adopting the appropriate control strategies. It should be emphasized that a proposed new fault-tolerant vector-control strategy applied to a prototype dual FS-PMSMs is supplied by two voltage source converters with real-time digital processor (DSP) control techniques and is based on vector pulse-width modulation (PWM). The control scheme is verified by both simulation in *Section 6* and experiential results in *Section 7* which are carried out with the prototype of the proposed fault-tolerant Flux Switching permanent magnet synchronous machine and six-phase motor drive system with a real-time DSP control. Experimental result backing simulation studies will illustrate the robustness of this drive topology to operate in safety-critical applications.

6 SIMULATION RESULTS

6.1 Simulink Simulation of FS-PMSM Control

To verify the effectiveness of the dual three-phase flux-switching permanent machine associated with field-oriented indirect vector-control, a variety of operation conditions under both healthy- and faulty-situations needs to be clearly investigated. The verification results have been carried on by using MATLAB Simulink. The simulation schematic of the entire motor drive system required in order to control the speed and torque of the machine without load and load conditions is presented in *Figure 6.1* . This schematic consists of two important parts. Firstly, the dual three-phase flux-switching permanent magnet machine model which is created by utilising the mathematic equations as previously described in *Section. 3.3*. Secondly, the filed-oriented indirect vector-control is employed to keep the machine running with adjustable speeds and load torques. The total electromagnetic toque can be obtained by summing the individual torque generated from each three-phase flux-switching permanent magnet machine. Therefore, under-healthy operation both the three-phase flux-switching machine participates in taking action to maintain the system operating conditions. Due to the merits of the dual-three-phase flux-switching permanent magnet machine in providing fault-tolerant capability the machine drive system can continue to operate in the event of either the first motor or the second motor being disconnected from the PWM voltage source inverter. It is clear that under healthy-operating condition each three-phase flux-switching permanent magnet motor takes responsibility to maintain half of the load. As a result, the total torque at the desired motor speed can be effectively achieved. On the other hands, during the absence of one motor the remaining motor and the modified controller need to maintain satisfactory performances of the whole motor drive system.

The mathematical equations of the FS-PM motor as derived previously are synthesized to create the simulink Matlab model. It is necessary to investigate the behaviours of the FS-PM motor corresponding to its vector-control under the different-operating conditions. The simulation results are presented to indicate that the designed controller has the ability to control the FS-PM motor in a wide range of speeds under no-load and applied load torque conditions.

To investigate the effectiveness of the fault-tolerant flux-switching permanent magnet motor, the simulation results can be classified into two sections: under-normal and fault-conditions. The system performances under the different-operating conditions are presented to demonstrate the feasibility of the dual three-phase flux-switching permanent magnet motor control system.

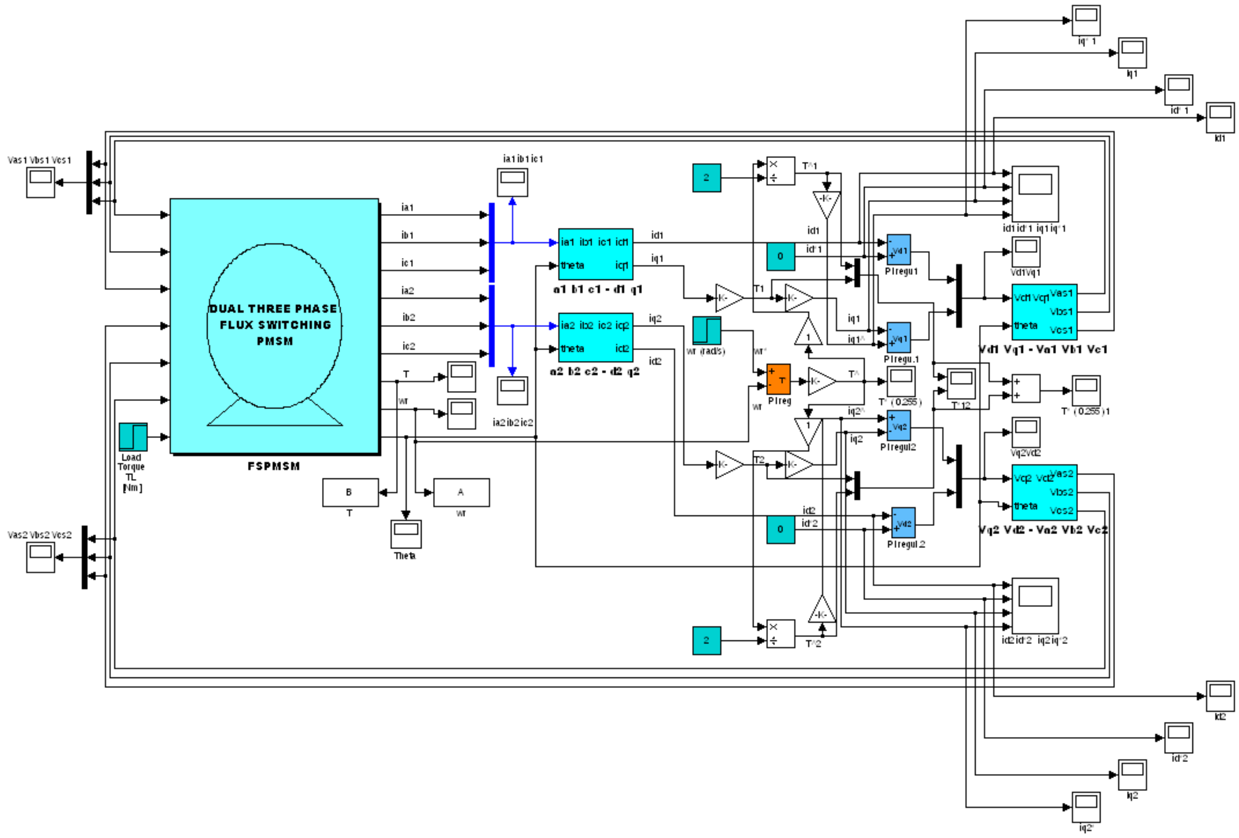

Figure 6.1 The simulation schematic of a dual three-phase flux-switching permanent magnet motor.

6.2 Healthy-Operation Conditions

To demonstrate the effectiveness of the dual three-phase flux-switching permanent magnet motor control the operation of both directions of motor rotation should be investigated. *Figure 6.2* shows the speed response of the considered flux-switching motor operating under speed reversal mode from reverse direction rotation (-500rad/s) to forward direction rotation (500rad/s). The motor starts operating from standstill to the command speed in the reverse direction. As can be seen, the motor can constantly rotate at the desired speed. After that at the time of 13 s, the motor is forced to operate in the opposite direction. It is clearly seen that the motor can follow the required speed.

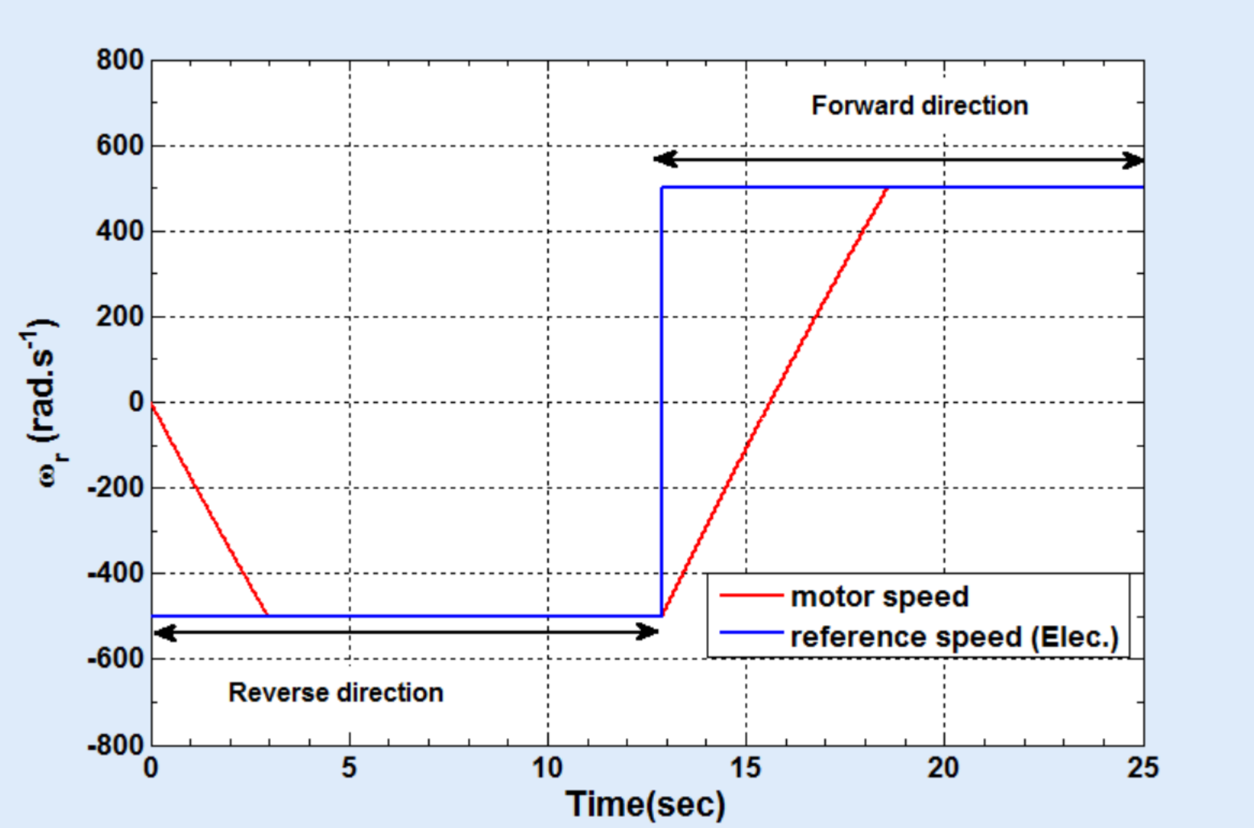

Figure 6.2 The speed reversal of the motor from -500rad/s to 500rad/s

In adjustable speed drive systems the motor needs to operate in a variety of speed ranges. In order to achieve the desired speeds the controller plays an important role in regulating the speed of the motor. To demonstrate the effectiveness of the dual three-phase flux-switching permanent magnet motor control under speed variations, the simulation results of the motor speed at 500rad/s, 1000rad/s and 1500rad/s is presented in *Figure 6.3*. It is clearly seen that the controller can regulate the speed of the flux-switching permanent magnet motor at the reference speeds.

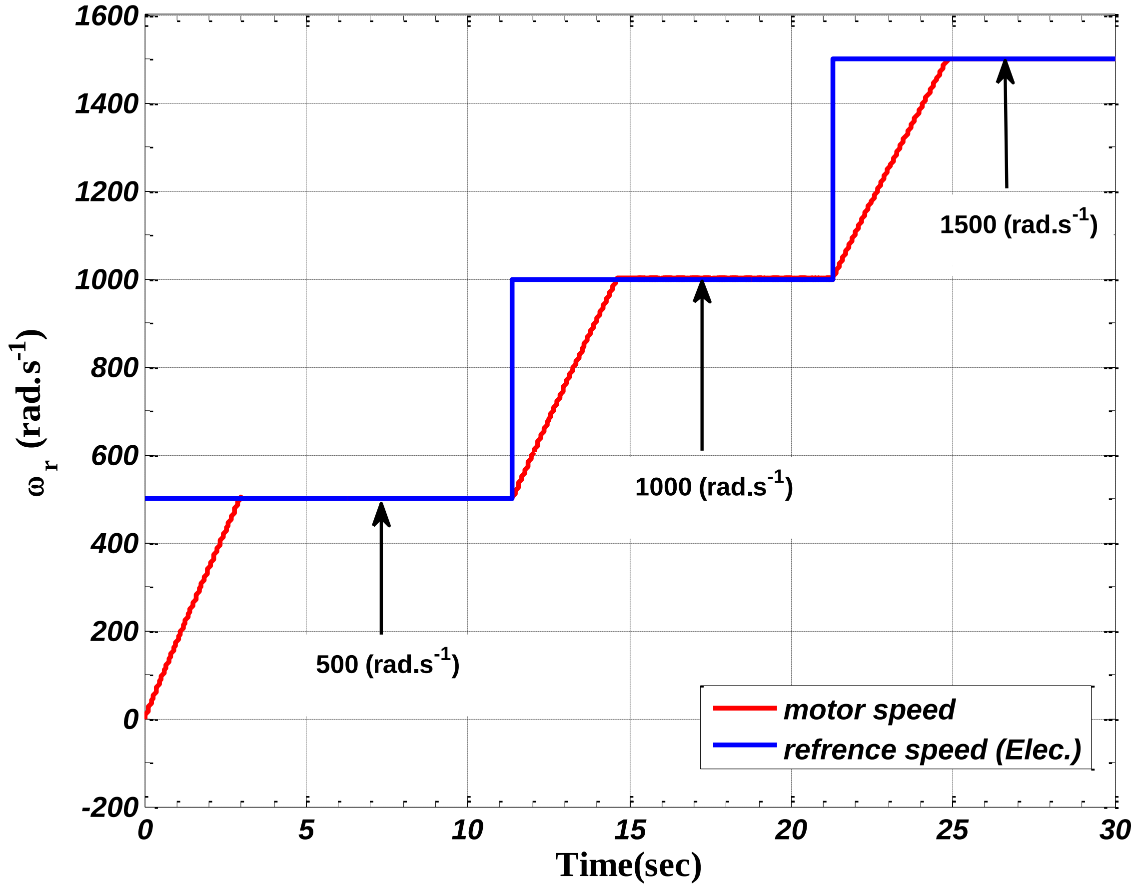

Figure 6.3 The speed response of the motor at 500rad/s, 1000rad/s and 1500rad/s

6.3 Faulty-Operation Conditions

A fault-tolerant system should have the ability to respond to any hardware or software failure, keeping the minimum functionality which allows the system to continue to operate. This is crucial in safety-critical aerospace applications [54]. The model described in *section 5* can be easily programmed into most simulation environments and has a rapid solution time. For the work undertaken here, the model was incorporated into a Matlab/Simulink model of the full motor-drive system, including a vector-control algorithm oriented with the PM flux linkage and a mechanical load model. The inverter in this case has been modelled by ideally controlled voltage sources but could easily be extended to incorporate real device models if required.

This section demonstrates the effectiveness of the fault-tolerant dual three-phase flux-switching permanent magnet motor drive control system in the presence of a fault. The fault being considered is the loss of one three-phase flux-switching permanent magnet motor. Therefore, the remaining healthy three-phase flux-switching permanent magnet motor needs to be controlled in order to keep the drive system operating continuously under fault-situation.

6.3.1 Open-Circuit Fault

Figure 6.4 shows an indirect vector-control of a FS-PMSM under faulty (unhealthy) operating conditions (Three-phase open-circuit fault). *Figure 6.5* shows the *q* and *q* current components during a speed transient, followed by the application of a 1-N m load step at *t=7.5* and an open-circuit fault at *t* = 10 s, respectively. The drive system is speed controlled. The speed reaches the steady state at 5s due to moment of inertia. As expected, the variation of iq_1 and iq_2 is proportional to the torque produced by the respective machine unit. It can be observed that the torque is equally shared by the machine units until the open-circuit fault. At *t* = 10 s, when an open-circuit-phase condition is introduced to motor 2, motor 1 picks up the entire load. *Figure 6.6* shows the two motors' phase currents before and after the fault occurs.

It can be observed that the simulated phase currents of the two-machine units (*Figure 6.6*) contain a significant amount of even harmonics, which is in the nature of this machine topology as will be further demonstrated later on in *section 7.*

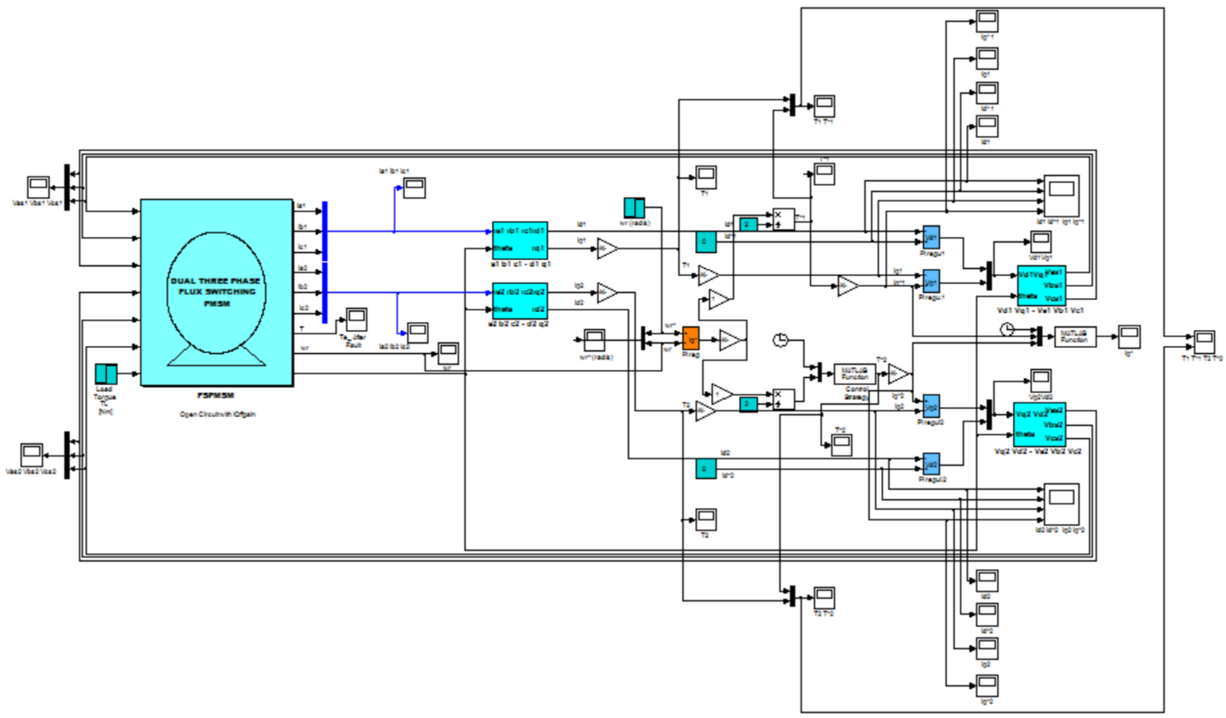

Figure 6.4 The simulation schematic of a vector-control of FS-PMSM under open-circuit fault operating conditions

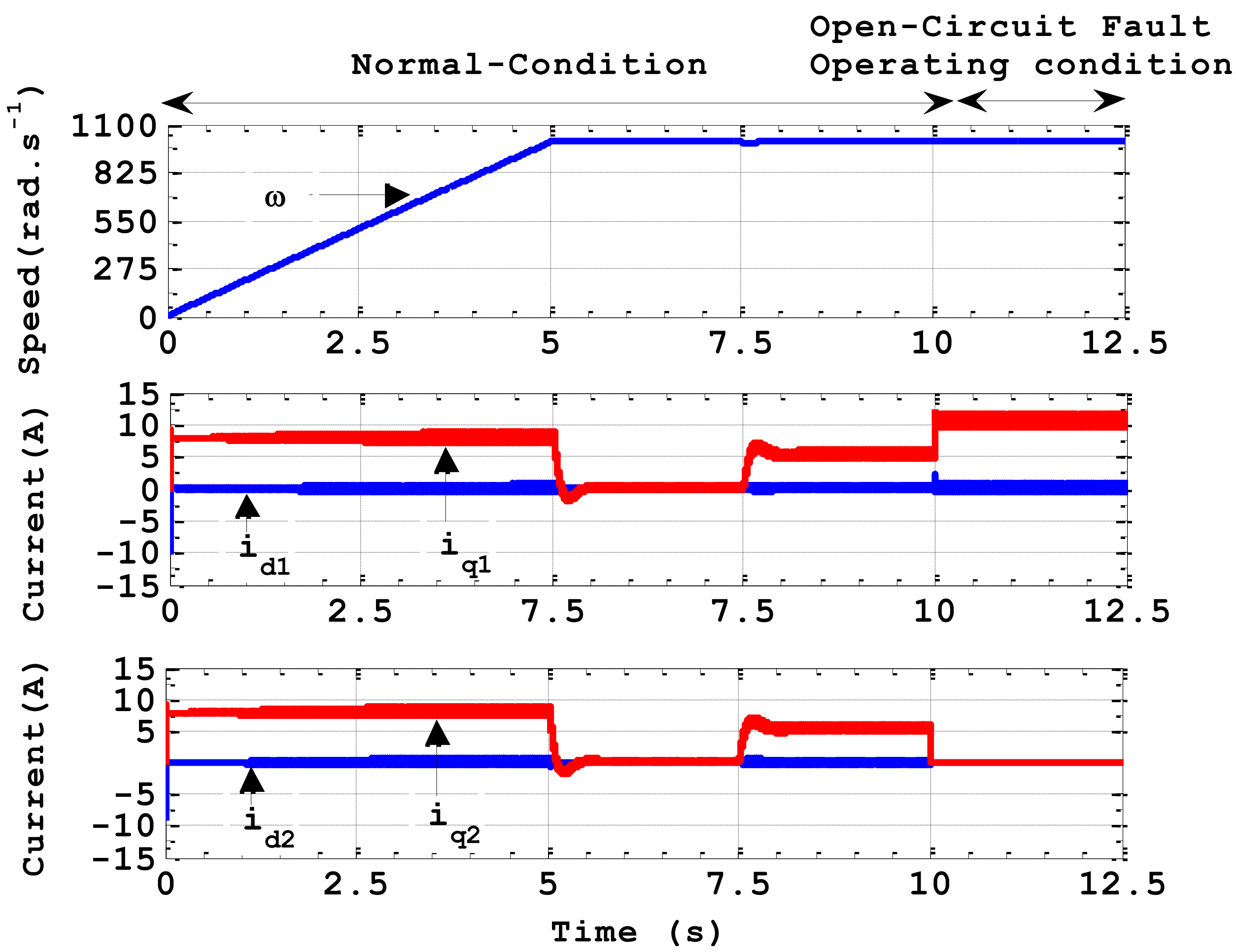

Figure 6.5 Behavior of the FS-PMSM at the speed of 1000 rad/s under normal- and open-circuit fault operating conditions

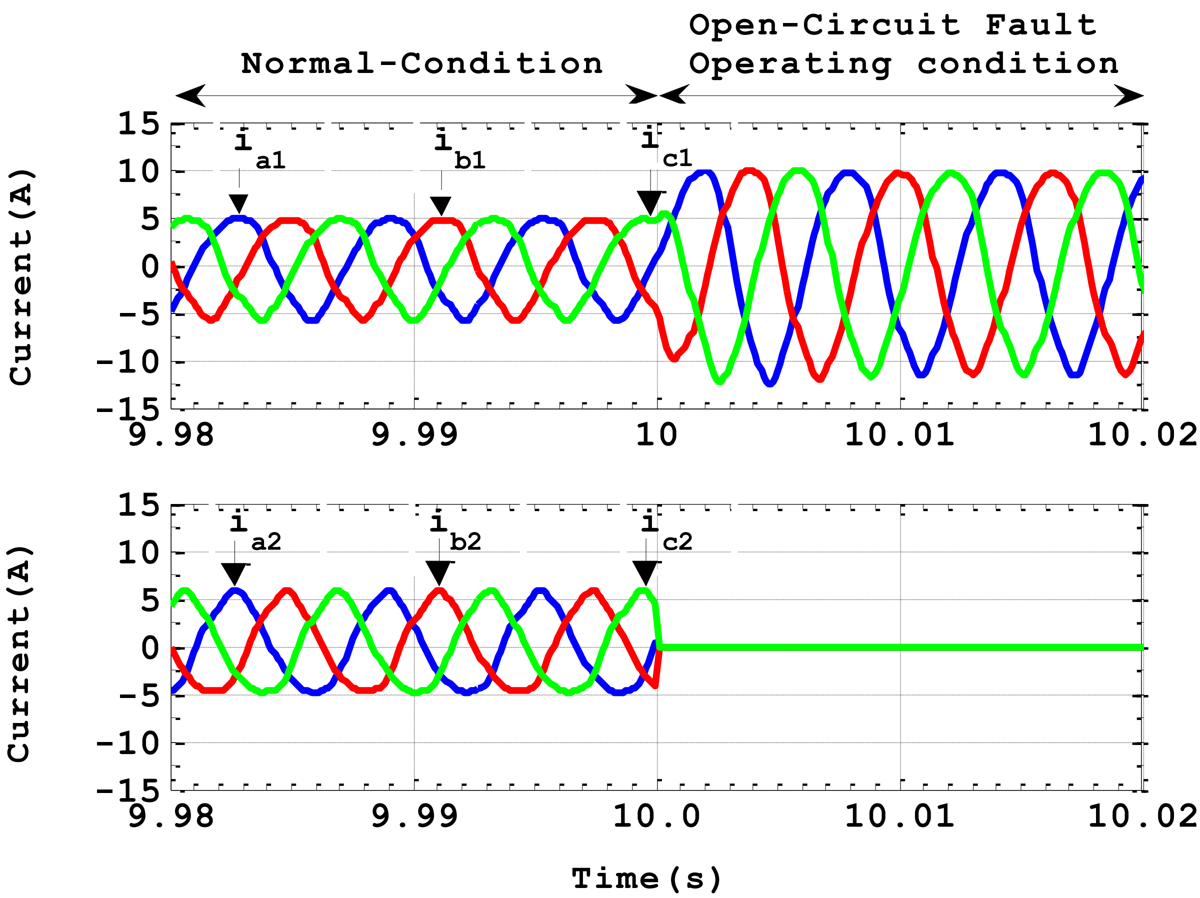

Figure 6.6 Behavior of the currents of the FS-PMSM at the speed of 1000rad/s under normal- and open-circuit fault operating conditions

6.3.2 Short-Circuit Fault

Figure 6.7 shows the simulation schematic of a vector-control of FS-PMSM under faulty-operation condition. The scheme is based on a dual three-phase FS-PMSM supplied from two separate vector-controlled voltage-sourced inverter drives. *Figure 6.8* shows the two-machines-unit phase currents before and after a balanced short-circuit fault is applied on motor 1. *Figure 6.9* shows the corresponding drive behaviour. It can be observed that the speed is maintained with motor 2 having to overcome the lost torque from motor 1 as well as the-braking-torque due to the short-circuit currents. In this case, i_{q1} is fed back to compensate for the braking-torque. This resulted in the current increasing by 160% in the healthy machine and by 40% in the faulty one.

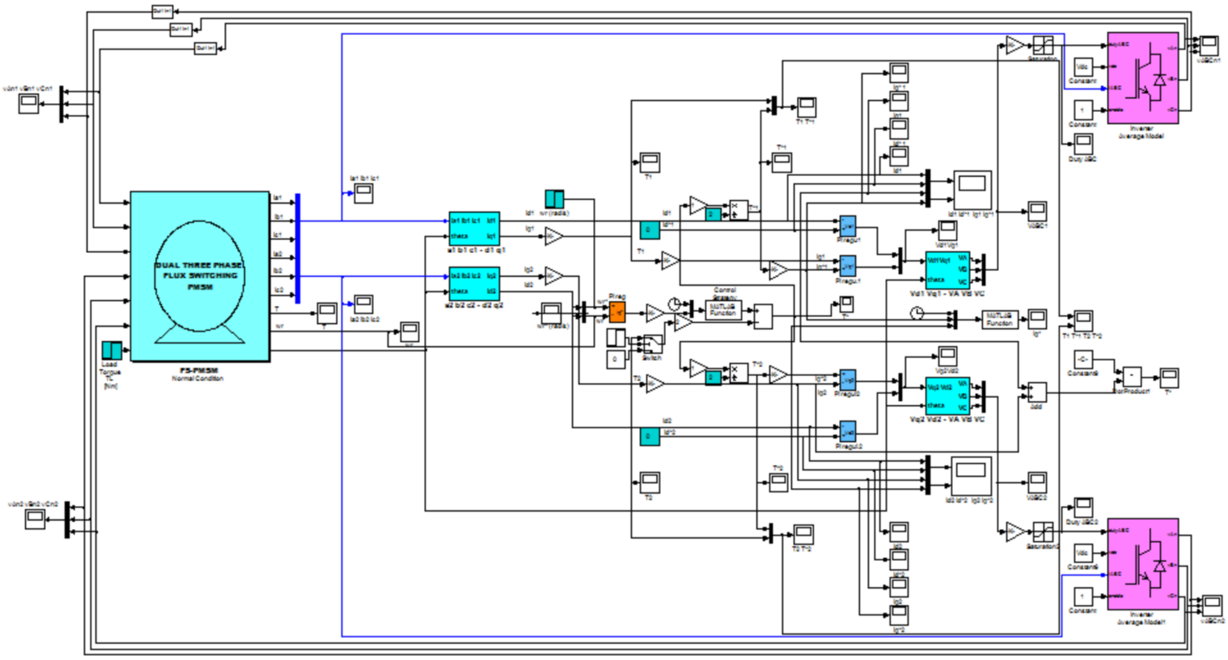

Figure 6.7 The simulation schematic of a vector-control of FS-PMSM under short-circuit fault operating conditions

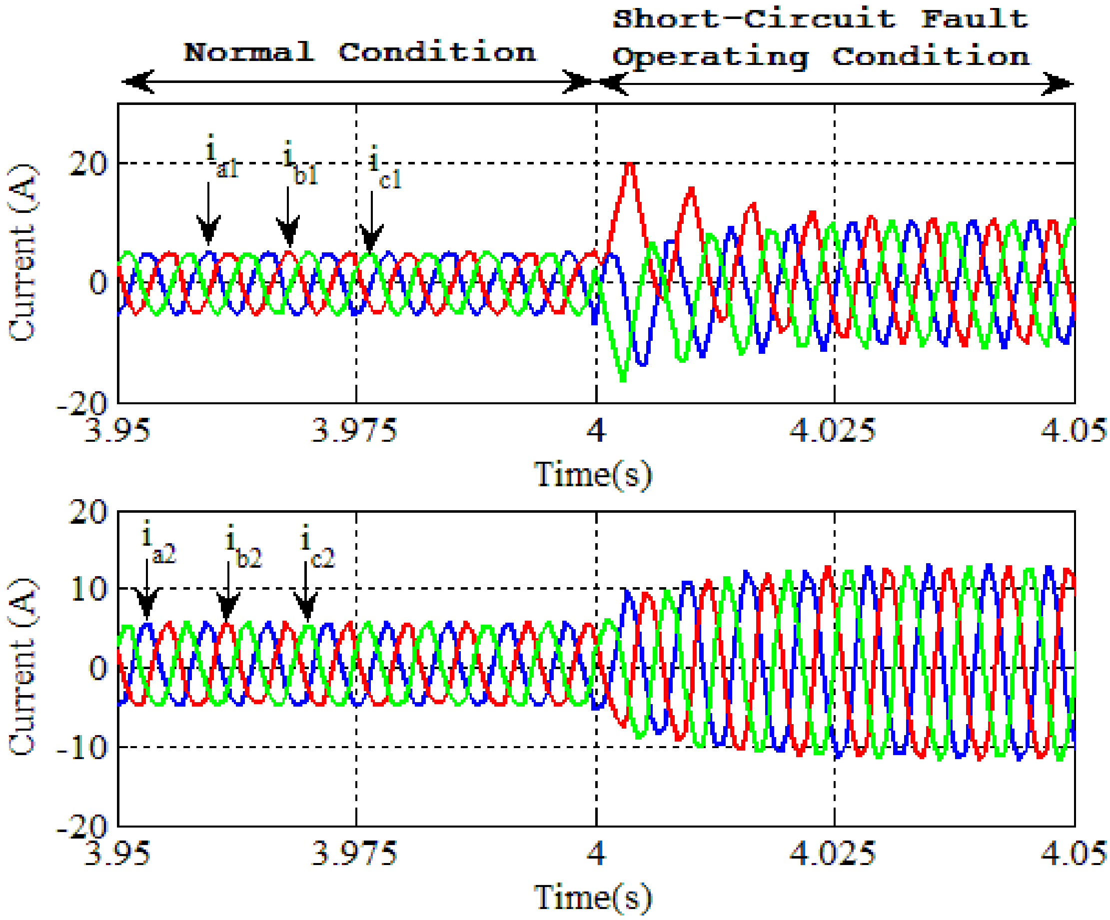

Figure 6.8 Simulation performance of the proposed dual FS-PMSM (M_1 is short-circuited) under different-operating conditions. (a) Currents of motor 1. (b) Currents of motor2.

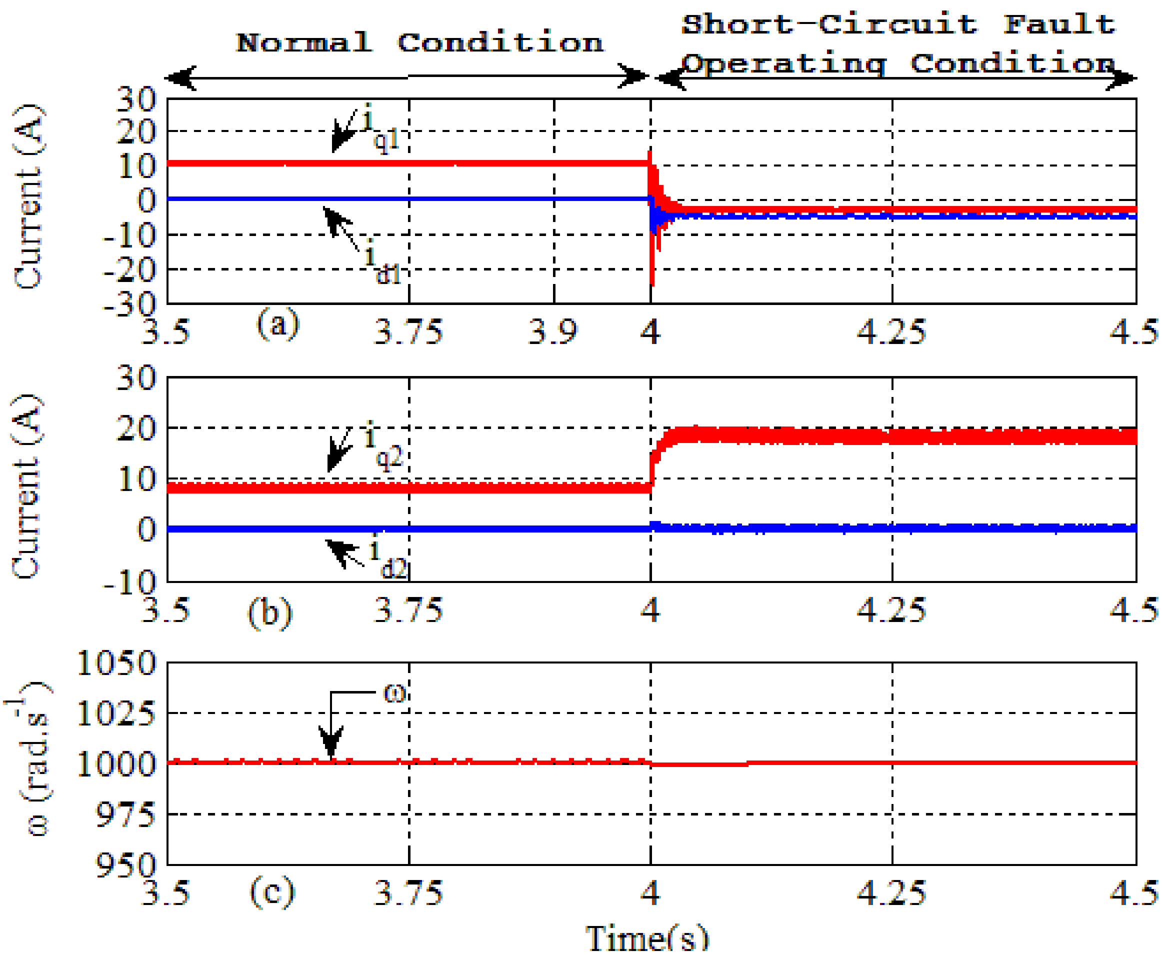

Figure 6.9 Simulation performance of the proposed dual FS-PMSM (M_1 is short-circuited) under normal-mode of operation and under a balanced short-circuit condition (a) Transformed currents of motor 1. (b) Transformed currents of motor 2 (c) Motor speed.

The next condition to be tested is a single-phase fault. The motor is initially operated under normal-condition, and then a single-phase fault is introduced. After a period of time, a balanced three-phase short-circuit fault (simultaneous short-circuit across all the three-phases) is applied to the faulty-motor through the converter. The simulation results of the currents are plotted in *Figure 6.10* and *Figure 6.11*

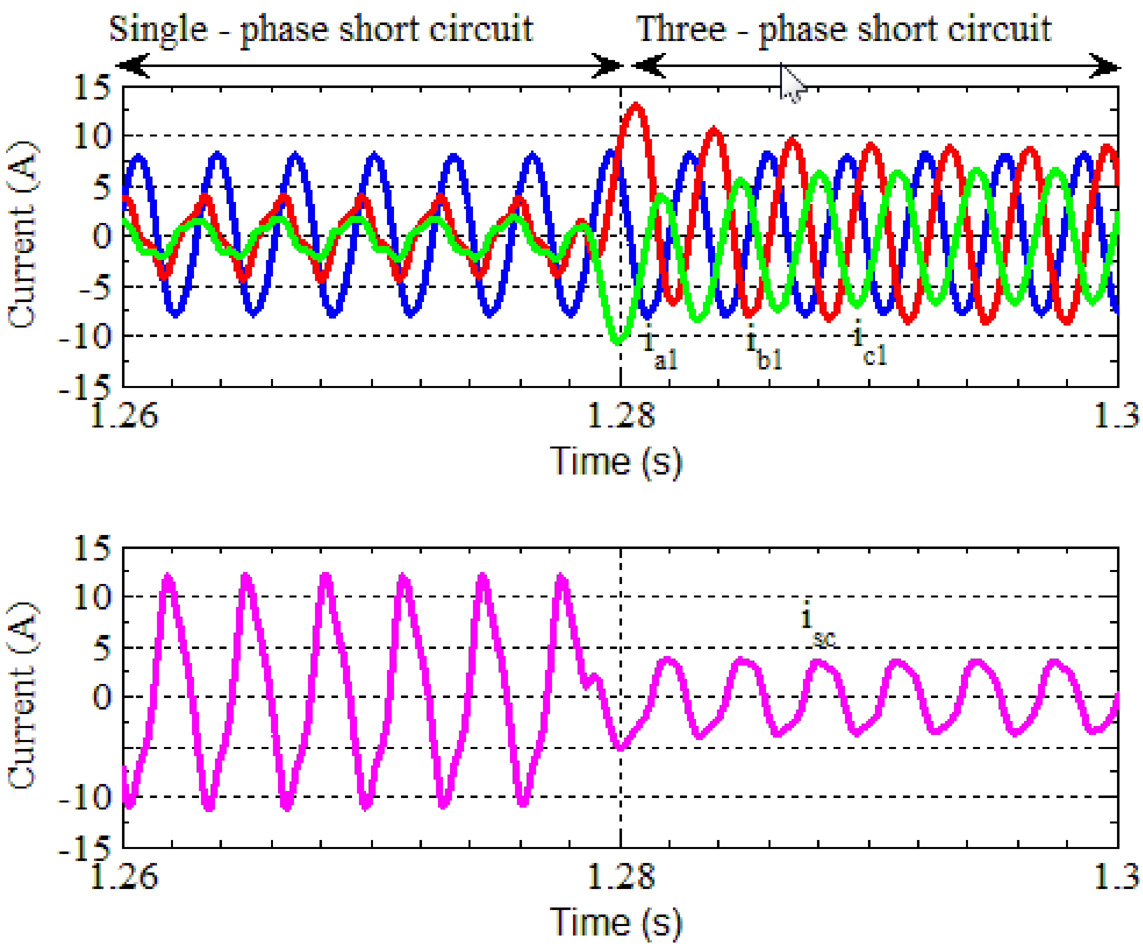

Figure 6.10 Simulation short-circuit current under different-operating conditions (M_2 is short-circuited) at the speed 2000 rad/s

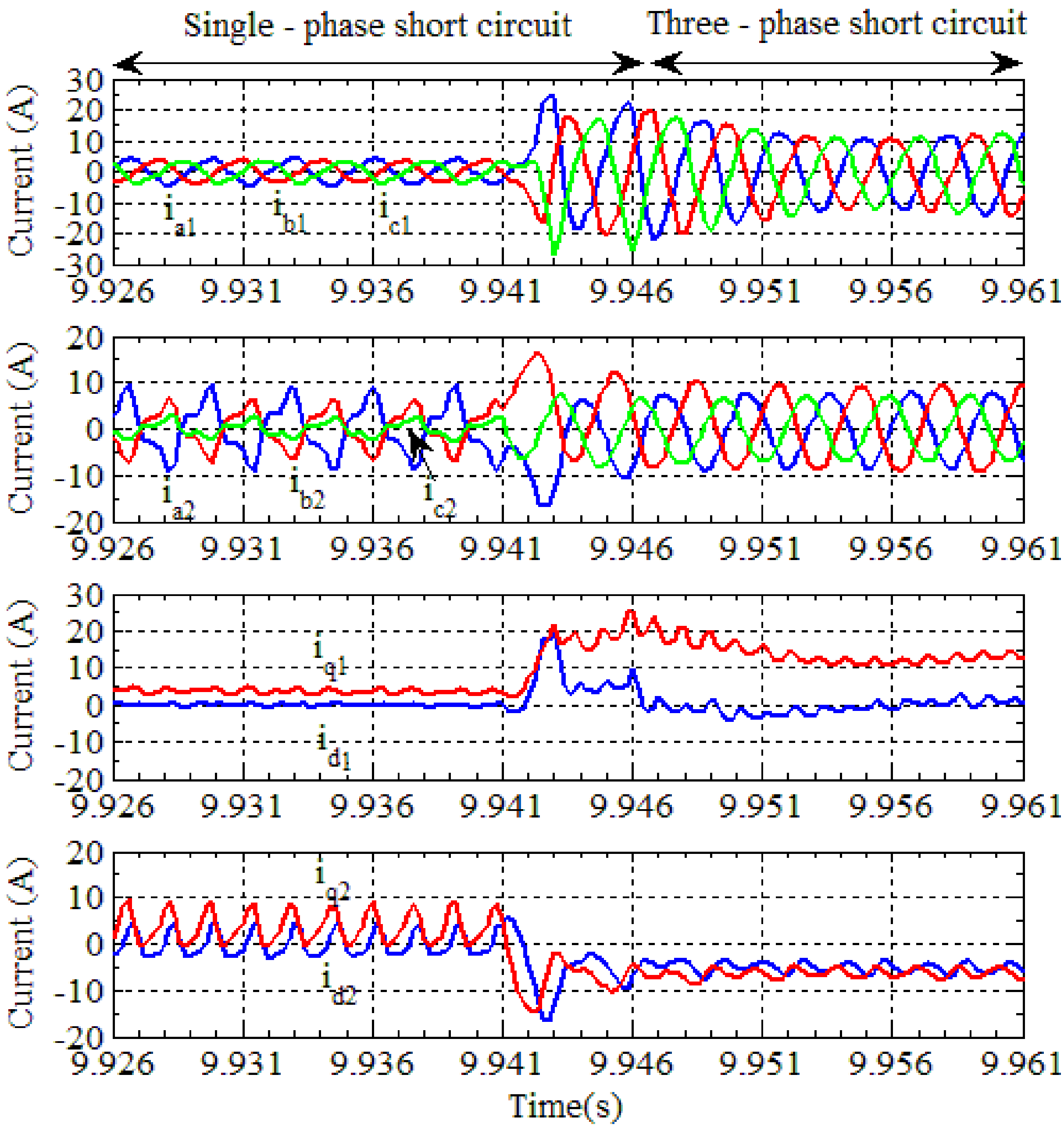

Figure 6.11 Simulation performance of the proposed dual FS-PMSM (M_2 is short-circuited) at the speed of 2000 rad/s under single- and balanced short-circuit operating conditions a) Currents of motor1 (b) Currents of motor2 (c) Transformed currents of motor1 (d) Transformed currents of motor 2.

6.4 Field-Weakening Operation

The field-oriented control is also called an indirect-control (the torque is indirectly controlled through the currents). *Figure 6.12* shows the simulation schematic of a vector-control of FS-PMSM with lookup table under no-load and with field-weakening based on voltage controller (*I-controller*). The voltage controller is using the voltage error signals between the maximum voltage output (voltage demand) and back-EMF (Actual voltage). The Back-EMF is calculated from the direct and quadrature voltages v_d and v_q. The field-weakening controller must identify all delays between the demand and actual voltage. The output of the voltage regulator (*I-regulator*) determined the required mount of the demagnetizing current (current demand). In addition, the onset of flux-weakening could be adjusted to prevent the saturation of the current regulators required by vector-controllers of FS-PMSM. Conventionally, two current controllers are always required to achieve torque (*q-axis current*) and flux (*d-axis current*) control. The reference value of quadrature current i_q is obtained from the saturation limiter. The input of the saturation limiter is the reference speed and the maximum upper/lower limit of the quadrature current ($\pm i_{qmax}$). The maximum upper/lower limit value of the quadrature current ($\pm i_{qmax}$) is obtained from equation (4.57).

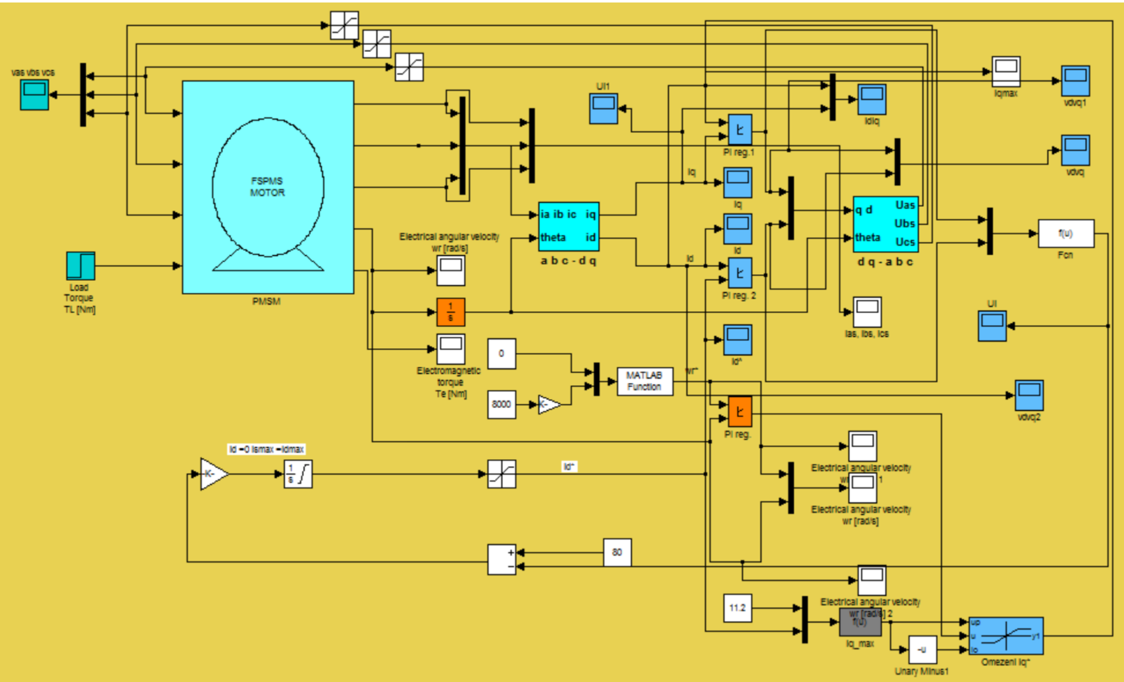

Figure 6.12 The simulation schematic of a vector-control of FS-PMSM with field-weakening based on a voltage controller

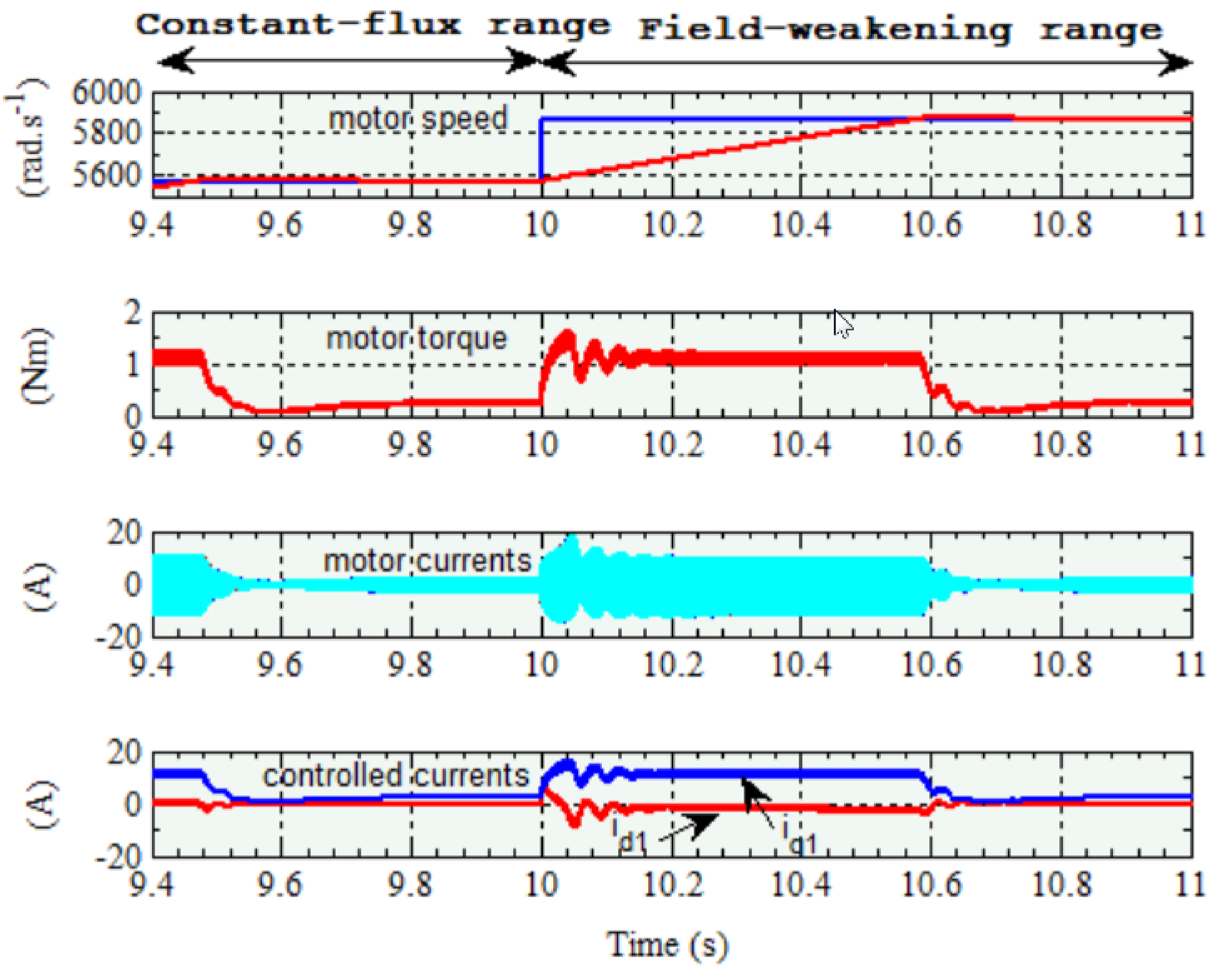

Figure 6.13 Performance of the proposed dual FS-PMSM during operation below /above rated speed of 7600 rpm a) Motor speed (b) Motor torque (c) Motor currents (d) Transformed currents of motor 1

Figure 6.13 shows the Performance of the proposed Dual FS-PMSM during operation, below and above the rated speed 7600 rpm. The effect of field-weakening can be achieved by advancing the current vector beyond $\delta = \pi/2$ i.e. introducing a current component in the negative d-axis to create a d-axis flux in opposition to that of the stator permanent magnets, resulting in a decrease air-gap flux. As a consequence i_q and then the torque are reduced in order not to exceed the maximum output current 11.2 A.

Figure 6.14 shows the motor speed Performance of the proposed dual FS-PMSM during the operation (below and above the rated speed 7600 rpm). *Figure 6.15* shows the zoomed in reference voltages and motor currents under both constant-flux and field-weakening range.

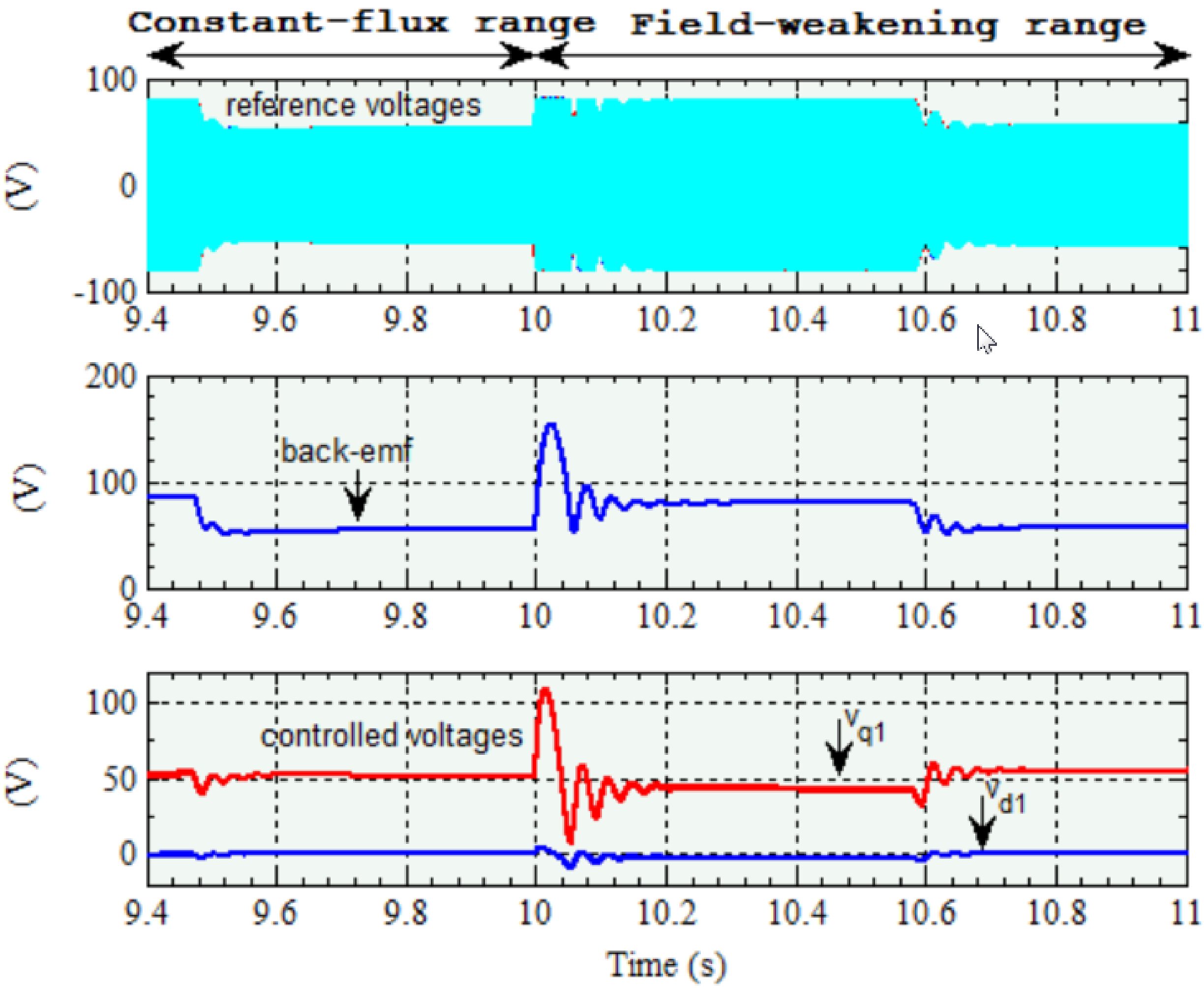

Figure 6.14 Performance of the proposed dual FS-PMSM with during operation below/above rated speed 7600 rpm a) Reference voltages (b) Back-EMF (c) Transformed voltages of motor 1

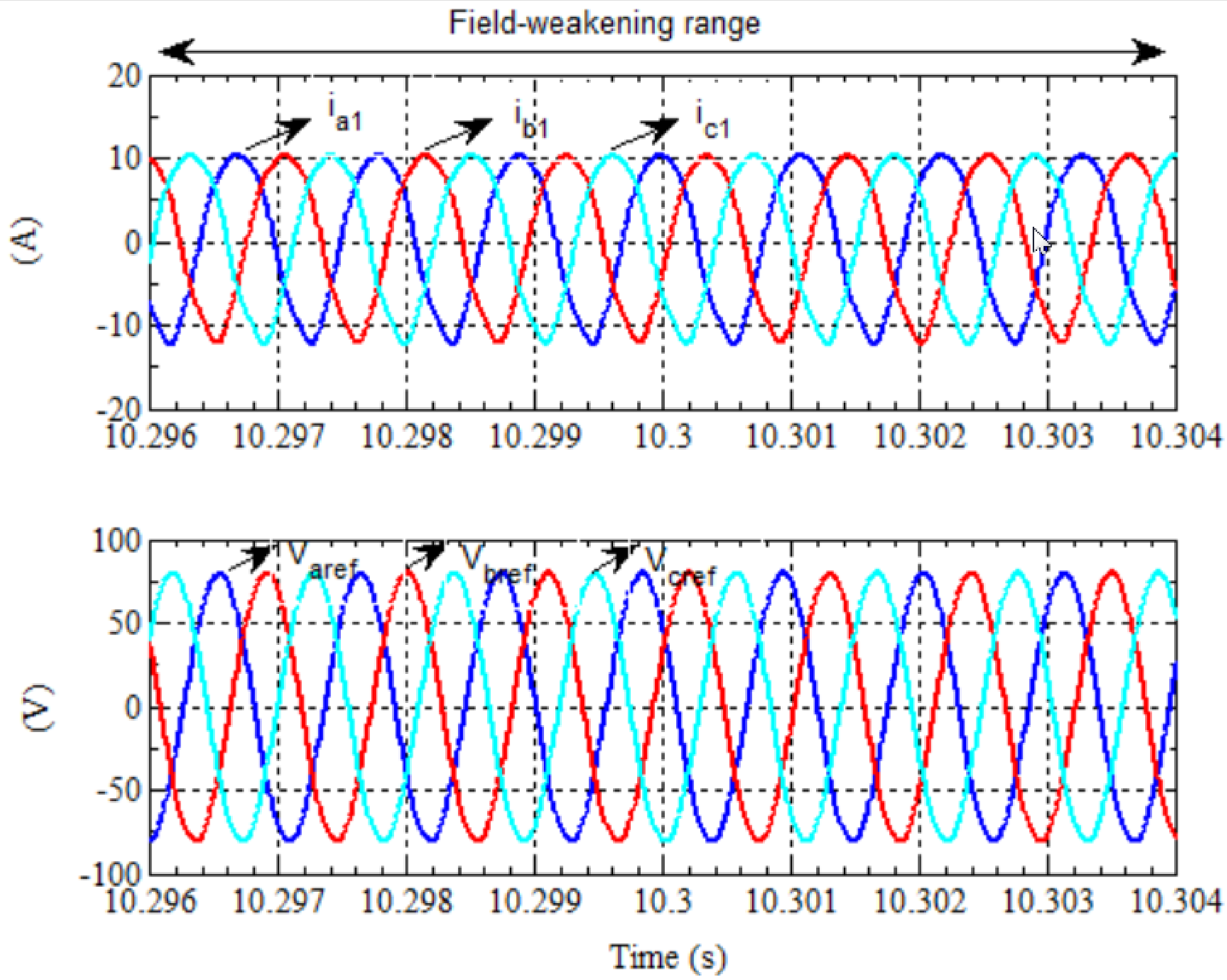

Figure 6.15 Performance of the proposed dual FS-PMSM with during operation below/above rated speed 7600 rpm a) Reference voltages (b) Motor currents (Zoomed in) (c) Transformed voltages of motor 1 (zoomed in)

6.5 Summary

This chapter provides a brief description of the vector-control technique applied for a dual three-phase Flux-Switching Permanent Magnet (FS-PM) motor which has two separate three-phase windings, each supplied separately. This high-speed motor is designed to achieve the fault-tolerant capability, which in the event of a fault in one of the three-phase motors the other one can continue to operate unaffected. In addition, this modular approach also provides the minimal electrical, magnetic and thermal interaction between phases of the drive. The three-phase mathematical model of permanent magnet synchronous motor is primarily studied to create the dual three-phase FS-PM motor model. To investigate the behaviour of the fault-tolerant FS-PM motor under the different-operating conditions, the considered FS-PM motor model has been carried out using Matlab-Simulink. The simulation results of the FS-PM motor with the vector-control method are presented at the different speed operations. The results show that the motor can operate properly under base-speed (7600rpm). However, the field-weakening strategy needs to be taken into consideration in order to enhance the above based-speed operations. Moreover, the loss minimization optimal control technique should be applied to the system in order to enhance the performance and efficiency of the considered FS-PM motor. A novel flux-weakening control of FS-PMSM based on voltage controller incorporating wide-range speed regulation is presented. The cross-coupling effect between d and q-axis is re-examined and a speed and flux-weakening control proposed. Definitely has been proved that the controller is able to achieve the closed-loop speed control and flux-weakening control simultaneously.

In this chapter the fault-tolerant capability is demonstrated in the presence of faults. Simulation results are presented in this chapter to validate the effectiveness of the fault-tolerant FS-PMSM drive. Simulation results have been compared in both healthy- and faulty-mode operations. Short-circuit faults as well as open-circuit faults have been considered. The experimental testing is implemented and will be shown in *Section 7* to validate the ability of FS-PM motor under a wide-range of operations.

7 EXPERIMENTAL DRIVE SYSTEM

In order to experimentally validate experimentally the effectiveness of the proposed voltage source inverter and flux-switching permanent magnet synchronous machine introduced in Chapters 3 and 4, a laboratory prototype should be considered for implementation In this chapter, the overall structure of the voltage source inverter prototype is presented. Voltage source inverter control implementation for the motor drive application is based on a digital signal processor (DSP) and a field programmable gate array (FPGA) as will be explained.

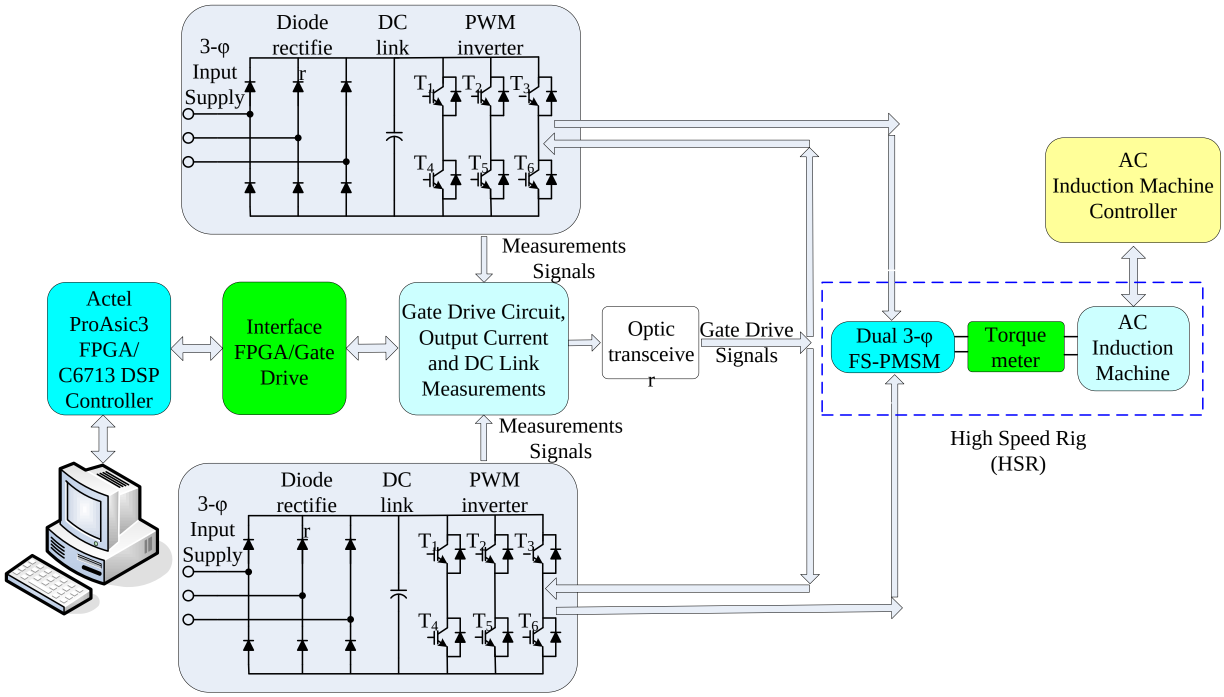

Figure 7.1 Block diagram of the experimental system.

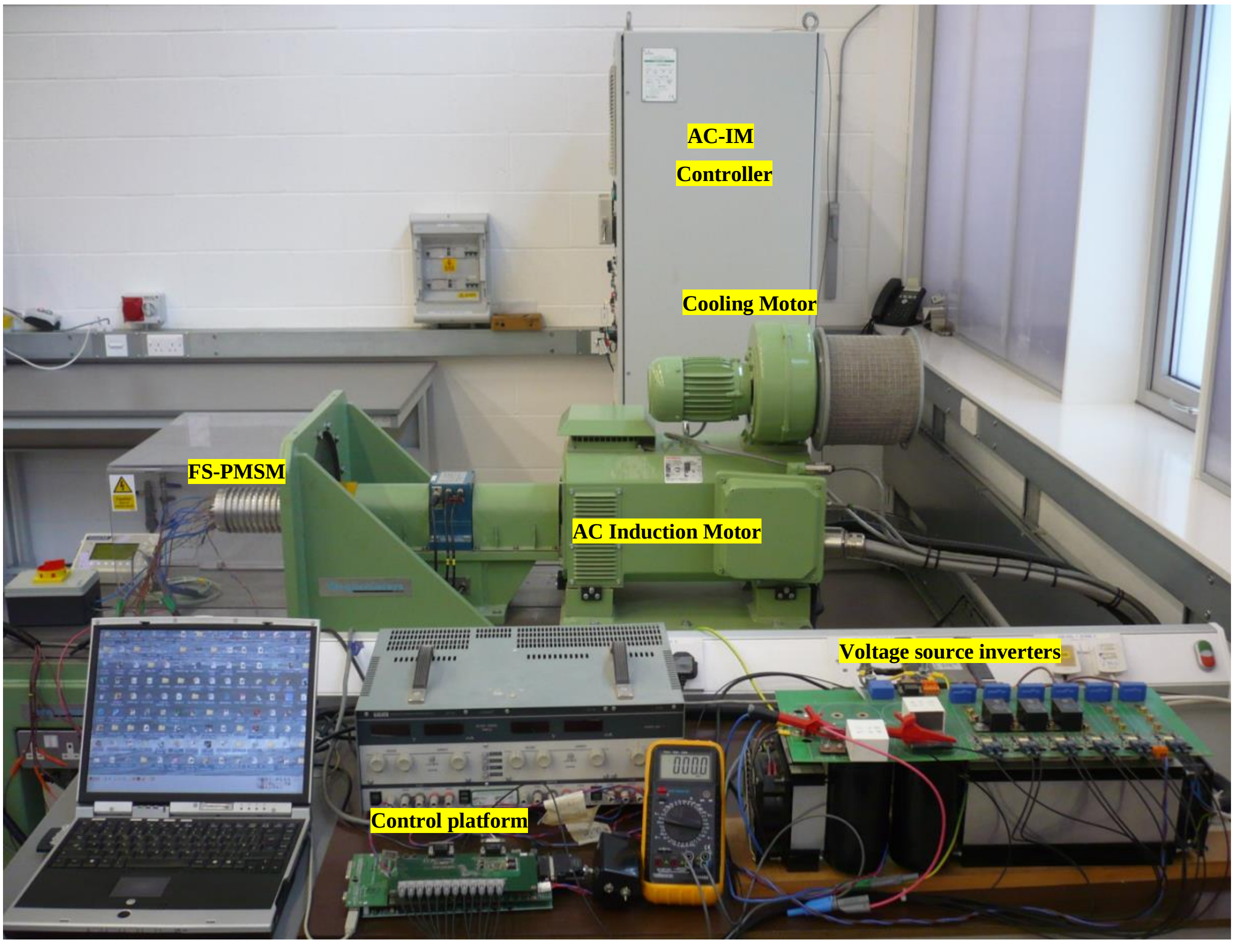

Figure 7.2 Experimental setup

A vector-controlled dual three-phase inverter and machine were set up on an instrumented test rig as shown in *Figure 7.1* and *Figure 7.2*. The machine coils were separately brought out to enable experimentation with different winding connections and apply faults to different winding locations. The machine was loaded using a vector-controlled induction machine with a rated power of 60 kW at 20 000 r/min coupled through a torque transducer as shown in *Figure 7.2*. The overall vector-control scheme adopted is shown in *Figure 7.3*. where the torque demanded by the speed loop is shared equally by the two-motor units in healthy-operation. The field-oriented scheme is implemented on a control board consisting of a Texas Instruments C6713 processor and Actel ProAsic3 FPGA. The PWM switching signals are transmitted to the gate drivers using high-performance fiber-optic links. The two three-phase channels of the FS-PMSM are fed from separate converter units, these are shown in *Figure 4.2(b)* and *Figure 7.2*. The rotor position is obtained from a resolver transducer.

The six stator-pole seven-rotor-pole flux-switching machine was constructed from 0.35-mm silicone laminations and samarium cobalt PMs. The machine was totally enclosed and naturally ventilated.

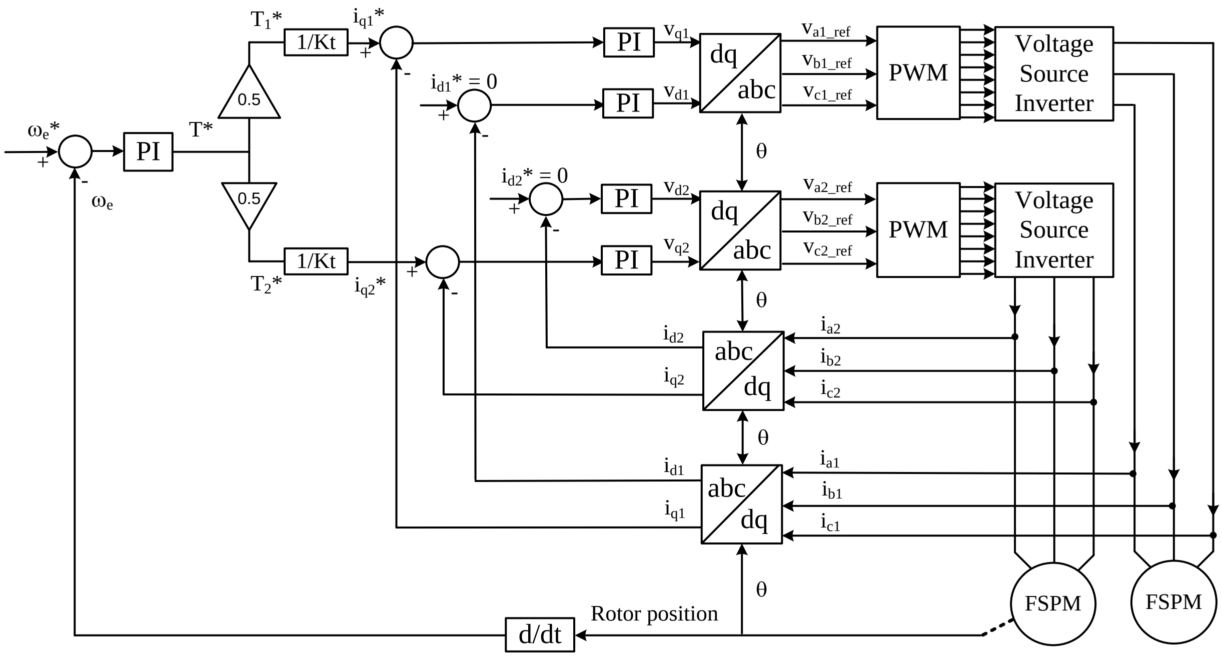

Figure 7.3 Vector control structure of dual-three-phase flux-switching permanent-magnet motor under normal-operating condition.

Figure 7.4 shows the no-load BEMF of the different stator coils. It can be noted that the waveform is distorted with seven harmonics. It can also be observed that the respective phase BEMFs of each machine module have the even harmonics in phase opposition with respect to each other. These would naturally cancel each other out if the dual-channel machine was to be connected as a single three-phase machine with the phase coils connected in series.

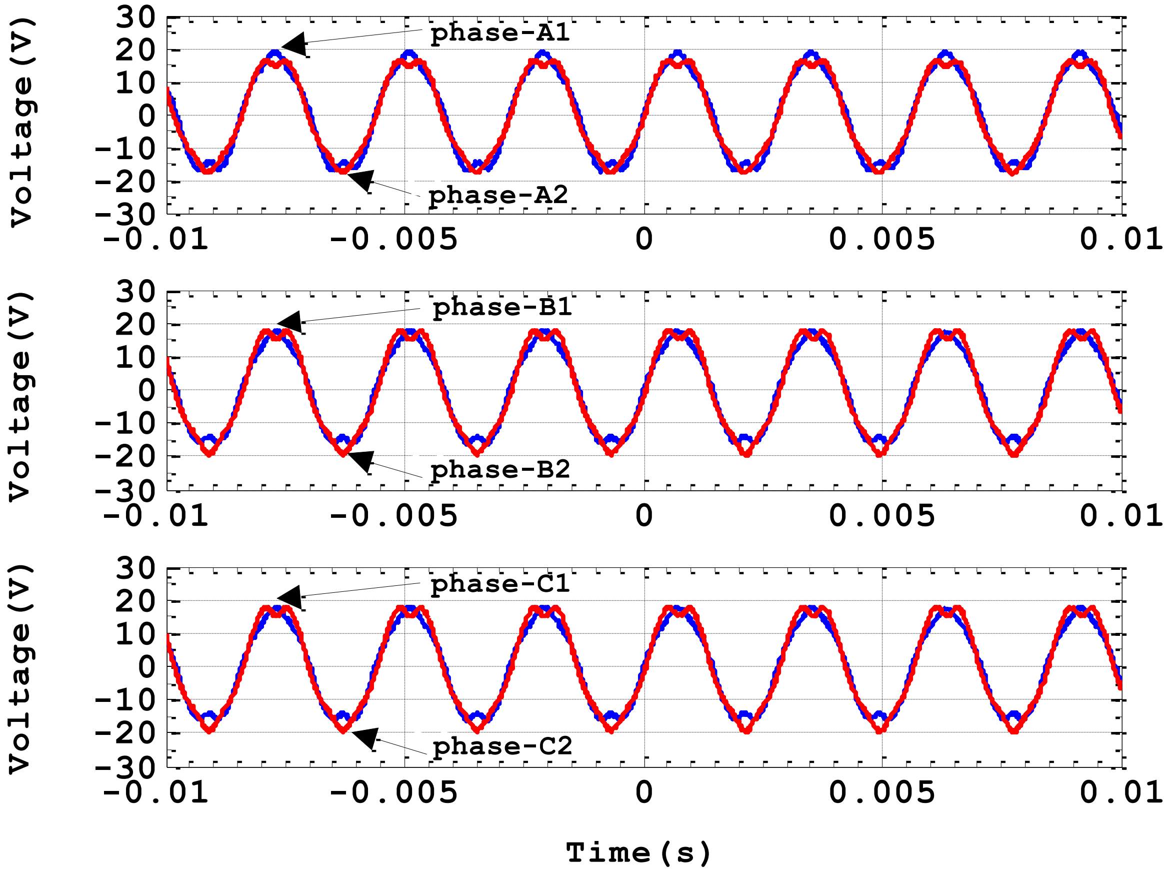

Figure 7.4 BEMF plots of the dual-channel three-phase machine.

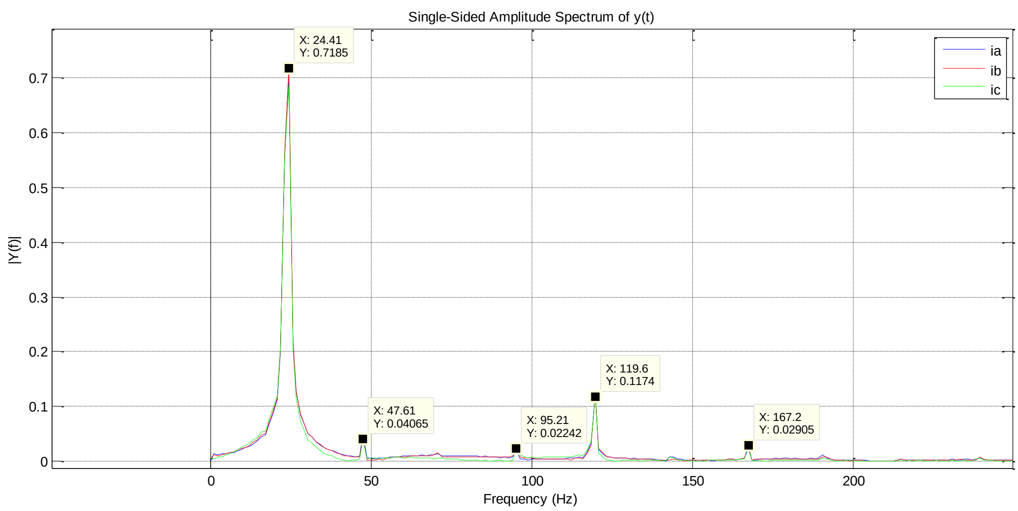

Figure 7.5 The FFT of the phase currents of M_1, for voltage source inverter FS-PMSM drive operating at 150rad/s under healthy-operating conditions.

Figure 7.5 *and* Figure 7.6 shows comparative spectra of the phase currents, (i_a, i_b, i_c), transformed currents (i_{d1}, i_{q1}) and speed of M_1 obtained from experimental result under healthy-operating condition. The fundamental component of phase currents occurs at a frequency of f_i = 24.41Hz. As can be seen in experimental waveform the phase currents contain a very small amount of the 3rd , 5th and 7th harmonics.

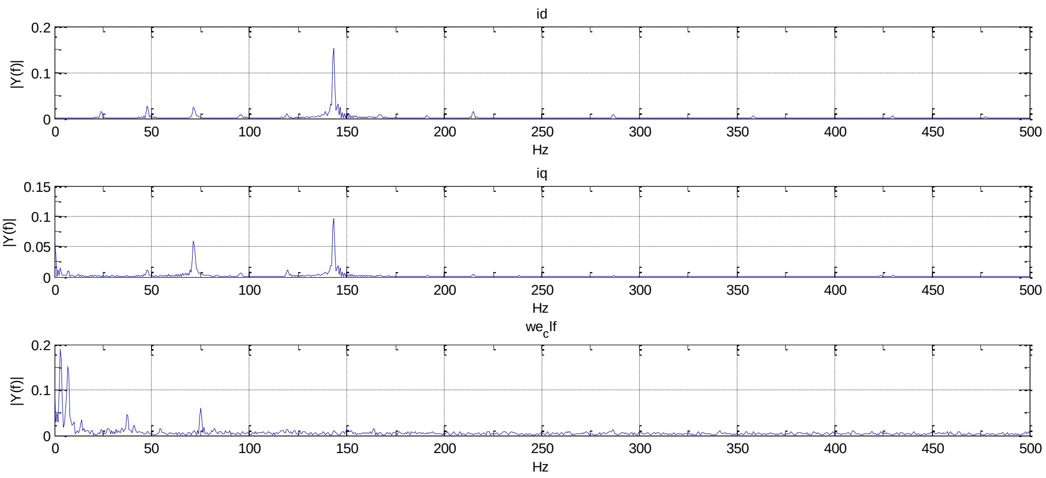

Figure 7.6 The FFT of the transformed currents of M_1, for voltage source inverter FS-PMSM drive operating at 150rad/s under healthy-operating conditions.

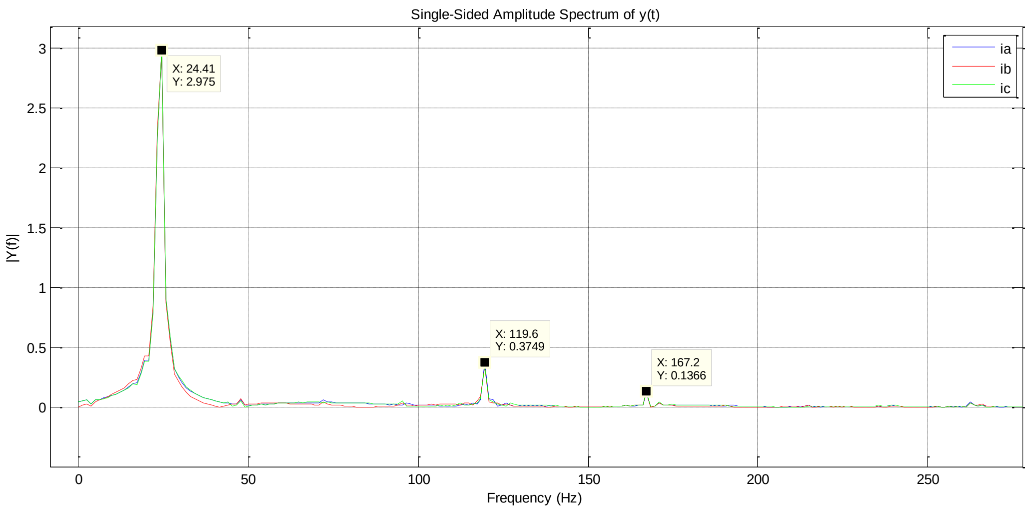

Figure 7.7 The FFT of the phase currents of M_1, for voltage source inverter FS-PMSM drive operating at 150rad/s under faulty-operating conditions.

Figure 7.7 and Figure 7.8 show comparative spectra of the phase currents, (i_a, i_b, i_c), transformed currents (id_1, iq_1) and speed of M_1 obtained from experimental result under faulty-operating conditions.

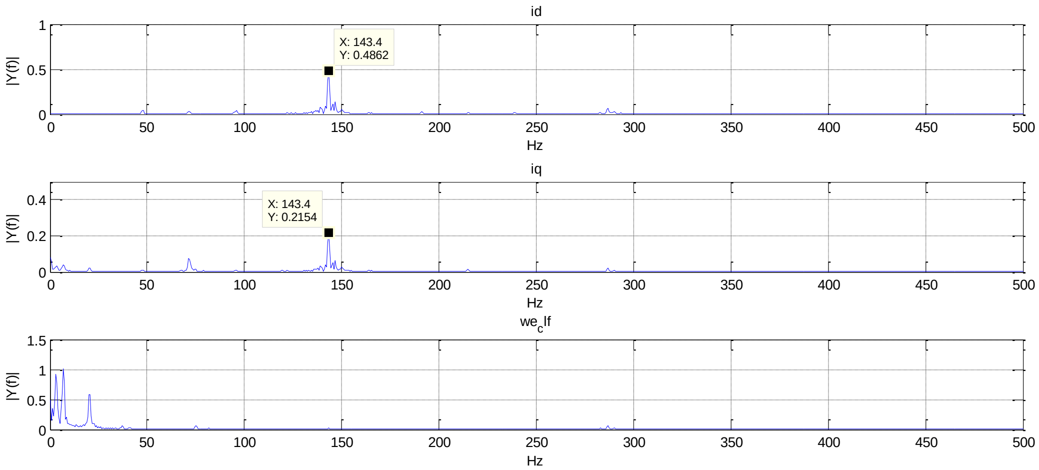

Figure 7.8 The FFT of the transformed currents of M_1, for voltage source inverter FS-PMSM drive operating at 150rad/s under faulty-operating conditions

7.1 Experimental Setup

Control platform – Operation of FSPM (Power converter and its control for a developed FSPM motor).

Traditionally motor control was designed with analog components as they are easy to design and can be implemented with relatively inexpensive components. However, there are several drawbacks with analog systems. Aging and temperature can bring about component variation causing the system to need regular adjustment, as the part count increases, the reliability of the system decreases. Analog components raise tolerance issues and upgrades are difficult, as the design is hardwired.

Digital systems offer improvements over analog designs. Drift is eliminated since most functions are performed digitally, upgrades can easily be made in software and part count is also reduced since digital systems can handle several functions on chip.

Digital Signal Processors go on further to provide high-speed, high-resolution and sensor-less algorithms in order to reduce system costs, providing a more precise control to achieve better consumption.

The performances of an AC synchronous motor are strongly dependent on its control. DSP controllers enable enhanced real time algorithms as well as sensor-less control. The combination of both allows a reduction in the number of components and optimizes the design of silicon to achieve a system cost reduction.

Figure 7.9 depicts a schematic diagram of the six-phase FS-PM drive system. The schematic block includes the power circuit and its control for experimental testing of a FS-PM motor.

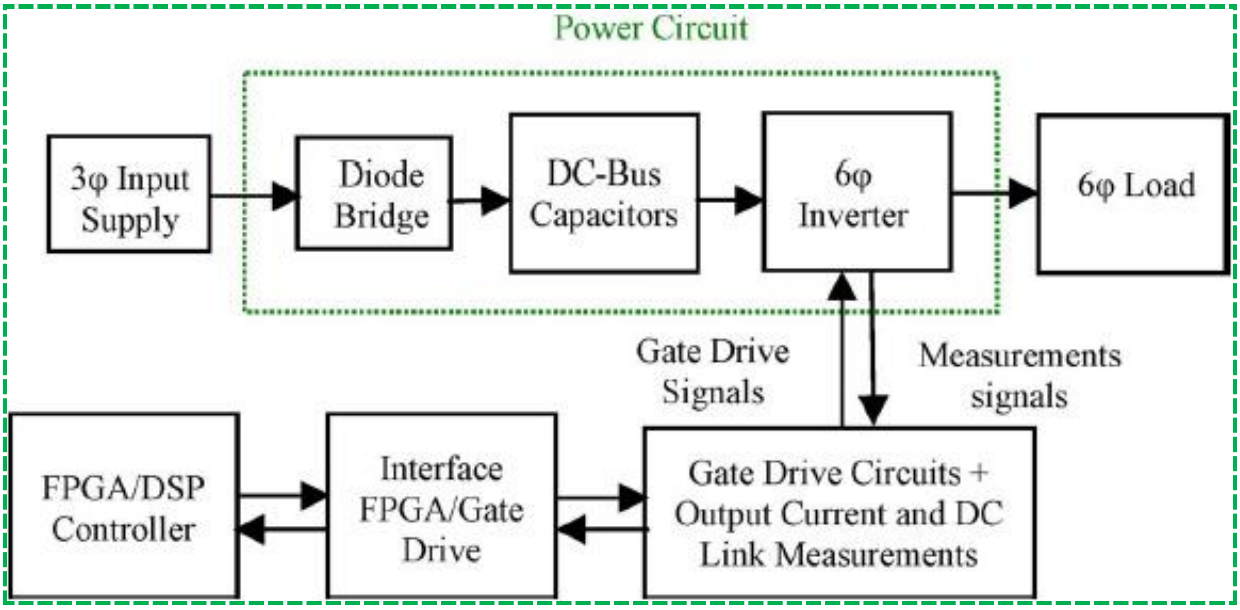

Figure 7.9 Six-phase drive system

Figure 7.10 shows the configuration of a three-phase diode bridge dc-link-six-phase two-level voltage source inverter which is chosen to experimentally implement using a 100GB 123 D IGBT transistor (see *Figure 7.11*) in order to operate the FS-PM motor under the different-operating conditions. The laboratory prototype six-phase inverter is presented in *Figure 7.12*. The inverter has been constructed using 100A 1200V inverter leg modules. The power plane also integrates the gate-drive circuits, output current measurement, and dc-link measurement transducers.

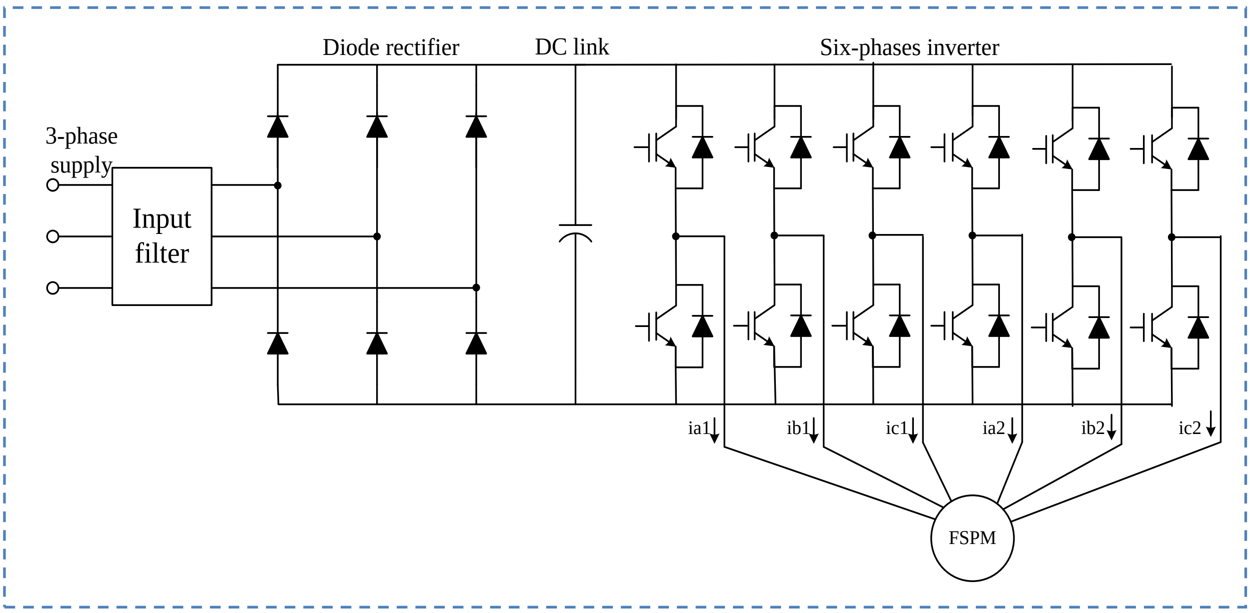

Figure 7.10 A three-phase diode bridge-dc link-six-phase two-level voltage source inverter configuration

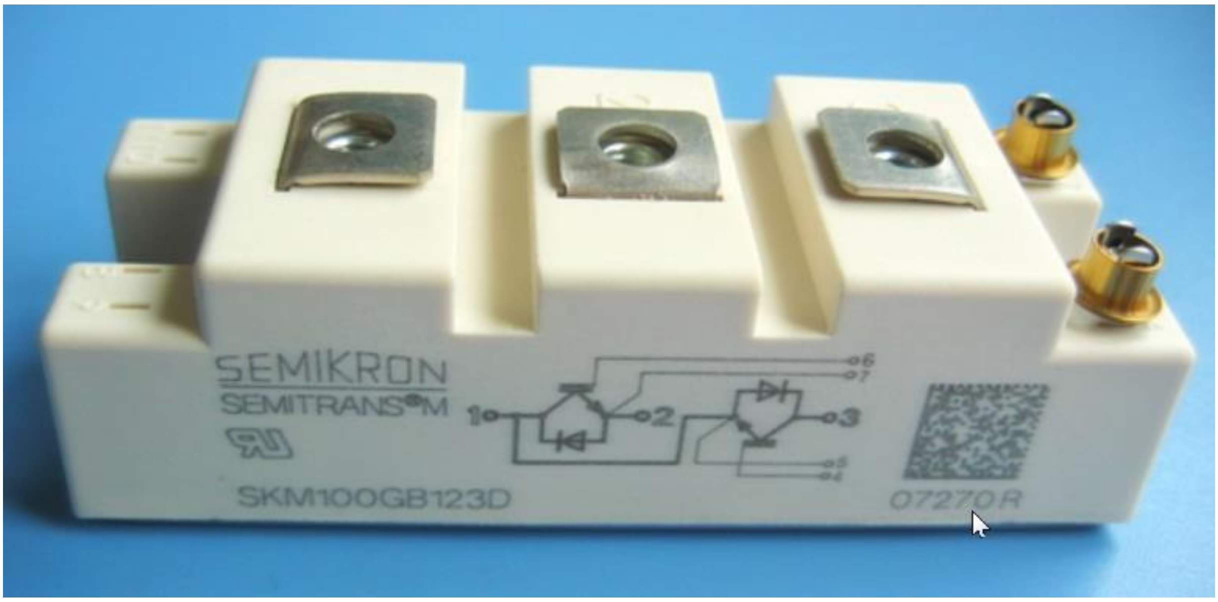

Figure 7.11 IGBT module-SKM 100GB 123 D

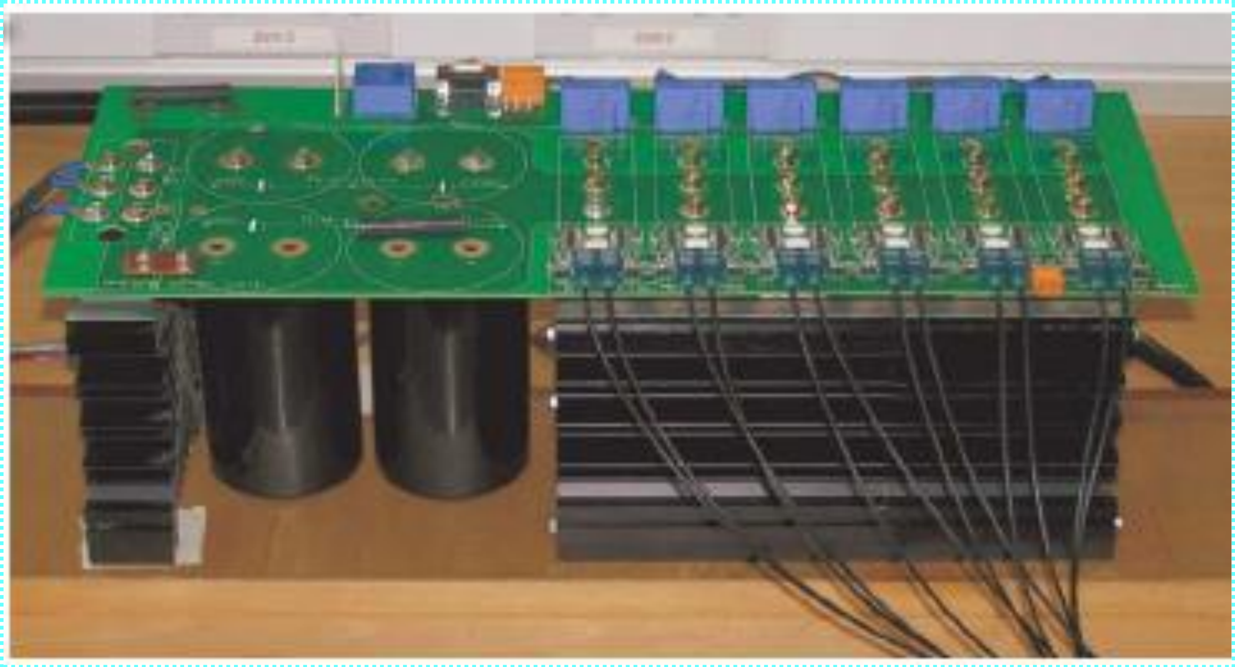

Figure 7.12 Three-phase diode bridge dc-link six-phase inverter implementation.

The controller was implemented using a high-speed digital signal processor (DSP) and a high-speed field programmable gate array (FPGA). The Texas Instruments C6713 floating-point processor and Actel ProAsic3 FPGAs were employed to achieve the desired motor performance. The control algorithm is implemented on DSP whereas the switching logic signals sent to the power switches are generated from FPGA.

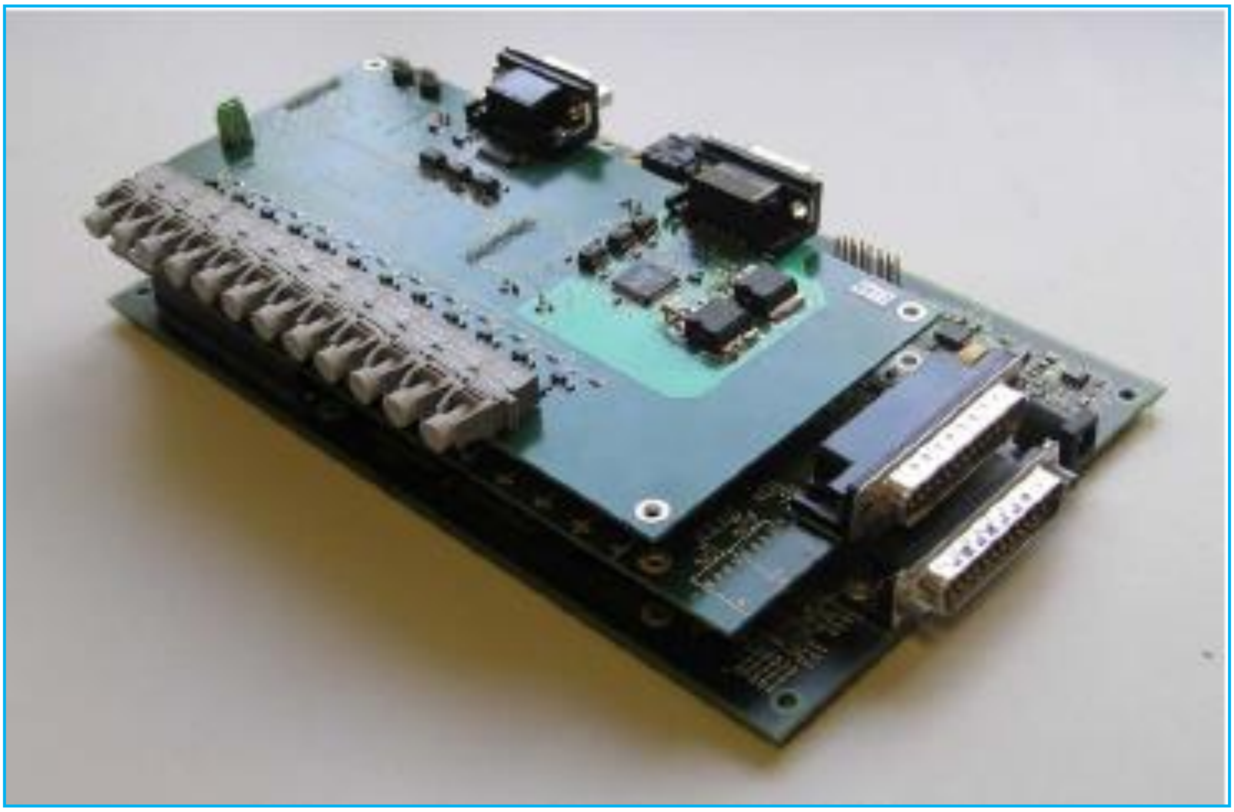

Figure 7.13 High-performance DSP-FPGA-based digital control platform

Figure 7.13 shows the control cards starting from the bottom with the TI C6713 DSK. The middle card contains the FPGA and also includes ten analog input channels which each input channel consisting of analog conditioning circuitry and a 14-b analog to digital converter (A2D). Finally, the top card is an interface card which provides the fiber-optic links (to increase noise immunity) for the gate-drive signals both a rotary resolver to digital converter and a rotary encoder interface circuit for higher flexibility and, finally, digital temperature sensor interface circuitry [54]. It has been shown that the control tasks are divided into two main parts of the controller. FPGA (connected to the DSP via its external memory interface) can be used to implement the high speed tasks such as the analog to digital (A2D) interface, high speed pulse-width modulation (PWM) generator, watchdog timer, trip/fault monitor and finally deadtime/communication control. The high speed floating point DSP (programmed in C using the code-composer integrated design environment.) can be used to perform all of the modulation and motor-control functions.

Host Port Interface Daughter Card

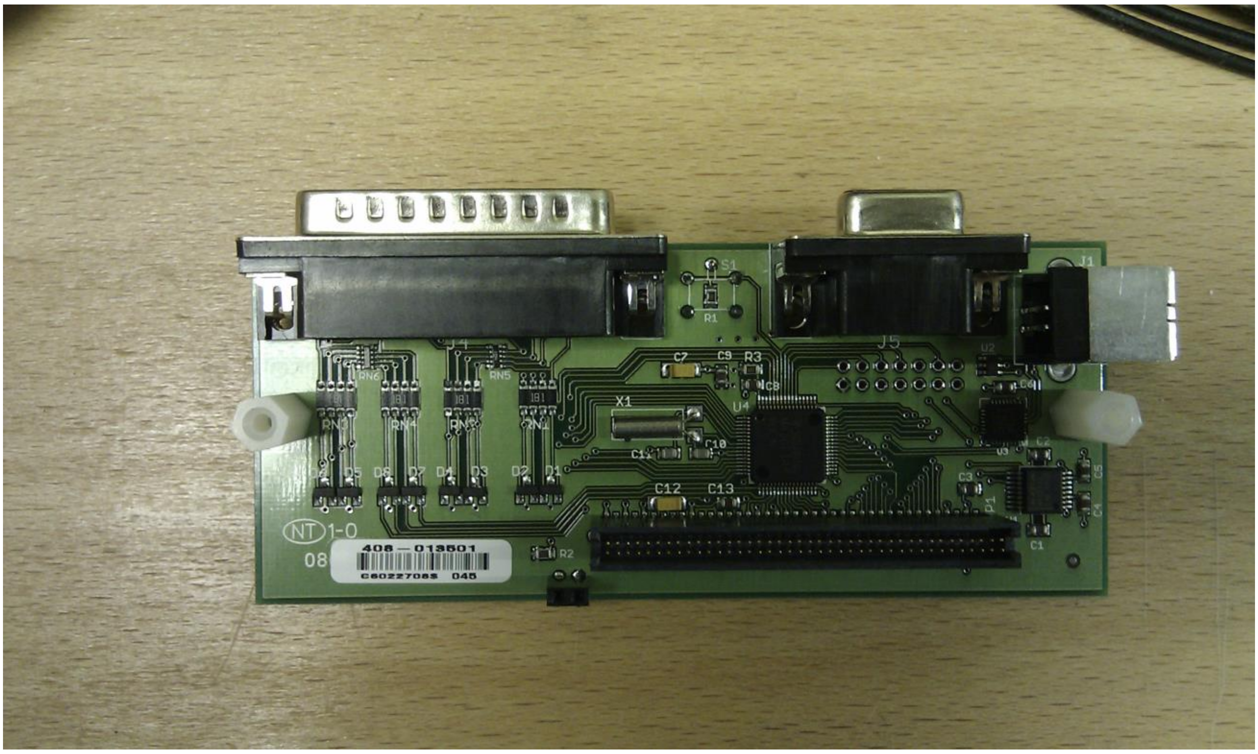

Figure 7.14 Host port interface daughter card

Figure 7.14 shows the Host Port Interface (HPI) daughter card. The Educational DSP DSK6713HPI daughter card is connected to the DSP card through the HPI parallel port. A host computer can communicate with the daughter card using a USB port, allowing access to the DSP memory space. Due to the memory accessibility, the direct DSP control operation can be achieved from the host computer. A MATLAB interface is employed for data acquisition and real-time control of the DSP without the requirement for the Code Composer Studio connection. With this advantage, MATLAB can download a .out file to the DSP memory map, resulting in the stand-alone application development.

Field Programmable Gate Array (FPGA)

A high performance Actel ProASIC3 FPGA card shown in *Figure 7.15* has been designed and developed by Lee Empringham from the PEMC group at the University of Nottingham [55]. This very flexible and versatile FPGA card is interfaced with the high speed TMS320C6713 DSP in order to control the voltage source inverter. The ten 12-bit A/D conversion channels and their individually software-configurable trip circuits are included on the FPGA card [54]. The switching signals are transmitted to the gate drive circuits through the output pins. The input connector receives the analogue signals provided by the measurement circuits which represent the measured voltages and currents. Eight A/D channels are employed to measure the two input voltages, four output currents, clamp voltage and clamp current. The measurement resistors are designed on the basis of the voltage and current transducers used in order to provide the input voltage for each A/D channel in the range of ± 5V. In addition, the output current direction for each output phase is also sent to the FPGA card through the input connector. Using a memory-mapped interface between the FPGA and the DSP, the information of the digital signals from the A/D channels extracted from the FPGA registers can be transferred to the DSP for processing.

In order to protect the voltage source inverter, the FPGA can turn off the power switches automatically when a trip signal is observed. Several types of trip are taken into consideration to ensure the safe operation of the voltage source inverter. Firstly, a watchdog trip is used to turn the converter off in the event of a communication failure between the DSP and the FPGA. Secondly, the hardware trips which are the fastest responding trips in the system have been configured through the hardware comparators located in the A/D circuitry. The trip levels for clamp voltage and the four output currents are defined by the DSP. Thirdly, the software trips which are responsible for the overcurrent and overvoltage protection are implemented on the DSP and are then latched at the FPGA. Finally, the resolver failure trip is set to ensure that the rotor position can be obtained from the resolver interface card.

When any trips occur, the LED displays feedback the trip signals. The information from these trips provides the opportunity to analyze failures in the converter. As can be seen in *Figure 7.15*, there are two switches, a push button switch and a toggle switch, connected to the FPGA card in order to reset the trips and enable/disable the voltage source inverter, respectively.

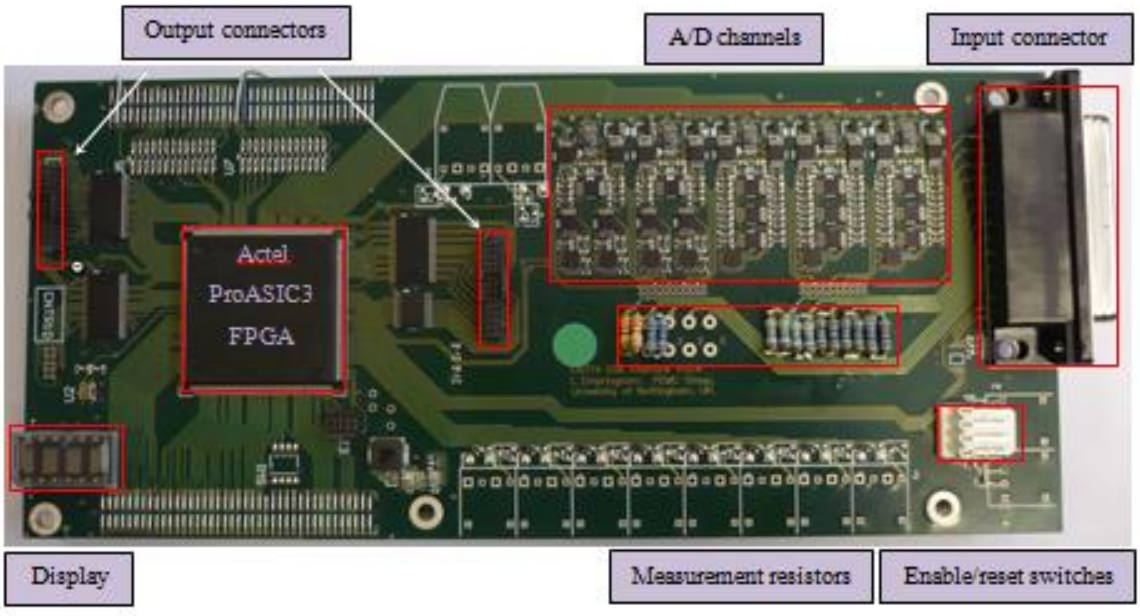

Figure 7.15 FPGA card

Digital Signal Processor (DSP)

A high-performance Texas Instruments TMS320C6713 floating-point digital signal processor with the DSP Start Kit (DSK) is shown in *Figure 7.16*. This DSP is employed to provide fast and effective control of the voltage source inverter motor drive. The TMS320C6713 DSP offers the benefit of peripheral capability that includes two Multichannel Buffered Serial Ports (McBSPs), two 32-bit general-purpose timers, a 16-bit host port interface (HPI) and a 32-bit glueless external memory interface (EMIF). The EMIF is capable of expanding the memory interface through an expansion memory interface connector for the FPGA board. The Code Composer Studio (CCS), an Integrated Development Environment (IDE) for the host PC, communicates with the DSK using a USB host interface in order for DSP code creation, debugging and analysis for the real-time applications. . The voltage signals which represent the measured voltages and currents are simultaneously transmitted from the FPGA to the DSP through the register memory map. These signals are reconverted to the actual analog values by scaling with their multiplicative factors. The maximum permissible levels of the output currents and clamp voltage are also determined in the DSP. If at least one of these signals is higher than the safe level the voltage source inverter needs to be immediately disabled [56].

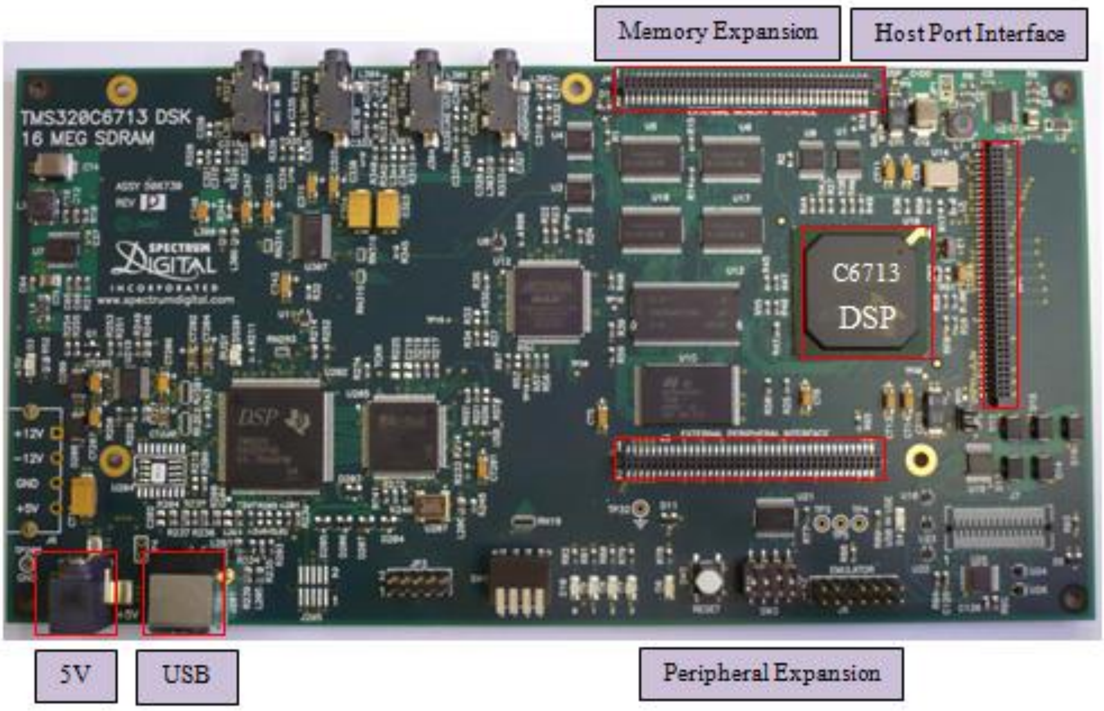

Figure 7.16 TMS320C6713 DSP board

7.2 Steady-State Performance

The first tests were performed to verify the steady-state performance of the machine units. *Figure 7.17* shows the measured torque as a function of *q-axis* current at a speed of 500 r/min. It can be observed that the two-machine units produce similar torque values. The torque values shown are those measured minus the torque measured without any excitation (no-load loss). This was done in order to have a direct comparison with the simulated results. It can be observed from *Figure 7.17(a)* that beyond i_{q1} + i_{q2} =10A, the two-machine units display a reducing torque constant due to magnetic saturation.

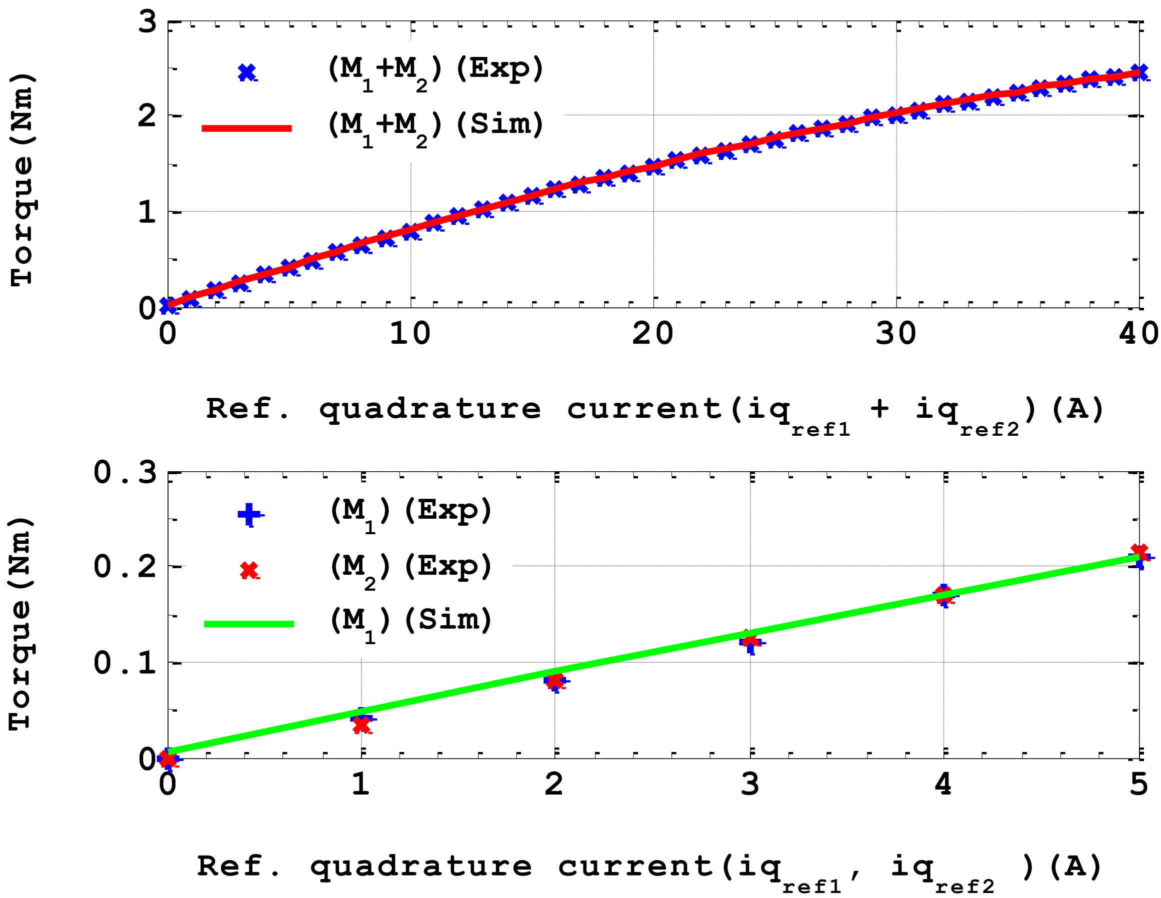

Figure 7.17 Torque of dual three-phase FS-PMSM :(a) Normal-condition and (b) Open-circuit condition

Figure 7.18 shows the total measured and simulated braking-torque as a function of speed when both machines are short-circuited in a balanced way. In this case, the machines are driven by the induction motor on the experimental rig. It can be observed that the model developed offers a close representation of the real machine behavior. As expected, the results show a reducing braking-torque as speed increases and as the inductive reactance becomes more dominant.

The experimental tests were carried out by feeding the dual-channel source inverters. *Figure 7.19* shows the experimentally measured steady-state short-circuit current (i_{sc}) values of the faulty motor during a balanced three-phase short-circuit operating condition at different speeds. In this case, the flux-switching machine drive system was operated in speed control with the induction machine providing a loading torque. With one flux-switching machine unit short-circuited, the healthy-machine unit had to overcome the loss of torque of the faulty-machine plus additional torque to overcome the braking-torque. The plot also illustrates the *q-axis* current component of the active healthy machine which varies as a function of speed in order to compensate for the speed dependent braking-torque generated by the shorted-machine. It is worth noting that, when a machine unit experiences a short-circuit-fault, as explained in *section 6.3.2*, the remaining unit takes over to deliver the remaining torque by doubling the *q-axis* current component to a linear approximation as well as needing an additional overhead to mitigate the braking-torque. This will result in a match higher machine thermal loading as the faulty unit would produce losses proportional to the fault current squared, and the healthy unit will see its losses increase proportionally to the square of the *q-axis* current.

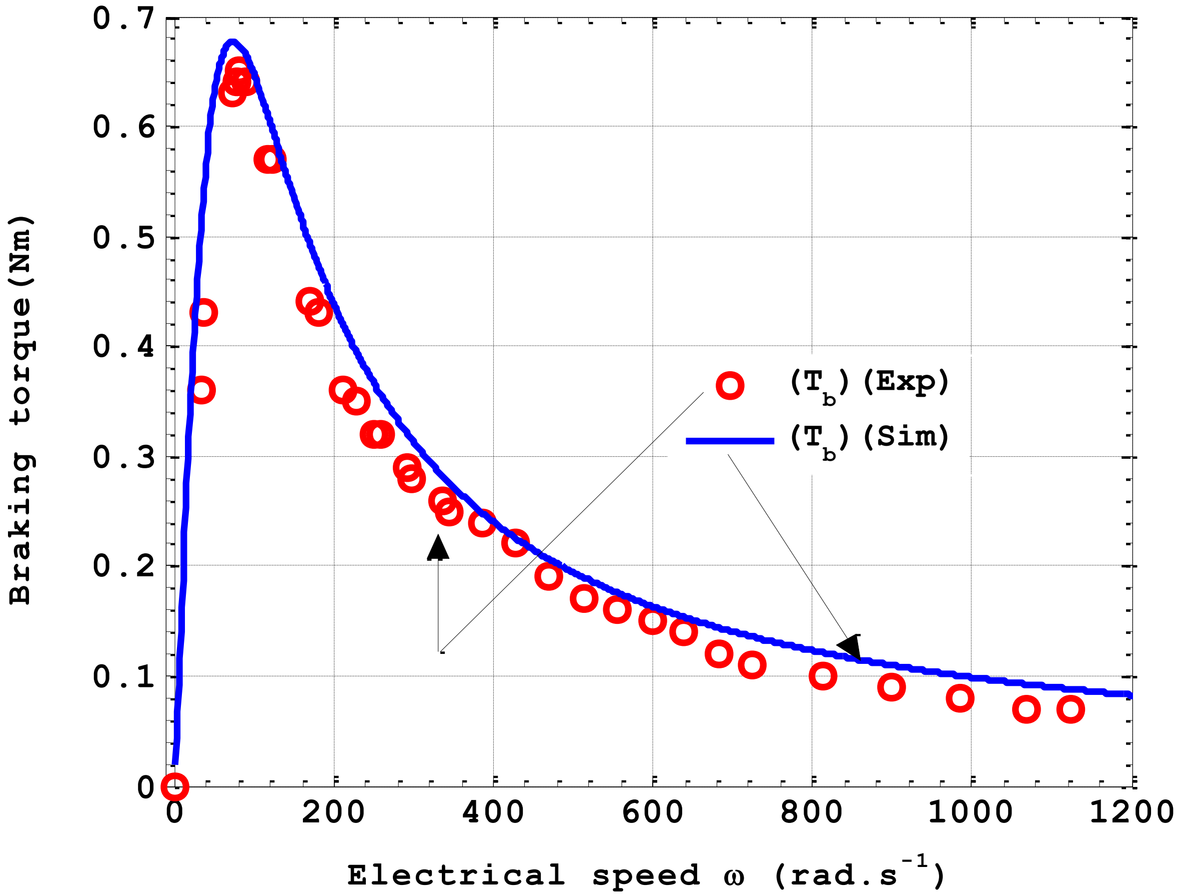

Figure 7.18 Braking-torque of dual three-phase FS-PMSM with the peak braking-torque appearing at 82 rad/s.

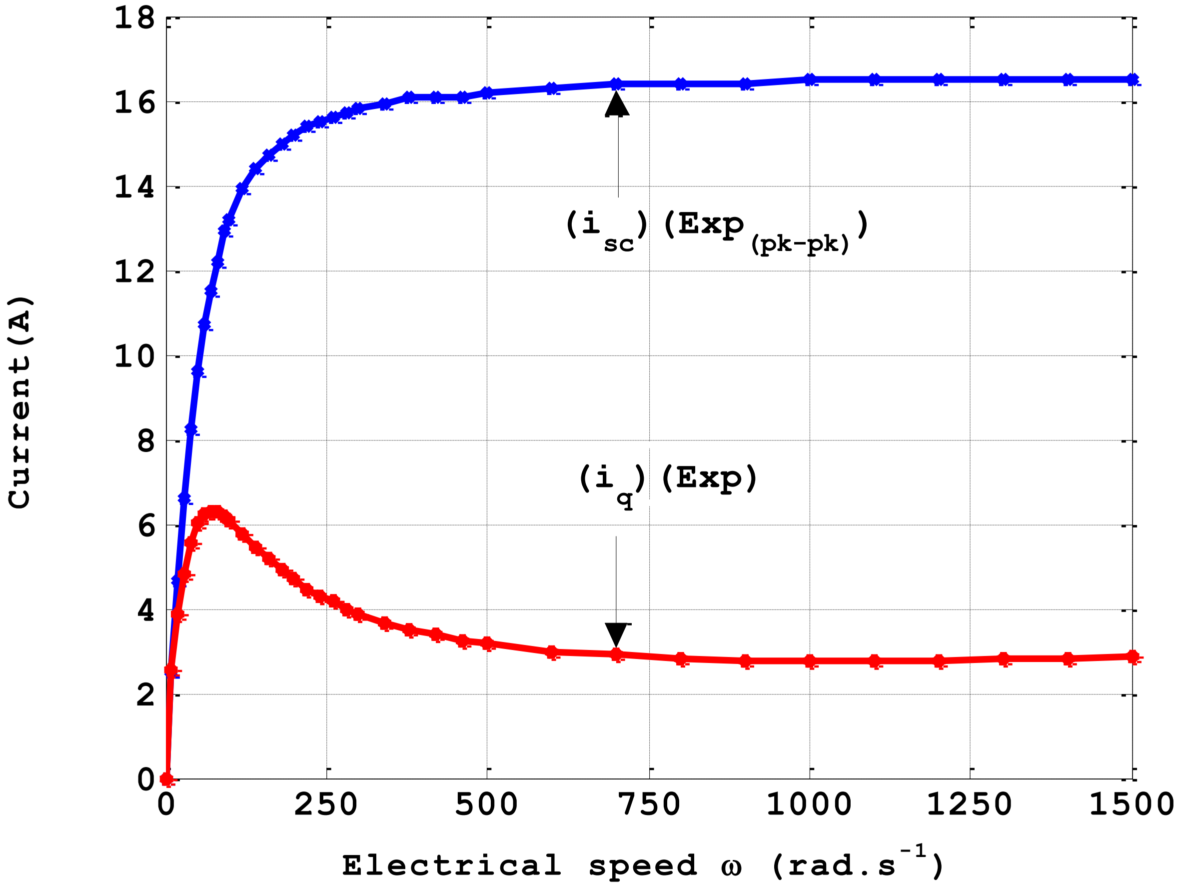

Figure 7.19 Dual three-phase FS-PMSM: one-phase short-circuit (pk-pk) current and quadrature current of the remaining motor as a function of speed

7.3 Transient Performance

This section will present the transient behaviour of the dual-channel flux-switching machine during both healthy- and faulty-conditions. The robustness of the drive operating during open- and short-circuit converter faults will be demonstrated in this section.

When a winding short-circuit is detected, the machine terminals are shorted to limit the fault current to a value below rated, and the remaining three-phase winding set is used to produce the torque requirement.

The adjustable speed operating conditions have been tested to show the ability of the drive control system. *Figure 7.20* shows the speed response of the motor operating at the different speeds, 500 rad/s, 1000rad/s and 1500rad/s. As can be seen, the actual motor speeds keep following the reference speeds.

The experimental result of the flux-switching motor drive system operating under load condition with adjustable reference speeds are demonstrated in *Figure 7.21*. The speed response of the motor operating at 500rad/s, 600rad/s and 700rad/s with a load applied to the drive system at t = 3s is presented. It can be seen that the motor speed can retain its reference speed.

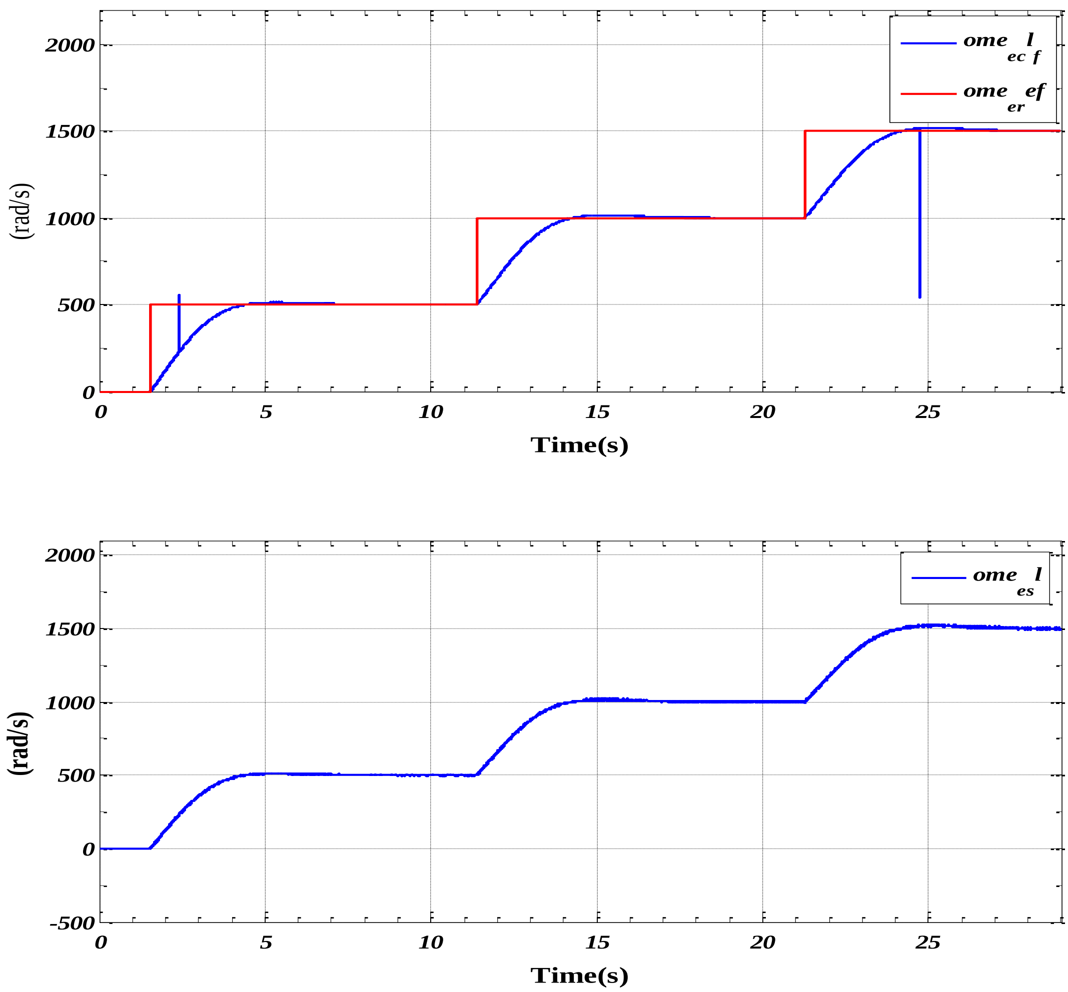

Figure 7.20 The speed of the motor operating at 500rad/s, 1000rad/s and 1500rad/s

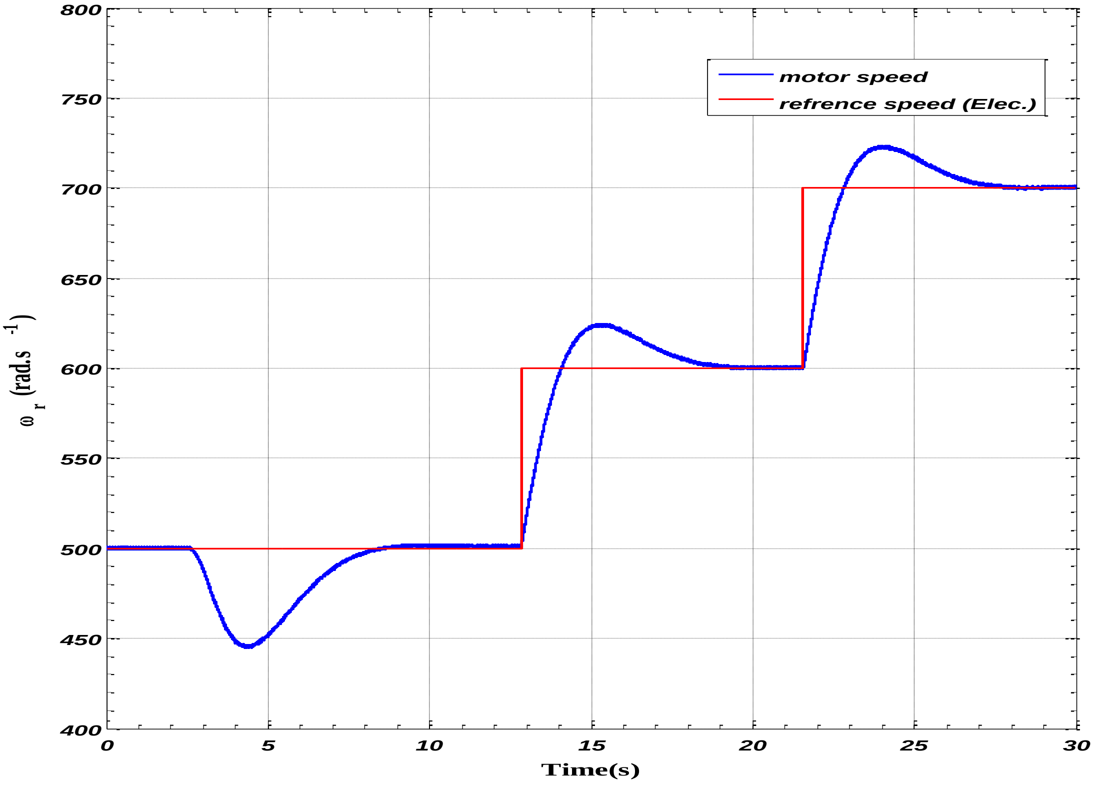

Figure 7.21 The speed of the motor operating at 500rad/s, 600rad/s and 700rad/s under load conditions

Figure 7.22 shows the phase currents of the dual three-phase motors before and after an open-circuit fault at *1000 r/min*. It can be seen that the resulting output torque is maintained as a result of doubling the healthy-machine current. When a balanced three-phase short-circuit is present in a one-machine unit, a speed dependent braking-torque will be produced. A balanced three-phase fault is applied after any converter or motor short-circuit failure. In order to attain a good dynamic performance, the braking-torque is estimated from the fault current of the faulty-machine unit and is compensated for in a feed-forward fashion to the healthy-motor unit.

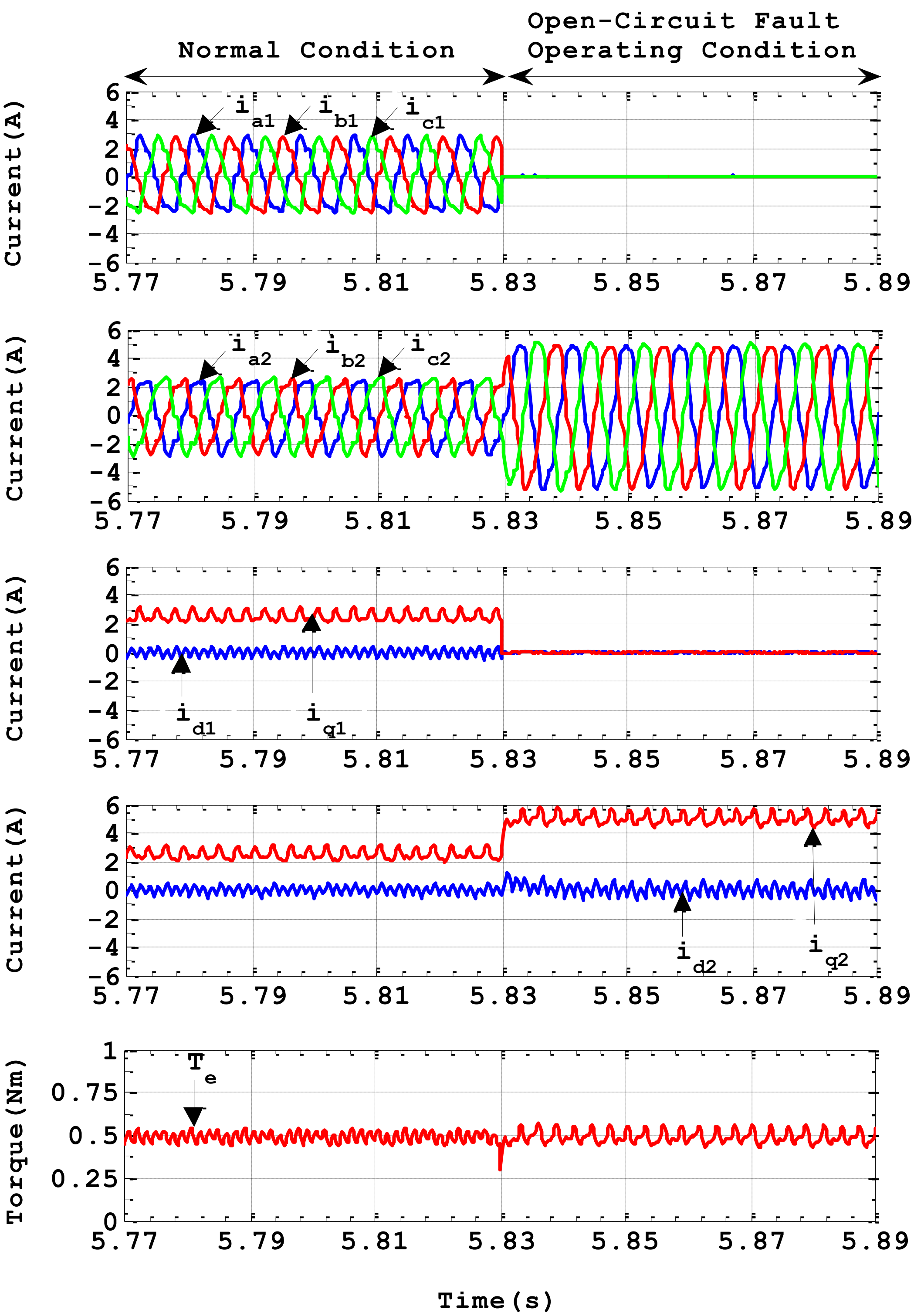

Figure 7.22 Experimental performance of the proposed dual FS-PMSM (M_1 is open-circuited) under normal-mode of operation and three-phases open-circuit (a) Currents of motor 1 (b) Currents of motor 2 (c) Transformed currents of motor 1 (d) Transformed currents of motor 2 (e) Total motor torque

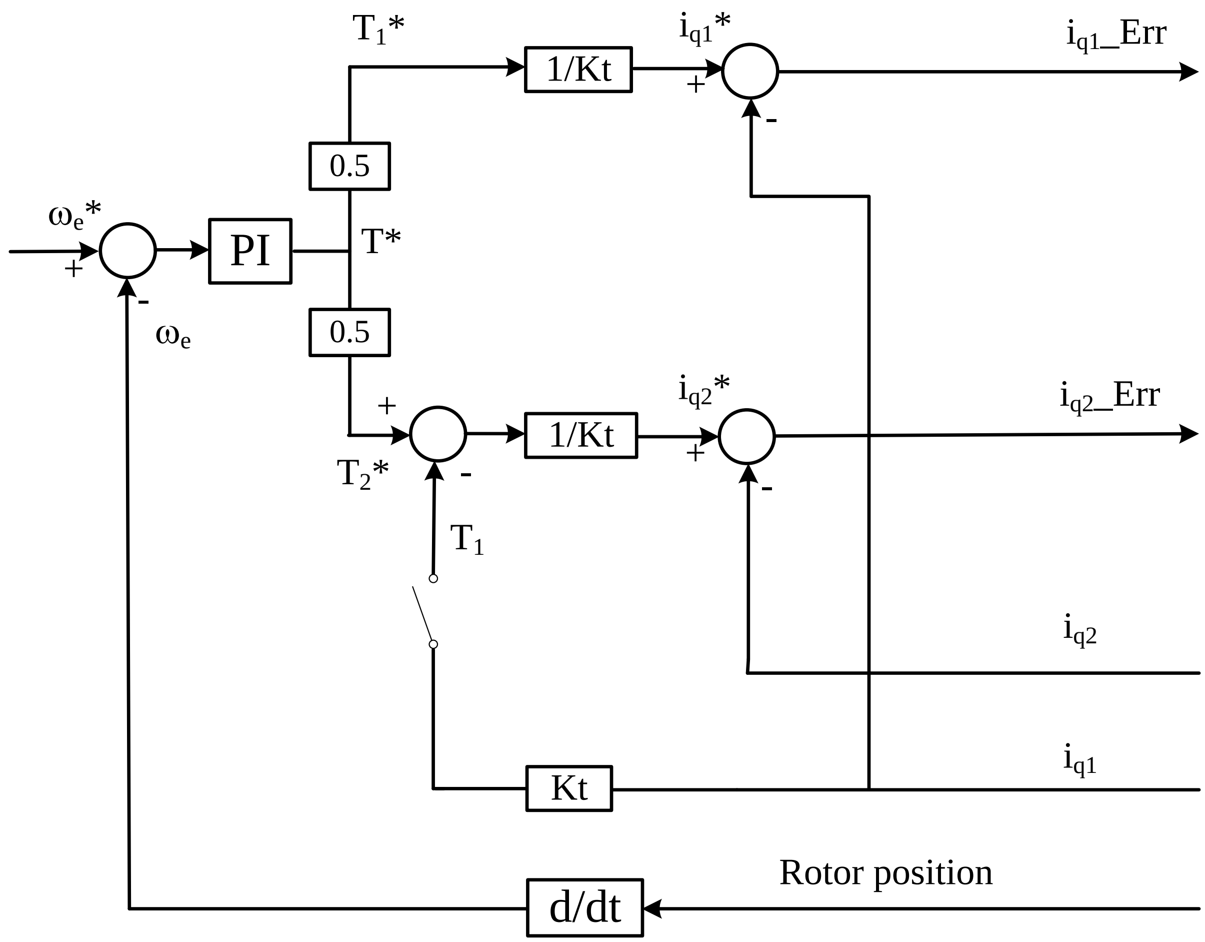

Figure 7.23 Torque compensation when motor 1 is short-circuited

The implemented system is shown in *Figure 7.23*. In the presence of short-circuit fault, the proposed torque compensation scheme is applied to the healthy-channel of the FS-PMSM after a balanced short-circuit is applied across the faulty-machine channel. This requires a diagnostic methodology able to detect the fault occurrence. As it can be observed, assuming motor unit M_1 is shorted, the q-component of the short-circuit is used in the feed-forward compensation. This current component is speed dependent, and two inaccurate assumptions are made. The first is that there is no saliency torque in the machine, i.e., the d-component of the short-circuit current is not producing any torque. The second is that the torque constant is assumed constant. Both assumptions are inaccurate as there is a small saliency, and the d-component of the short-circuit will alter the magnetic circuit saturation level which will in turn affect the torque constant. In spite of these inaccuracies, adding the compensation strategy significantly improved the machine's dynamic performance.

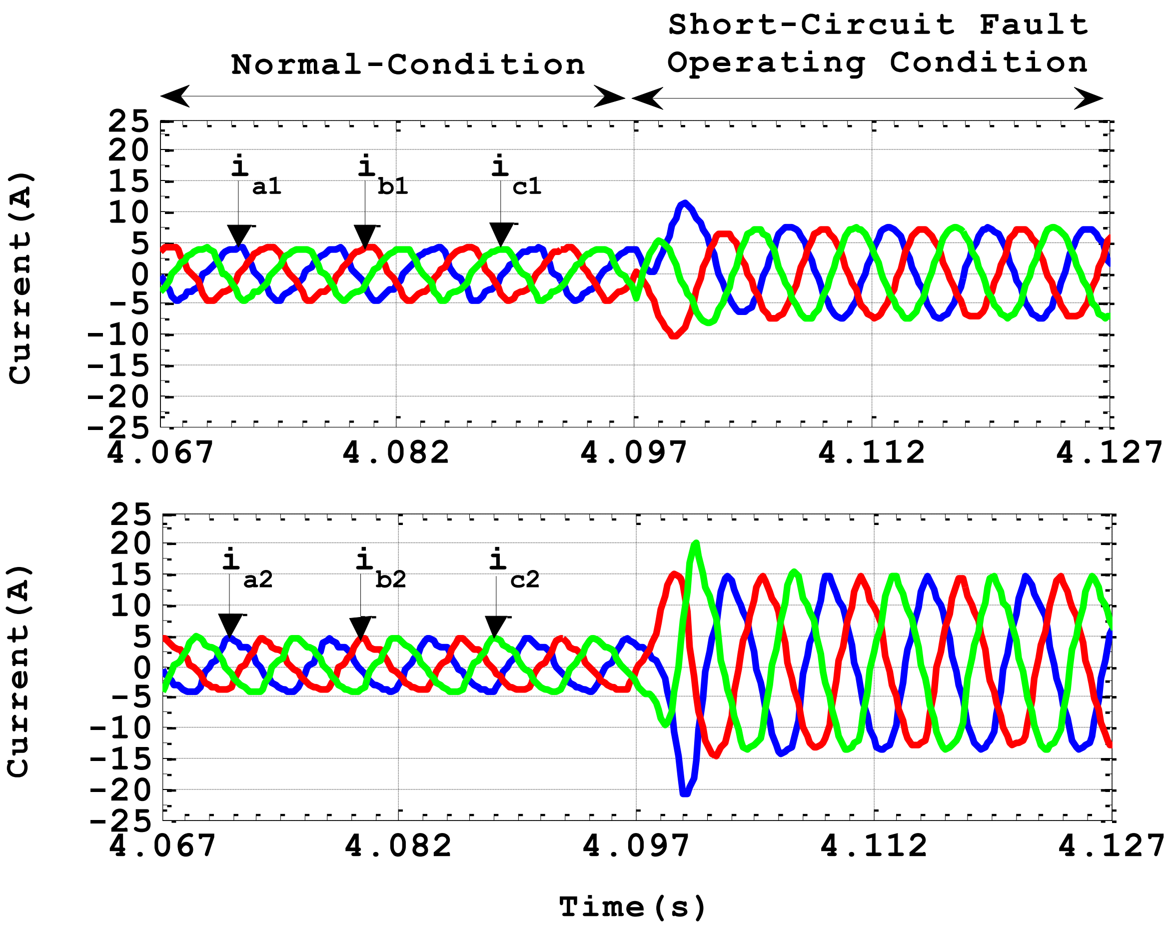

Figure 7.24 Experimental performance of the proposed dual FS-PMSM (M_1 is short-circuited) under different-operating condition (a) Currents of motor1 (b) Currents of motor2.

Figure 7.24 shows the two-machine unit phase currents before and after a balanced short-circuit fault is applied on motor 1. *Figure 7.25* shows the corresponding drive behavior. It can be observed that the speed is maintained with motor 2 having to overcome the lost torque from motor 1 as well as the braking-torque due to the short-circuit currents. In this case i_{q1} is fed back to compensate for the braking torque. This resulted in the current increasing by 160 % in the healthy-machine and by 40 % in the faulty-one. Naturally, this increase is speed and load dependent according to the braking characteristic shown in *Figure 7.18*.

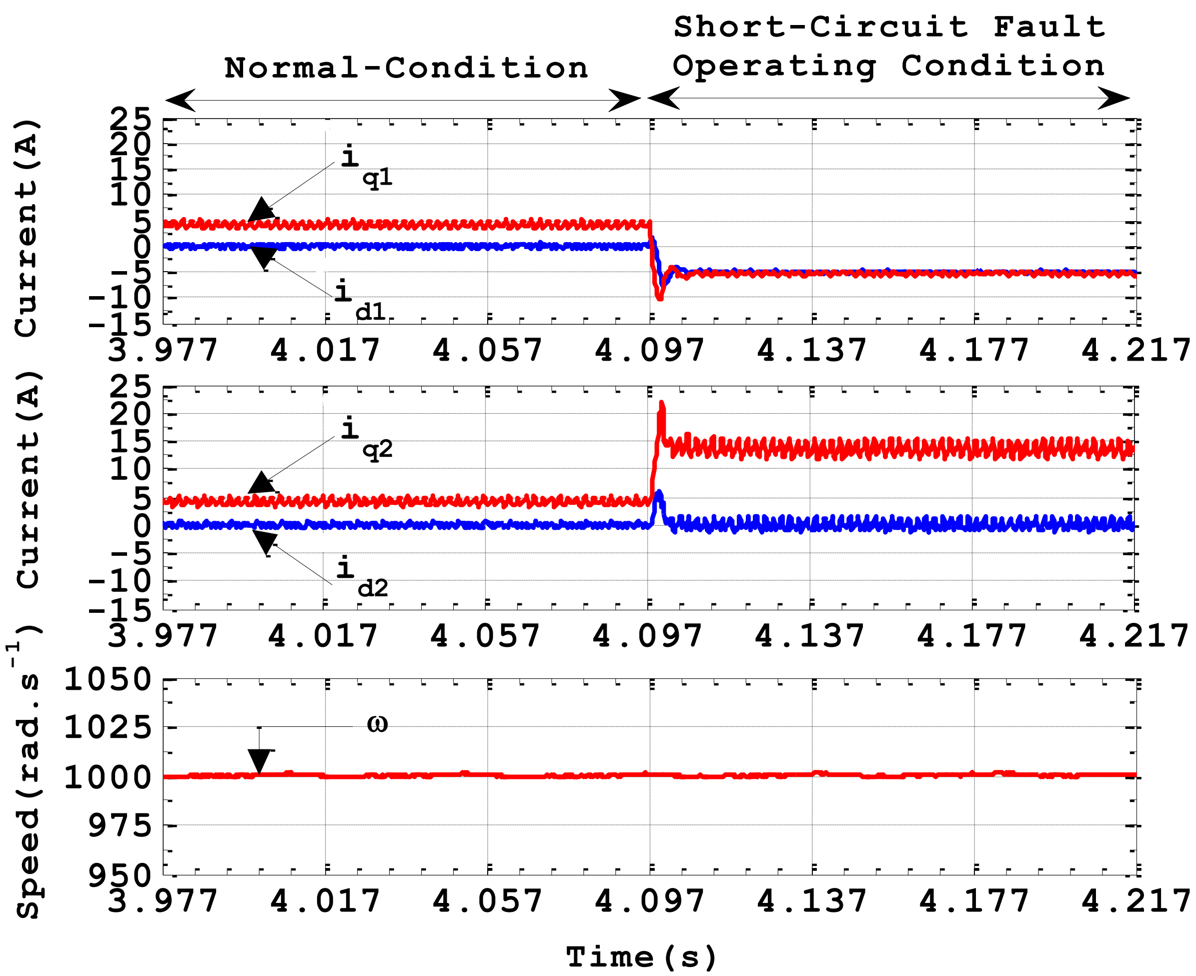

Figure 7.25 Experimental performance of the proposed dual FS-PMSM (M_1 is short-circuited) under normal-mode of operation and under a balanced short-circuit condition (a) Transformed currents of motor1 (b) Transformed currents of motor2 (c) Motor speed.

The next condition to be tested is a single-phase fault. *Figure 7.26* shows the experimental setup to test this condition. As is demonstrated in this figure, phase A of motor 2 can be shorted through an external contactor. This exact fault condition is not likely to occur in a practical scenario. It is representative of an internal winding failure. The most likely electrical failure is within the converter [43], and this condition has been evaluated in the proceeding experiments. In safety-critical applications, it is however sometimes necessary to consider the drive performance when an internal motor fault occurs. In the machine structure considered, only faults within the some coil are possible due to their physical isolation. As a worst case scenario in terms of torque disturbance in a random wound coil, an entire coil short-circuit is considered.

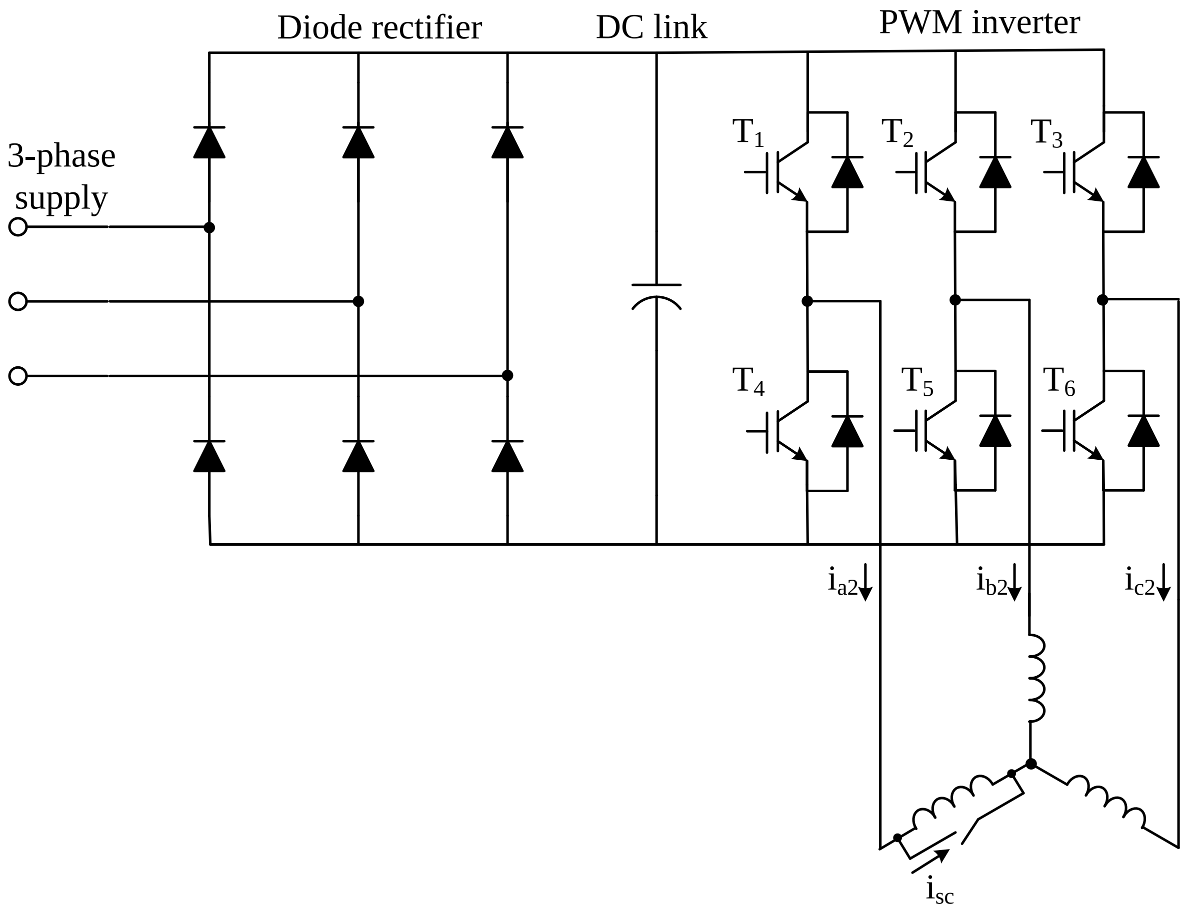

Figure 7.26 The FS-PMSM under short-circuit fault conditions

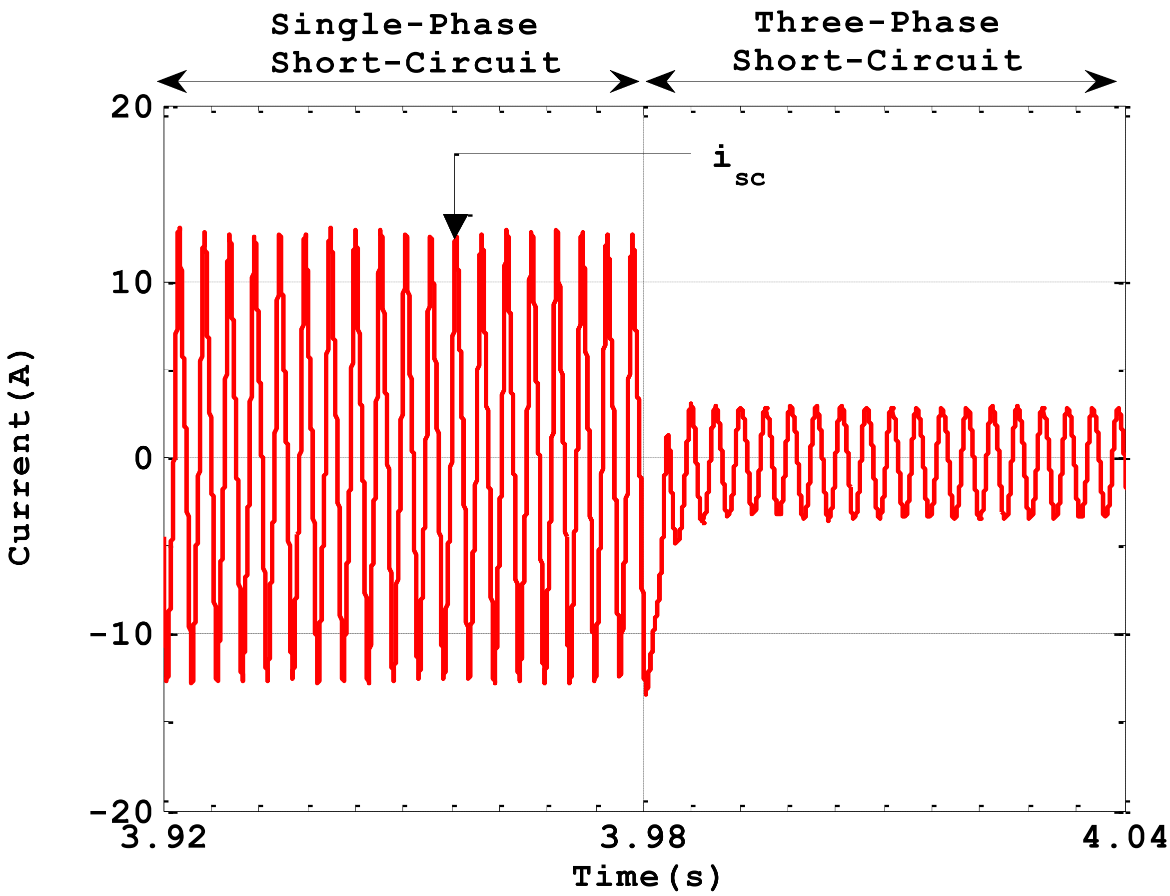

Figure 7.27 Experimental short-circuit current under different-operating condition (M_2 is short-circuited) at the speed of 2000 rad/s.

The motor is initially operated under normal-conditions, and then a single-phase fault is introduced. After a period of time, a balanced three-phase short-circuit (simultaneous short-circuit across all the three-phases) is applied to the faulty-motor through the converter.

The measured currents are plotted in Figs. *Figure 7.27-Figure 7.29*. When one phase is short-circuited, the unbalanced motor impedance results in negative sequence currents and corresponding torque-ripple at twice the fundamental frequency. This can be also observed in the *q-axis* current component of the faulty-machine in *Figure 7.29*. This is considerably reduced, as expected, when the balanced SC is applied. The aforementioned results clearly demonstrate the viability of this machine to operate with faults, given that the appropriate remedial control strategies are applied.

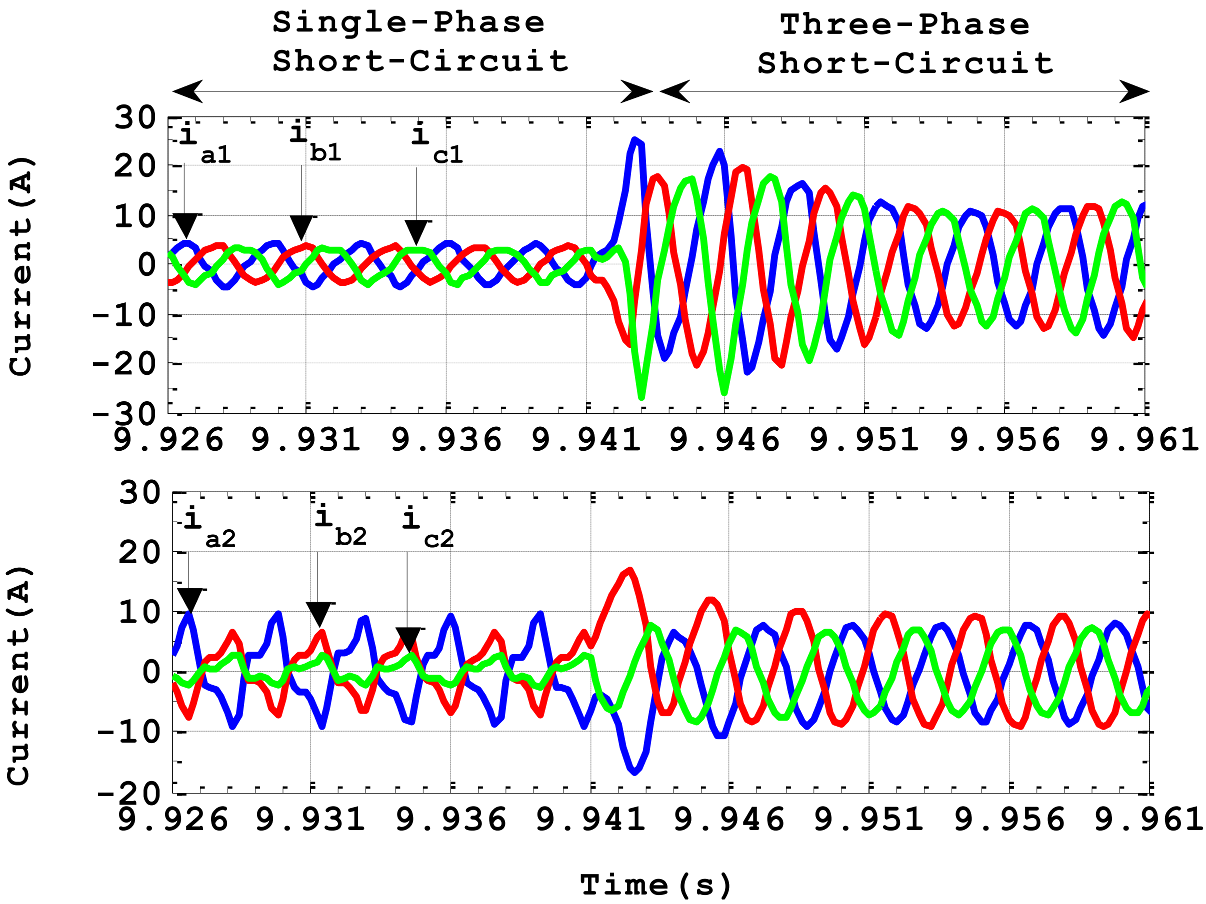

Figure 7.28 Experimental performance of the proposed dual FS-PMSM (M_2 is short-circuited) under single- and balanced short-circuit conditions a) Currents of motor1 (b) Currents of motor2.

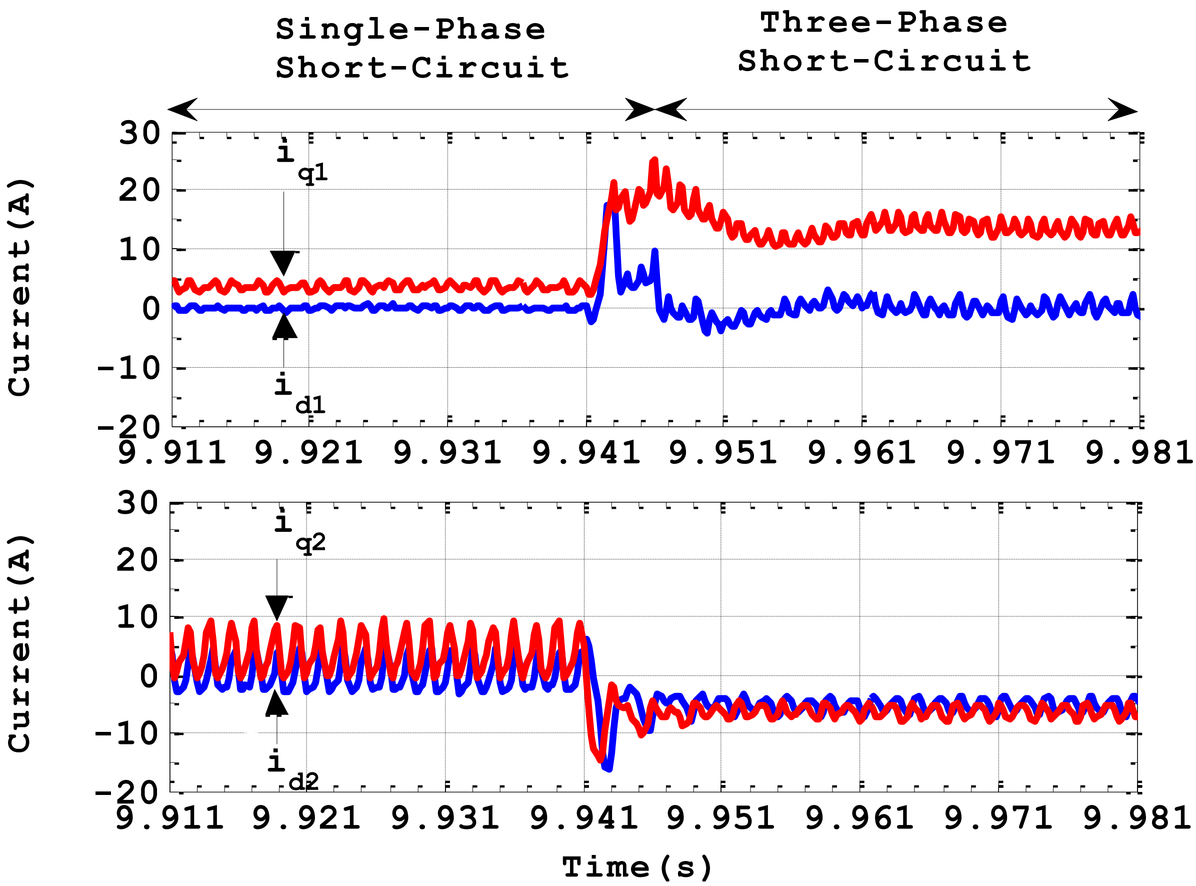

Figure 7.29 Experimental performance of a proposed dual FS-PMSM (M_2 is short-circuited) at the speed of 2000 rad/s under single- and balanced short-operation (a) Transformed currents of motor1 (b) Transformed currents of motor2.

Figure 7.30 shows LeCroy WaveRunner 64Xi Oscilloscope's single-and balance three-phase short-circuit current of M_2 (single-phase) and M_1 (three-phase).

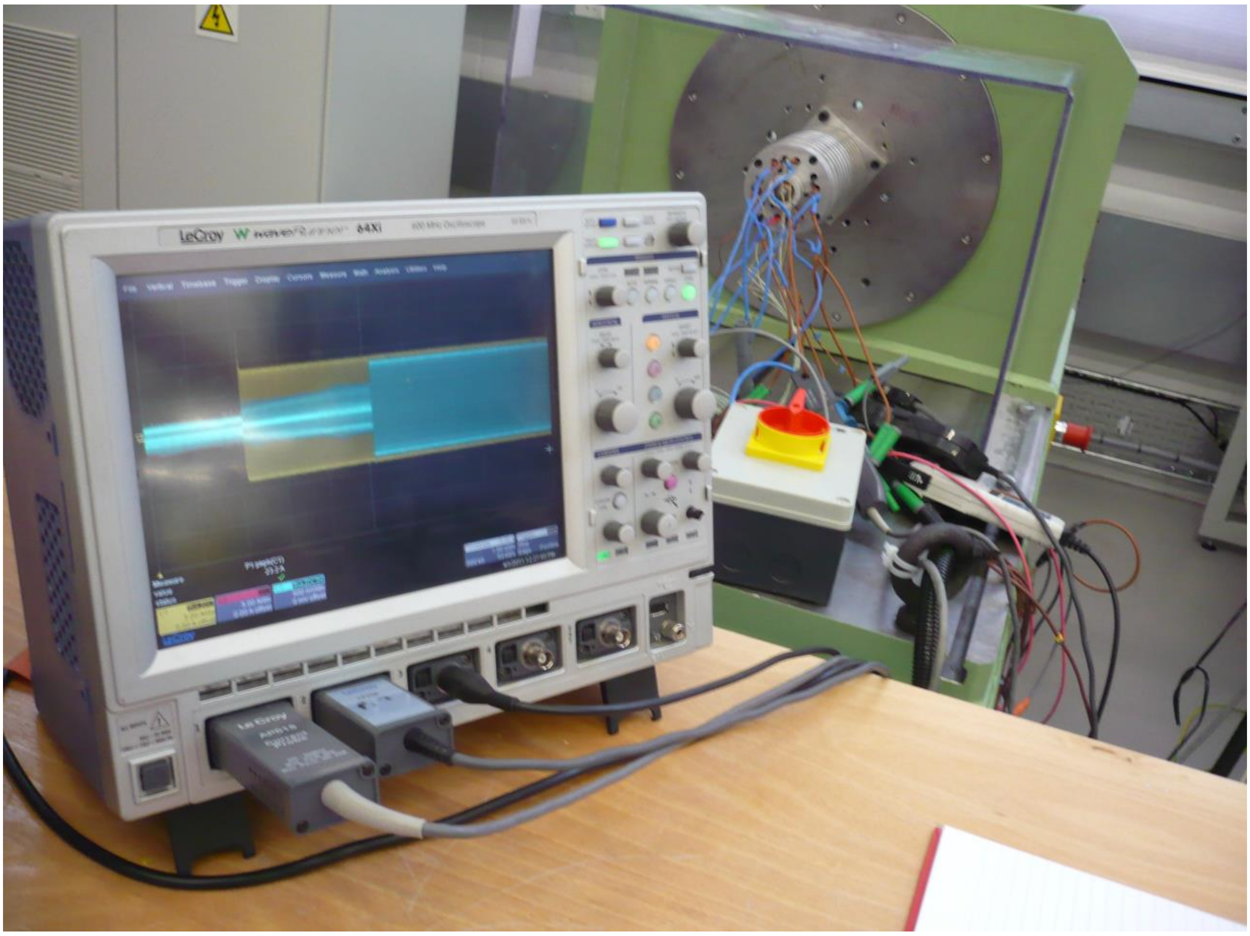

Figure 7.30 Oscilloscope LeCroy WaveRunner 64Xi (M_2 is short circuited)

7.4 Summary

In this Chapter the experimental study of the laboratory prototype flux-switching permanent magnet synchronous machine has been described. The operability of a flux-switching machine as an integral part of a high-performance fault-tolerant vector-controlled drive has been demonstrated. Experimental tests have demonstrated the validity of a nonlinear-machine model. The drive has been shown to operate reliably in the presence of open-circuit and short-circuit faults with minimum braking-torque and torque-ripple [57]. The control implementation of the voltage source inverter has been achieved using the high-performance DSP and FPGA platform to drive the motor under healthy- and unhealthy-operating conditions.

8 CONCLUSION AND FUTURE WORK

8.1 Conclusion

Electrical servodrive is a control drive, consisting of one or more electrical motors, which is fed by an electronic power-converter which is powered by semiconductor devices and controlled by electronic circuits. The electronic power-converter converts voltage and current from one to another applying power electronics device in the power circuit and microelectronics circuits to control the input-output values of the converter.

A brief description of the mathematical model of a PMSM has been given. A Permanent magnet synchronous motor (PMSM) has been modelled using the d-q variables to mimick the behaviour of a DC machine. The motor is assumed to be fed from a symmetric power supply. The model has been developed in the rotor reference frame. It means the electrical angular velocity is equal to the synchronous angular velocity. The rotor reference frames model is useful where the switching elements and power are controlled on the rotor side.

In a closed-loop positioning system, a sensor detects the actual position and feeds the information to the motor controller. The controller compares the actual position to the desired position, and moves the motor to correct any error. This allows the motor to reach a precisely controlled position. Similarly, controlled speed is achieved by adjusting the driver gain to minimize the difference between the required position and the actual position at regular time intervals.

For feedback cascade control, the estimated position is compared to the actual position and the error is inputted to a proportional controller used to drive the steady-state estimation error to zero. Most designers place the position sensor on the motor shaft. While this ensures precise motor position, it does so at the expense of load position. Naturally, the greater the backlash beyond the motor shaft, the further off the load is likely to be. The alternative, placing the sensor on the load, presents another set of problems. Here, backlash becomes part of the closed loop, and hence, system dynamics. The dynamic response of backlash itself, essentially a delay, makes the position loop less stable and prone to oscillation.

This thesis presents a fault-tolerant flux-switching permanent magnet motor drive control system driven by a six-phase voltage source inverter. A dual three-phase flux-switching permanent magnet motor, which consists of two separate three-phase stator windings, has an ability to provide the fault-tolerant capability under faulty-operating conditions. In the event of faults when the one three-phase motor stops working, the remaining healthy three-phase motor can continue to operate unaffected. In addition, this modular approach also provides the minimal electrical, magnetic and thermal interaction between phases of the drive. The dual three-phase flux-switching permanent magnet motor model is created in order to investigate the behaviour of the motor drive control system under healthy- and faulty-operating conditions. Moreover, the field-orientated indirect vector-control is employed to control the drive system at a wide range of speeds and load-torque applied. Under the fault operation mode the modified control strategy is adopted to the drive system in order to keep the motor operating continuously as well as to maintain the system performance as before the fault occurrence. The simulations of the considered motor drive control system have been carried out using Matlab Simulink. The simulation results of the entire system operating with no-load and load-torque applied are presented under both normal- and fault-operating conditions. The experimental setup is implemented to validate the effectiveness of the fault-tolerant flux-switching motor drive control system operating under a wide range of operations even in the presence of a fault. The simulation and the experimental results show that the proposed fault-tolerant flux-switching permanent magnet motor drive system has an ability to maintain the system performance under both normal- and fault-operation modes.

This thesis has demonstrated the operability of a flux-switching machine as an integral part of a high-performance fault-tolerant vector-controlled drive. A nonlinear-machine model has been described, which is able to predict the drive's performance during both healthy- and faulty-operations. Experimental tests have demonstrated the validity of the model. The drive has been shown to operate reliably in the presence of open-circuit and short-circuit faults with minimum braking-torque and torque-ripple.

The aim of this thesis has been has been primarily to show the robustness of the machine and drive topology to operate under faults originating either from the converter or from the machine itself. Further work is however required to determine the losses and, consequently, the efficiency of machine operation during both healthy- and faulty-conditions. The faulty-conditions would likely be the machine-drive sizing case if full rated operation is required after experiencing a fault. The machine-drive design optimization is an important aspect if such a system was to be adopted as many tradeoffs between machine size and efficiency, filtering requirement, and converter VA requirement need investigation. Both simulated and experimental results verify that the FS-PMSM can be operated effectively by adopting the developed control strategy and offers good steady-state and dynamic performance.

8.2 Future Work

The filed-oriented control (FOC) method can be used to control the FS-PMSM drive. The recent trend in field-oriented control is towards the use of sensor-less techniques that avoid the use of speed sensors. The sensors in the hardware of the drive can be replaced with state observers to minimize the cost, increase the reliability and estimate the used states in the field oriented control algorithms frequently.

The control structure of a state-feedback is not very robust with respect to the control error, because this error is not fed back. Uncertainties in the plant model parameters or disturbance acting on the plant may cause steady-state control errors. It has been shown that while working with the P-regulator in conjunction with the subsidiary speed loop there is a state feedback-control mechanism which requires all state variables to be measured. In many cases it is not possible, either for technical or economic reasons. In this case we may use an observer (estimator), which can estimate the state variables knowing only the input and output signals and can deliver the information about the states so that they can be used for control.

A state feedback-controller or a cascade state feedback-control system is involved with an observer which has non-zero error in a steady-state. For zero error in a steady-state one of the following regulating structures should be used-Structure with an integrator (because error is fed back to an integrator) or Structure with a disturbance observer.

The motor losses consist of mechanical loss, copper loss and iron loss. The mechanical loss is speed dependent and not controllable. The controllable losses are copper loss and iron loss. The copper loss can be minimized by the maximum torque-per-ampere control, in which the armature current vector is controlled in order to produce the maximum torque per armature current ampere [58].

The iron loss can be reduced by the flux-weakening control [59]-[62], in which the d-axis current is controlled in order to reduce the air-gap flux by the demagnetizing effects due to the d-axis armature reaction, because the iron loss is roughly proportional to flux density squared.

Within FS-PM machines, it has been shown that the magnet eddy loss may contribute a large part of the total machine losses due to the volume of magnet material within the motor topology. However, radial and/or axial segmentation of the permanent magnets can reduce the magnet eddy losses significantly [63].

Future work will focus on creating a representative sensor-less control model of FS-PMSM with an observer and integrator using program Matlab or Labview, combining this with Finite element using the Magnet program. Also to create a representative loss minimization model of FS-PMSM with field weakening, experimental evaluation of the simulation results has to be taken into account.

In the future more faulty conditions should be studied (i.e power converter fault). Special attention should be given to the torque-ripple minimization by increasing the number of poles, number of converter legs or applying an advanced control technique. The future work will also focus on fault detection hardware and power supply, minimization of torque pulsation, improvement of fault-tolerant operation, advanced control algorithm and more applications.

LIST OF APPENDICES

APPENDIX (A) - LIST OF PUBLICATIONS

The work described in this thesis has resulted in the following journal and conference papers being published:

[1] M. O. E. Aboelhassan, T. Raminosoa, A. Goodman, L. De Lillo, C. Gerada “Performance Evaluation of a Vector-Control Fault-Tolerant Flux-Switching Motor Drive,” *IEEE Transactions on Industrial Electronics*, Vol. 60, No. 8, August 2013, pp. 2997-3006.

[2] M. Aboelhassan, T. Raminosoa, A. Goodman, L. De Lillo, C. Gerada “A fault-tolerant control scheme for a dual flux-switching permanent magnet motor drive,” *in Proc. International Conference on Electrical Machines and Systems, ICEMS '11*, August 2011, pp. 1-6.

[3] M. Aboelhassan, J. Skalický “A fault tolerant control strategy for a flux-switching permanent magnet motor drive under open phase fault,” *in Proc. 11th International Conference on Low Voltage Electrical Machines, LVEM '11*, November 2011, pp. 1-4.

[4] M. Aboelhassan, J. SKALICKÝ “Control of synchronous motor with permanent magnet (PM) excitation,” *in Proc. 14th Scientific Conference Computer Applications in Electrical Engineering, ZKwE'09*, April 2009, pp. 271-272.

[5] M. Aboelhassan “Position control of field oriented PMSM using Matlab/Labview,” *in Proc. 9th International Conference on Low Voltage Electrical Machines*, November 2009, pp. 63-66.

[6] M. Aboelhassan “Speed control of DC motor using combined armature and field control,” *in Proc. 15th Conference Student, EEICT'09*, April 2009, pp. 87-91.

[7] M. Aboelhassan, “A proportional integral derivative (PID) feedback control without a subsidiary speed loop,” *Acta Polytechnica*, Vol. 48, No. 3, pp. 7-11, October 2008.

[8] M. Aboelhassan, J. SKALICKÝ “Position servodrives with an elastic coupling and integrator,” *Computer Applications in Electrical Engineering, pp. 339-350*, 2008.

[9] M. Aboelhassan, J. SKALICKÝ “Nonlinear control of servodrives with dynamic backlash,” *in Proc. 8th International Conference on Low Voltage Electrical Machines LVEM '08*, November 2008, pp.14-17.

[10] M. Aboelhassan, “Proportional integral derivative control,” *in Proc. 12th International Student Conference on Electrical Engineering*, May 2008, pp.1-4.

[11] M. Aboelhassan, “Position control of servodrives using BLDC motor,” *in Proc. 14th Conference student, EEICT'08*, April 2008, pp.134-138.

[12] M. Aboelhassan, J. SKALICKÝ “State feedback control with an observer and integrator,” *in Proc. 13th Scientific Conference Computer Applications in Electrical Engineering, ZKwE'08*, April 2008, pp. 221-222.

[13] M. Aboelhassan, J. SKALICKÝ “Position servodrives with an elastic coupling,” *in Proc. 7th International Conference on Low Voltage Electrical Machines LVEM '07*, November 2007, pp.18-21.

APPENDIX (B) –FS-PMSM MODEL

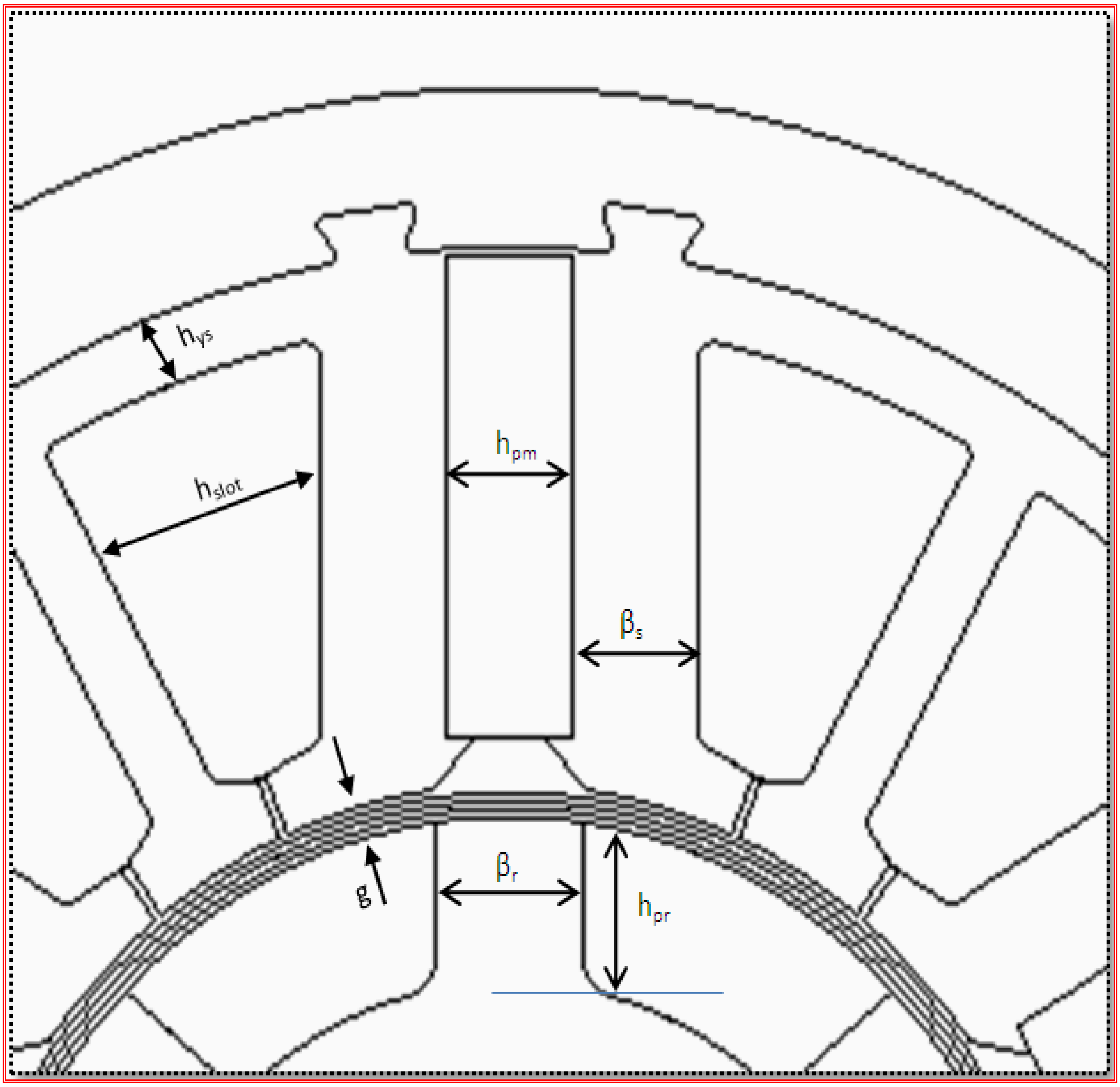

Determination of machine dimensions in original design.

where:

h_{ys}	=	*Stator yoke thickness.*
h_{slot}	=	*Slot opening width.*

β_s	=	*Stator segment tooth width.*
β_r	=	*Rotor pole width.*
h_{pm}	=	*PM thickness in magnetisation direction.*
h_{pr}	=	*Rotor pole height.*
g	=	*Airgap length.*

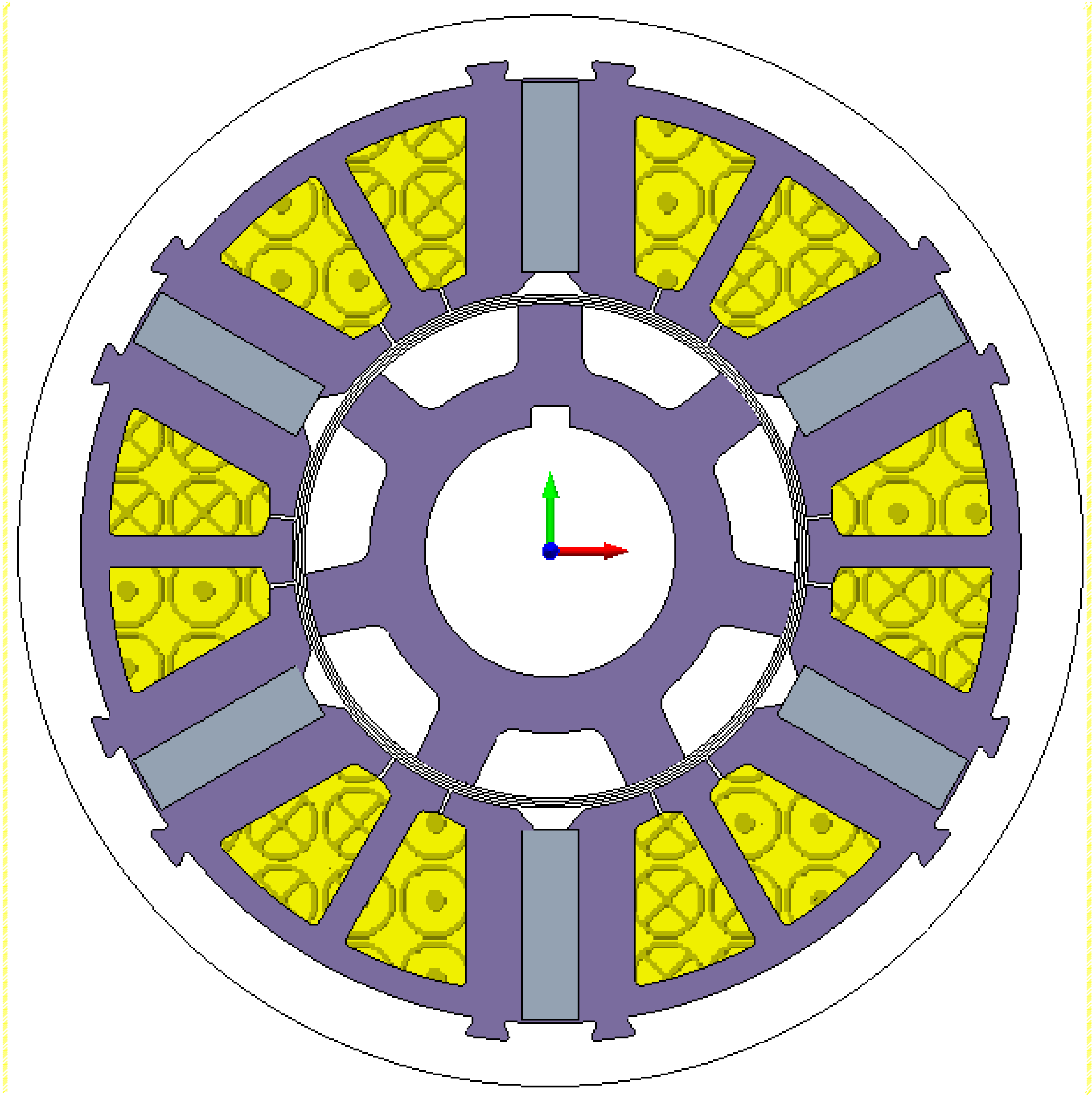

The finite element model of FS-PMSM.

APPENDIX (C) – FINITE-ELEMENT ANALYSES (FEA) RESULTS

The distribution of no-load magnetic fields at the four specific rotor positions (Flux plotting from finite element modelling)

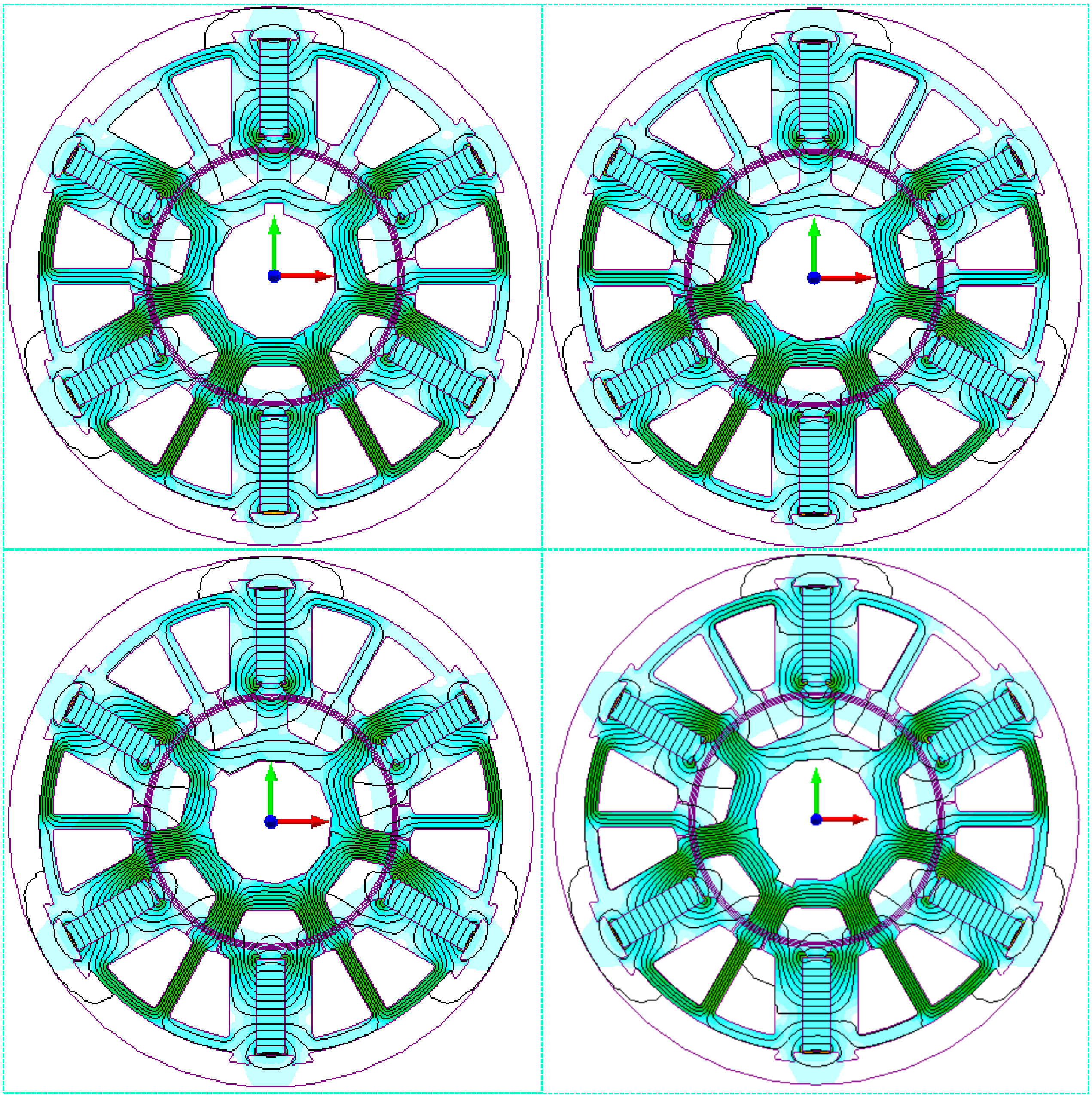

Cross-sectional design and magnetic flux distribution of magnetic field at no-load for the proposed fault-tolerant 7-pole rotor FS-PMSM

$\theta_r = 0°$ (b) $\theta r = 51°$ (c) $\theta r = 102°$ (d) $\theta r = 153°$

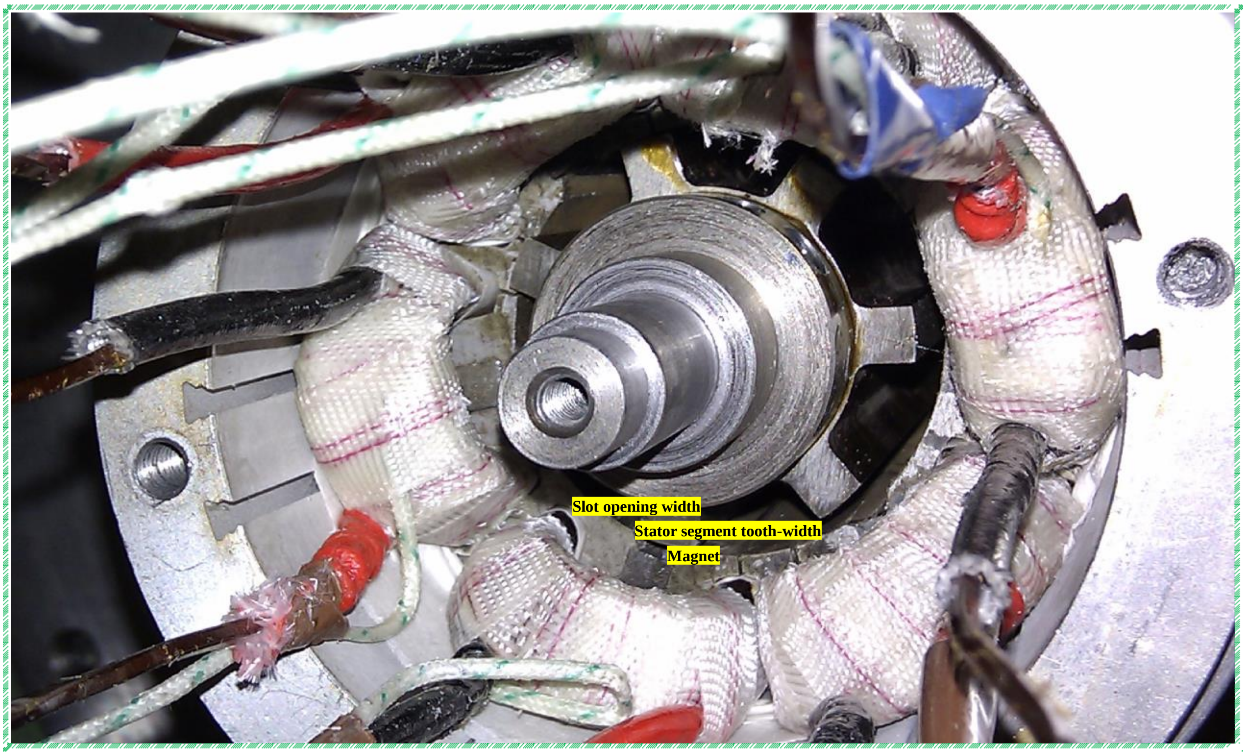

The prototype of the proposed fault-tolerant dual three-phase FS-PMSM (Stator of FS-PMSM and close up showing arrangement of magnet, stator segment tooth width and slot opening width)

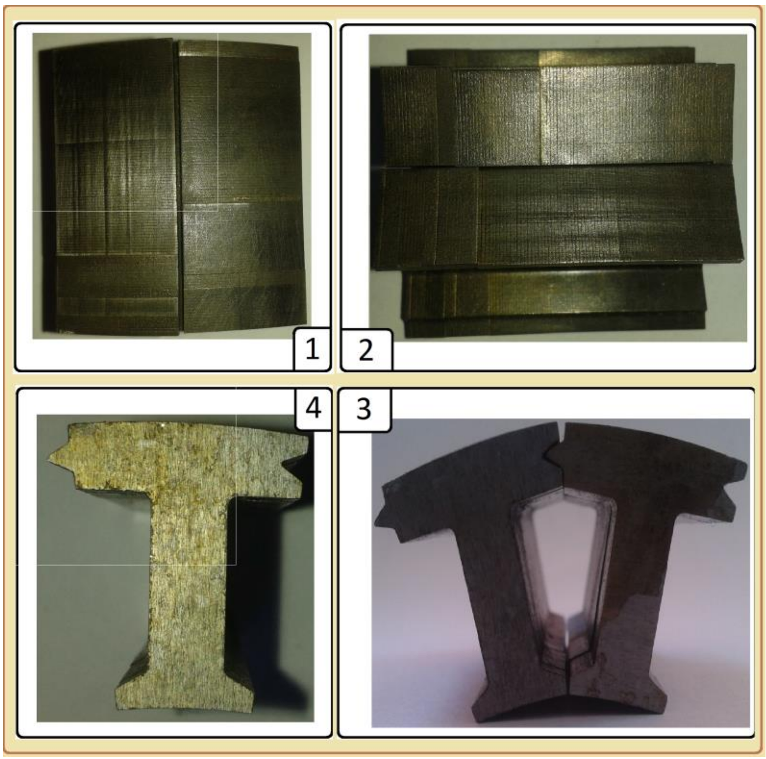

FS-PMSM slot

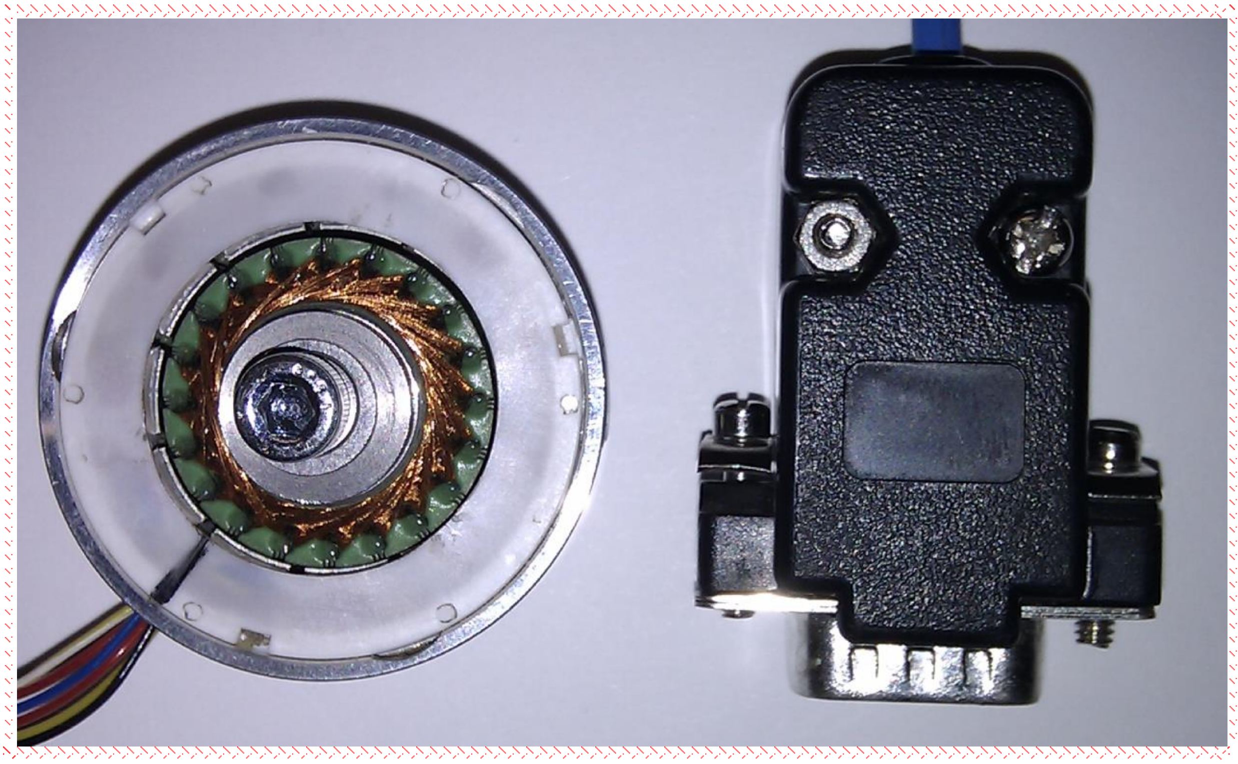

Resolver transducer mounted on the rotor shaft (rotor position data is acquired using a resolver)

Since the rotor position is required for the close-loop control algorithm of the motor, a resolver to digital (R/D) converter is needed. The resolver transducer is mounted on the motor shaft for the rotational angle measurement.

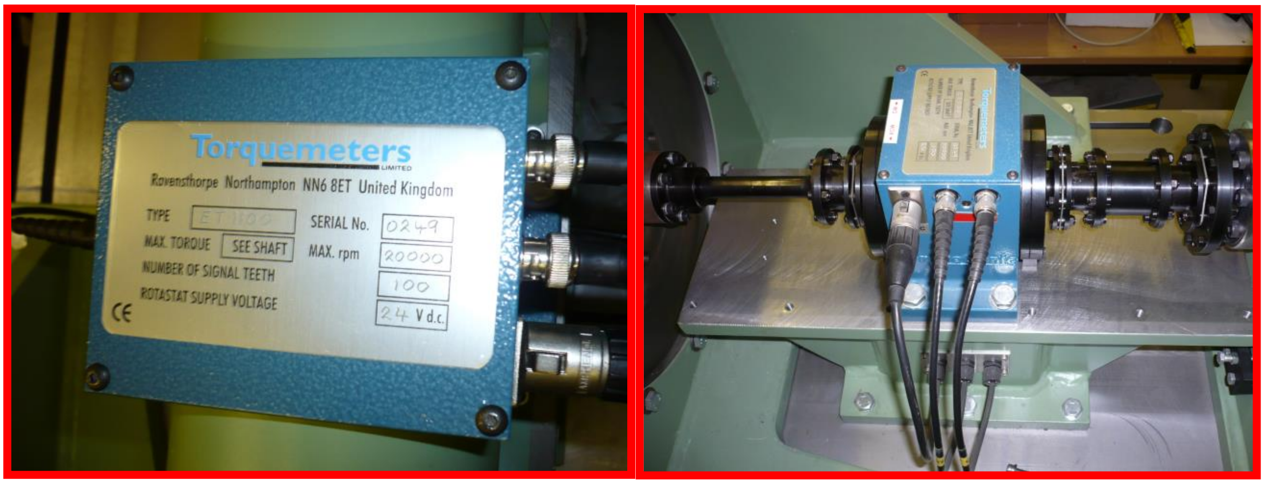

Torquemeters

UadTech 1730 LCR Digibridge

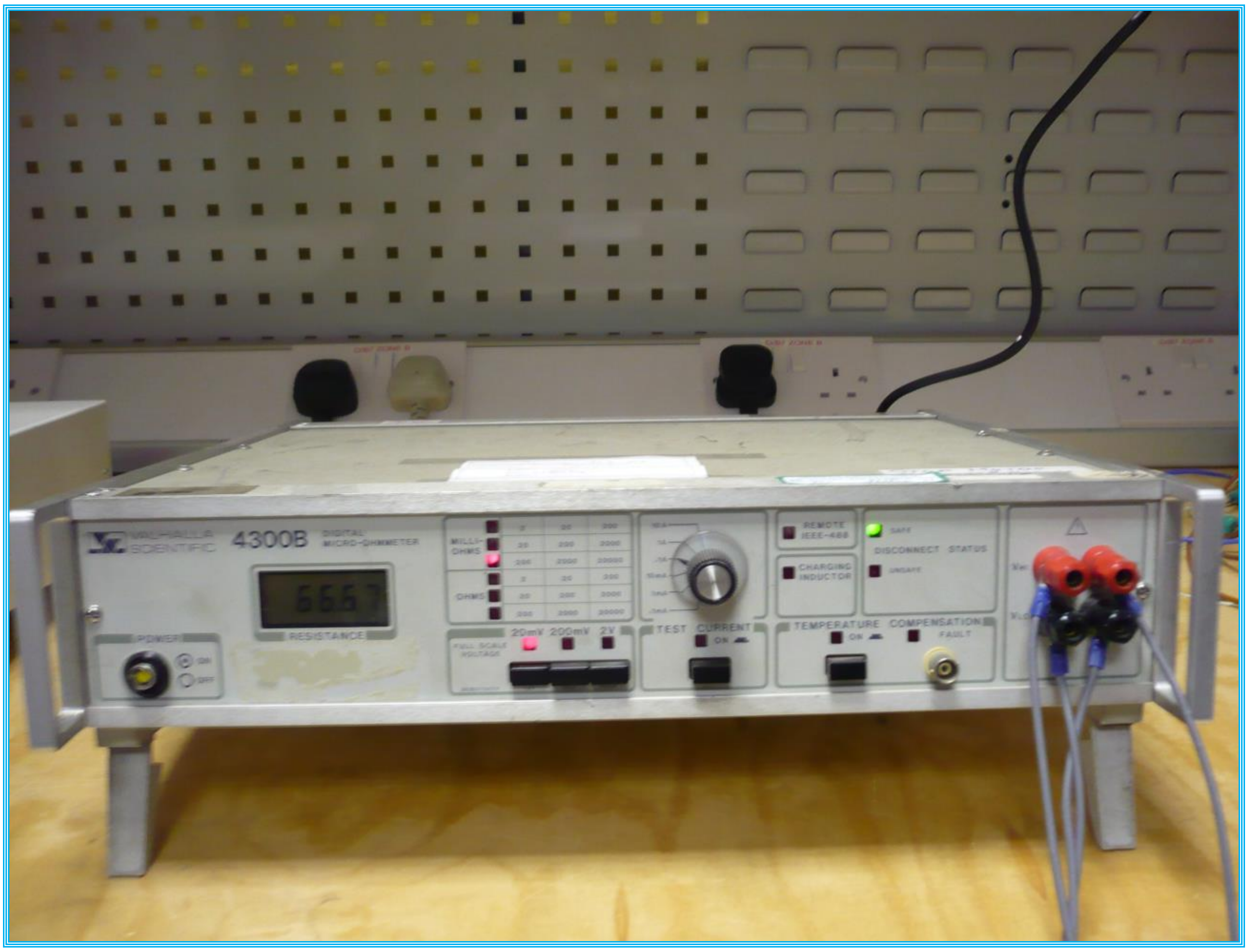

Digital Micro-Ohmmeter 4300B

APPENDIX (D) – SIMULATION IN PROGRAM MATLAB

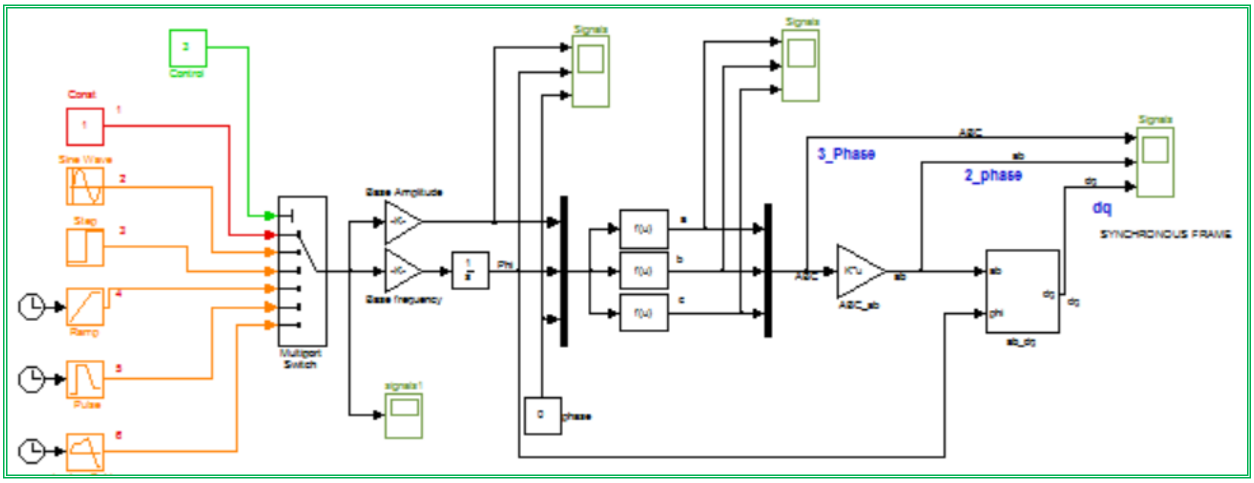

abc-dq transformation (variable-amplitude variable-frequency sinusoidal signals)

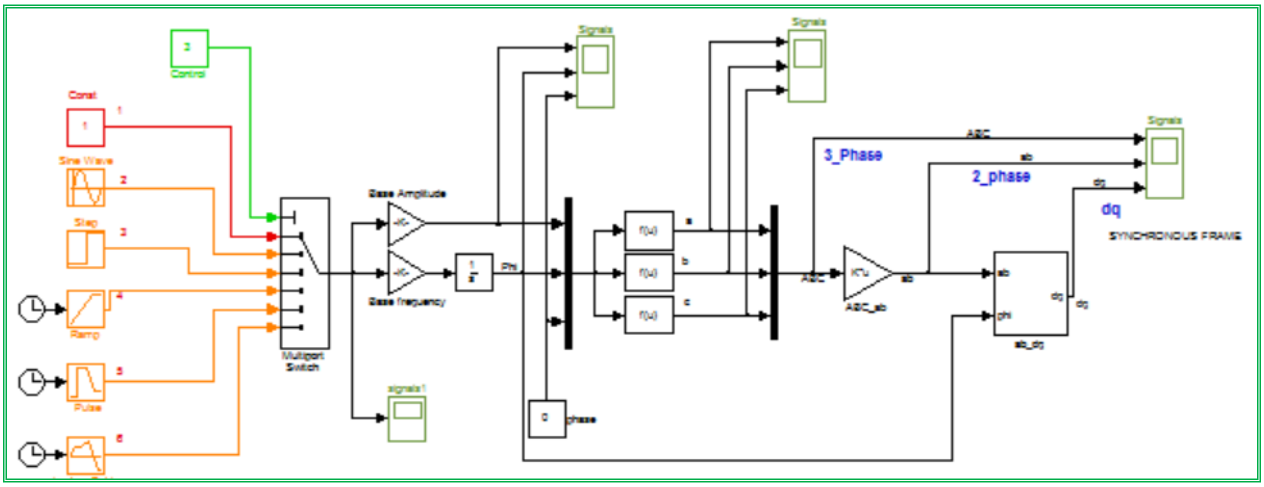

abc-dq and dq-abc transformation (variable-amplitude variable-frequency sinusoidal signals)

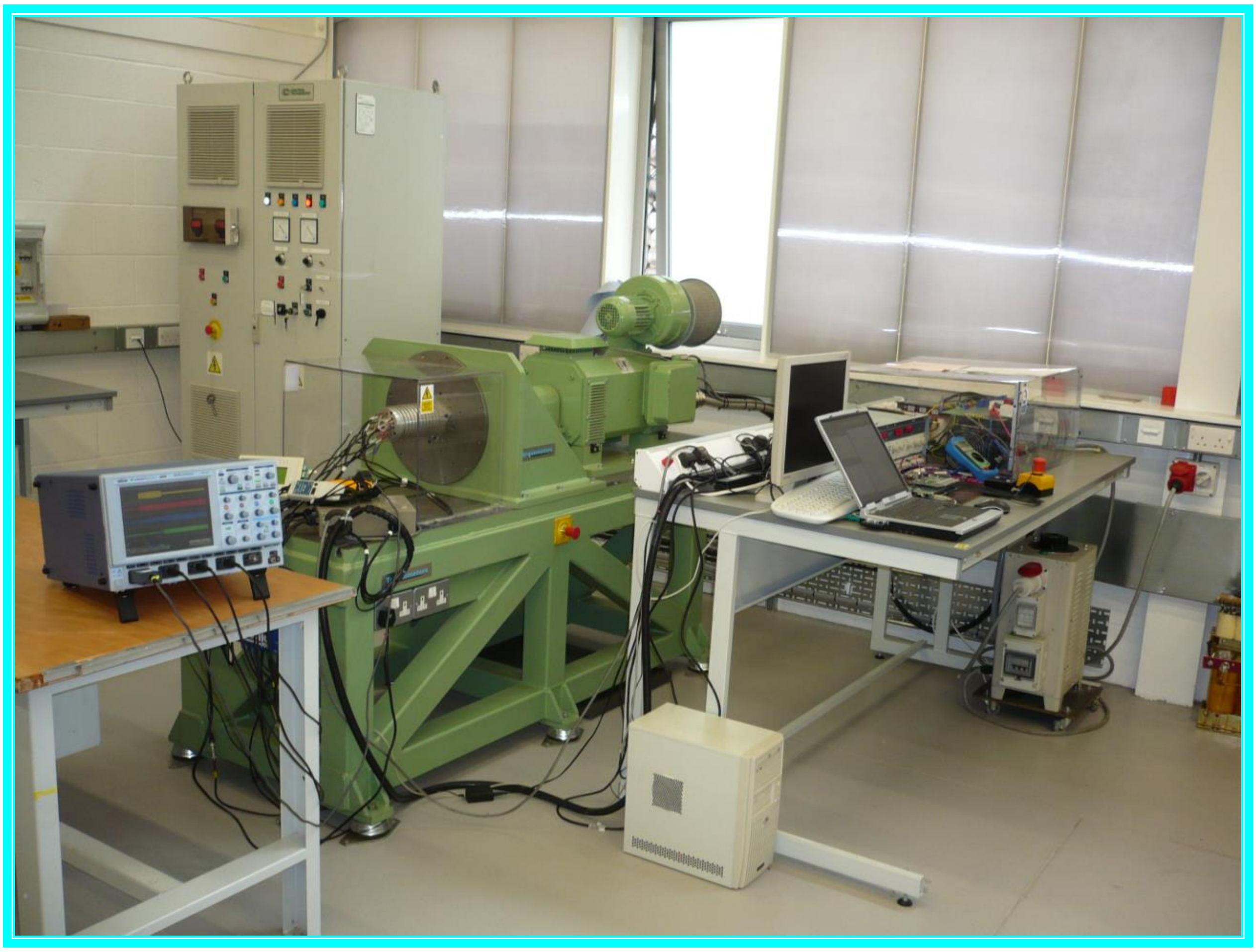

Experimental setup

BIBLIOGRAPHY

[1] H. Jia, M. Cheng, W. Hua, W. Zhao, W. Lu, "A New Stator-Flux Orientation Strategy for Flux-Switching Permanent Magnet Drive Based On Voltage Space-Vector," *IEEE ICEMS*, Wuhan, China, October 17-20, 2010, pp. 3032-3036.

[2] Z.Q. Zhu, Y. Pang, D. Howe, S. Iwasaki, R. Deodhar, A. pride, "Analysis of electromagnetic performance of Flux-switching permanent magnet machines by non-linear adaptive lumped parameters magnetic circuit model," *IEEE Trans. Magnetics*, vol. 41, no. 11, pp. 4277-4287, November 2005.

[3] Y. Pang, Z. Q. Zhu, D. Howe, S. Iwasaki, R. Deodhar, A. Pride, W. Lu, "Comparative study of flux-switching and Interior permanent-magnet machines," *IEEE ICEMS*, Seoul, South Korea, October 8-11, 2007, pp. 757-762.

[4] W. Zhao, W. Hua, H. Jia, D. Howe, "A redundant flux-switching permanent-magnet motor drive for fault-tolerant applications," *IEEE VPPC*, Harbin, China, September 3-5, 2008, pp. 1-6.

[5] B. C. Mecrow, A. G. Jack, J. A. Haylock, J. Coles, "Fault-tolerant permanent-magnet machine drives," *IEEE Elect. Power Appl.*,vol. 143, no. 6, pp. 437-442, November 1996.

[6] K. T. Chau, C. C. Chan, C. Liu, "Overview of permanent-magnet brushless drives for electric and hybrid electric vehicles," *IEEE Trans. Ind. Electron.*, vol. 55, no. 6, pp. 2246-2257, June 2008.

[7] D. Gerada, A. Mebraki, C. Gerada, "Optimal design of a high speed concentrated wound PMSM ," *IEEE ICEMS*, Tokyo, Japan November 15-18, 2009, pp. 1-6.

[8] Z.Q. Zhu, Y. Liu, D. Howe, "Minimizing the influence of cogging torque on vibration of PM Brushless Machines By Direct torque control," *IEEE Trans. Magnetics*, vol. 42, no. 10, pp. 4512-3514, October 2006.

[9] J. Holtz, W. Lotzkat, A. Khambadkone, "On Continuous Control of PWM Inverters in the Overmodulation Range Including the Six-Step Mode ," *IEEE Trans. Power Electronics*, vol. 8, no. 4, pp. 546-553, October 1993.

[10] J. Zhu, N. Ertugrul, W. L. Soong, "Fault Remedial Strategies in a Fault-Tolerant Brushless Permanent Magnet AC Motor Drive with Redundancy," *IEEE IPEMC*, Wuhan, China, May 17-20, 2009, pp. 423-427.

[11] O. F. Jasim, *An Extended Induction Motor Model for Investigation of Faulted Machines and Fault Tolerant Variable Speed Drives:* University of Notttingham, 2009.

[12] J. Zhu, X. Niu, "Investigation of short-circuit in a fault-tolerant brushless permanent magnet AC motor drive with redundancy," *IEEE ICIEA*, Taichung, Taiwan, June 15-17, 2010, pp. 1238-1242.

[13] R. Dorf, System, *Controls, Embedded Systems, Energy, and Machines*: CRC press, 2006.

[14] B. Drury, *The Control Techniques Drives and Controls Handbook:* Cambridge University Press, 2001.

[15] W. Leonhard, *Control of Electrical Drives:* Springer, 1996.

[16] J. Gieras, M. Wing, *Permanent Magnet Motor Technology*: Marcel Dekker Inc. 2002.

[17] Available at: *http://www.yourdictionary.com/servomechanism.*

[18] J. Skalický, *Power electronics:* Brno University, 2002.

[19] R. Crowder, *Electric Drives and Electromechanical Systems*: Oxford OX2, 2006.

[20] G. Anderson, *Dynamics and Control of Electric:* EEH Power System Laboratory, Zürich, 2011.

[21] M. Aboelhassan, J. Skalický, "Control of Synchronous Motor with Permanent Magnet (PM) Excitation," *ZKwE*, Poznan, Poland, April 20-22, 2009, pp. 271-272.

[22] P. Vas, *Sensorless Vector and Direct Torque Control*: Oxford University Press, 1998.

[23] M. Aboelhassan, "A Proportional Integral Derivative (PID) Feedback Control without a subsidiary speed loop," *Acta Polytechnica*, vol. 48, no. 3, pp. 7-11, October 2008.

[24] S. Vukosavic, *Digital Control of Electrical Drives*: Springer, 2007.

[25] O. Chee-Mun, *Dynamic Simulation of Electric Machinery*: Printice Hall, 1998.

[26] M. Aboelhassan, "Nonlinear Control of sevodrives with Dynamic Backlash," *LVE*, *M*, Brno, Czech Republic, April 24-25, 2008, pp.14-17.

[27] T. Raminosoa, C. Gerada, N. Othman, L. D. Lillo,"Rotor losses in fault-tolerant permanent-magnet synchronous machines," *IET Elect. Power Appl*, vol. 5, no. 1, pp. 75-88, January 2011.

[28] T. Raminosoa, C. Gerada, "Novel fault-tolerant design of flux-switching machines," *IET PEMD*, Brighton, UK, April 19-21, 2010, pp. 1-6.

[29] T. Raminosoa, C. Gerada, M. Galea,"Design considerations for a fault-tolerant flux-switching permanent-magnet machine," *IEEE Trans. Ind. Electron.*, vol. 58, no. 7, pp. 2818-2825, July 2011.

[30] T. Raminosoa, C. Gerada, "Fault-tolerant winding technology comparison for flux-switching machine," *IEEE ICEMS*, Rome, Italy, September 6-8, 2010, pp. 1-6.

[31] W. Zhao, M. Cheng, K. T. Chau, J. Ji, W. Hua, R. Cao, "A new modular flux-switching permanent-magnet machine using fault-tolerant teeth," *IEEE ICEFC*, Chicago, USA, May 9-12, 2010, pp. 1.

[32] J. T. Chen, Z. Q. Zhu, "Comparison of all and alternate poles wound flux-switching PM machines having different stator and rotor pole numbers," *IEEE Trans. Ind. Electron.*, vol. 46, no. 4, pp. 1406-1415, August 2010.

[33] M. Cheng, W. Hua, J. Zhang, W. Zhao, "Overview of stator-permanent-magnet brushless machines," *IEEE Trans. Ind. Electron.*, vol. 58, no.11, pp. 5087-5101, November 2011.

[34] J. T. Chen, Z. Q. Zhu, "Influence of rotor pole number on optimal parameters in flux-switching PM brushless ac machines by lumped parameter magnetic circuit model," *IEEE IEMDC*, Miami, USA, May 3-6, 2009, pp. 1216-1223.

[35] W. Zhao, M. Cheng, W. Hua, H. Jia, R. Cao, "Back-EMF harmonic analysis and fault-tolerant control of flux-switching permanent-magnet machine with redundancy," *IEEE Trans. Ind. Electron.*, vol. 58, no.5, pp. 1926-1935, May 2011.

[36] W. Zhao, M. Cheng, K. T. Chau, W. Hua, H. Jia, J. Ji, W. Li,"Stator-flux-oriented fault-tolerant control of flux-switching permanent magnet motors," *IEEE Trans. Magn.*, vol. 47, no.10, pp. 4191-4194, October 2011.

[37] L. Alberti, N. Bianchi, "Impact of winding arrangement in dual three-phase induction motor for fault-tolerant application," *IEEE ICEMS*, Rome, Italy, September 6-8, 2010, pp. 1-6.

[38] J. J. Wolmarans, H. Polinder, J. A. Ferreira, D. Clarenbach, "Selecting an optimum number of system phases for an integrated, fault-tolerant permanent-magnet machine and drive," *IEEE EPE*, Barcelona, Spain, September 8-10, 2009, pp. 1-10.

[39] Y. Zhang, J. Zhu, W. Xu, Y. Guo, "A simple method to reduce torque ripple in direct torque-controlled permanent-magnet synchronous motor by using vectors with variable amplitude and angle," *IEEE Trans. Ind. Electron.*, vol. 58, no.7, pp. 2848-2859, July 2011.

[40] A. S. Thomas, Z. Q. Zhu, R. L. Owen, G. W. Jewell, D. Howe, "Multiphase Flux Switching Permanent-Magnet Brushless Machine foe Aerospace Application," *IEEE Trans. Industry Application*, vol. 45, no. 6, pp. 1971-1981, December 2009.

[41] E. Hoang, A. H. Ben-Ahmed, J. Lucidarme, "Switching flux permanent magnet polyphased synchronous machines," *EPE*, Trondheim, Norway, September 8-10, 1997, pp. 903-908.

[42] M. O. E. Aboelhassan, T. Raminosoa, A. Goodman, L. de Liliana, C. Gerada, "A fault-Tolerant Control Scheme for a Dual Flux-Switching Permanent Magnet Motor Drive," *IEEE ICEMS*, Beijing, China, August 20-23, 2011, pp. 1-6.

[43] J. W. Bennett, G. J. Atkinson, B. C. Mecrow, D. J. Atkinson, "Fault- tolerant design considerations and control strategies for aerospace drives, " *IEEE Trans. Ind. Electron.*, vol. 59, no. 5, pp. 2049-2058, May 2012.

[44] S. J. Nall, P. H. Mellor, "A compact direct-drive permanent-magnet motor for a UAV rotorcraft with improved faulted behaviour through operation as four separate three-phase machines," *IET PEMD*, York, United Kingdom, April 2-4, 2008, pp. 245-249.

[45] M. P. Kazmierkowski, R. Krishnan, F. Blaabjerg, *Control in power electronics, selected problems:*Academic press, 2002.

[46] J. R. Rodriguez, J. W. Dixon, J. R. Espinoza, J. Pontt, P. Lezana,"PWM regenerative rectifiers: state of the art," *IEEE Trans. Ind. Electron.*, vol. 52, no. 1, pp. 5-22, February 2005.

[47] C. klumpner, P. Nielsen, I. Boldea, F. Blaabjerg,"A new matrix converter motor (MCM) for industrial applications," *IEEE Trans. Ind. Electron.*, vol. 49, no. 2, pp. 325-335, April 2002.

[48] E. L. Lyshevski, *Electromechanical Systems and Devices:* CRC Pres, 2008.

[49] B. K. Bose, *Modern Power Electronics and AC Drives:* Patience Hall, 2002.

[50] E. Odvarka, A. Mebarki, D. Gerada, N. Brown, C. Ondrusek, "Electric motor generator for a hybrid electric vehicle," *Eng. Mechan.*, vol. 16, no. 2, pp. 131-139, February 2009.

[51] R. N. Argile, B. C. Mecrow, D. J. Aktinson, A. G. Jack, P. Sangha, “Reliability analysis of fault tolerant drive topologies,” *IET PEMD*, York, UK, April 2-4, 2008, pp. 11-15.

[52] Q. Shang, *A new Short Circuit Fault Detection Scheme for Fault Tolerant Drive Systems:* University of Newcastle Upon Tyne, 2009.

[53] B. C. Mecrow, A. G. Jack, D. J. Atkinson, J. A. Haylock, “Fault tolerant Drives for Safety Critical Application,” *IEEE*, London, UK, June 18-20, 1997, pp. 1-7.

[54] L. de Lillo, L. Empringham, P. W. Wheeler, S. Khwan-On, C. Gerada, M. N. Othman, X. Huang, “Multiphase Power Electronics Drive for Fault-Tolerant Machine Development in Aerospace Applications,” *IEEE Trans. Ind. Electron.*, vol. 57, no. 2, pp. 575-583, February 2010.

[55] P. Wheeler, J. Clare, L. Empringham, M. Apap, K. Bradley, C. Whitley, G. Towers, “A matrix converter based permanent magnet motor drive for an aircraft actuation system,” *IEEE IEMDC*, Madison, USA, June 1-4, 2003, pp. 1295-1300.

[56] S. Khwan-on, *Fault Tolerant Matrix Converter Motor Drives:* University of Nottingham, 2011.

[57] M. O. E. Aboelhassan. T. Raminosoa, A. goodman, L. de Lillo, C. Gerada, “Performance evaluation of a vector-control fault-tolerant flux-switching motor drive,” *IEEE Trans. Ind. Electron.*, vol. 60, no. 8, pp. 2997-3006, August 2013.

[58] T. M. Jahns, G. B. Klin, T. W. Neuron, “Interior permanent-magnet synchronous motor for adjustable-speed drives,” *IEEE Trans. Ind. Appl.*, vol. IA-22, no. 4, pp. 738-747, April 2008.

[59] B. Sneyers, D. W. Novotny, T. A. Lipo,“Field weakening in buried magnet ac motor drives,” *IEEE Trans. Ind. Appl.*, vol. IA-21, no. 2, pp. 398-407, April 2007.

[60] T. M. Jahns, “Flux-weakening regime operation of an interior permanent-magnet synchronous motor drives,” *IEEE Trans. Ind. Appl.*, vol. IA-23, no. 4, pp. 681-689, April 2008.

[61] B. K. Bose, *Modern Power Electronics and AC Drives:* Patience Hall, 2002.

[62] S. Morimoto, Y. Takeda, T. Hirasa, K. Taniguchi,“Expansion of operation limits for permanent magnet motor by current vector control considering inverter,” *IEEE Trans. Ind. Appl.*, vol. 26, no. 5, pp. 866-871, August 2002.

[63] A. Thomas, Z. Q. Zhu, G. W. Jewell, D. Howe, “Flux-switching PM Brushless Machines with alternative stator and rotor pole combinations” *Journal of Asian Vehicles*, vol.6, no. 1, pp. 1103-1110, June 2008.


The University of
Nottingham
UNITED KINGDOM · CHINA · MALAYSIA
East
Entrance
QS
WORLD
UNIVERSITY
RANKINGS
A Global Top 75 University
QS World University Rankings 2010/11